Synthesis, Characterization and Redox Properties of Antiaromatic Expanded Isophlorins

A Thesis

Submitted in Partial Fulfillment of the Requirements

for the Degree of

Doctor of Philosophy

By

Yadagiri Gopalakrishna Tullimilli

ID: 20093033

Indian Institute of Science Education and Research (IISER), Pune

2015

Dedicated to

My parents

Mr. & Mrs. Venkateswararao and

Lakshmidevi

&

My Sister Vani

भारतीय विज्ञान शिक्षा एवं अनुसंधान संस्थान, पुणे
INDIAN INSTITUTE OF SCIENCE EDUCATION AND RESEARCH (IISER), PUNE
Mendeleeve Block, Dr. Homi Bhabha Road, Pune – 411 008, Maharashtra, India

Dr. V. G. Anand
Associate Professor

Certificate

Certified that the work described in this thesis entitled "***Synthesis, Characterization and Redox Properties of Antiaromatic Expanded Isophlorins***" submitted by *Mr. Yadagiri Gopalakrishna Tullimilli* was carried out by the candidate, under my supervision. The work presented here or any part of it has not been included in any other thesis submitted previously for the award of any degree or diploma from any other university or institution.

Date: 13th March 2015

Dr. V. G. Anand
Research Supervisor

Ph: +91-20-25908091 | Fax: +91-20-25899790 *Email: vg.anand@iiserpune.ac.in*

Declaration

I declare that this written submission represents my ideas in my own words and wherever other's ideas have been included; I have adequately cited and referenced the original sources. I also declare that I have adhered to all principles of academic honesty and integrity and have not misrepresented or fabricated or falsified any idea/data/fact/source in this submission. I understand that violation of the above will result in disciplinary actions by the Institute and can also evoke penal action from the sources, which have thus not been properly cited or from whom appropriate permission has not been taken when needed.

Date: 13th March 2015

T. Y. Gopalakrishna

ID: 20093033

Acknowledgements

Foremost, I would like to express my sincere gratitude to my advisor Prof. V. G. Anand for the continuous support of my Ph.D. study and research, for his patience, motivation, enthusiasm, and immense knowledge. I thank him for believing in my abilities and giving work freedom during my Ph.D. It is difficult to compose appropriate sentence to express my gratefulness to him for his guidance and keen interest which made this work possible. I could not have imagined having a better advisor and mentor for my Ph.D. study.

I am extremely thankful to Prof. K. N. Ganesh for providing excellent research facilities and an outstanding research ambiance.

I am also grateful to the Research Advisory Committee members Dr. Sayam S. Gupta (NCL, Pune) and Dr. Sujit K. Ghosh (IISER, Pune) for their suggestions and advices.

I am thankful to Dr. T. S. Mahesh, Dr. H. N. Gopi, Dr. R. Boomishankar, Dr. R. G. Bhat, Dr. M. Jayakannan, Dr. Srinivasa Hotha, Dr. Jeetender Chugh, Dr. Arun Venkatnathan, Dr. M. Musthafa, Dr. Sunil Nair and Dr. Surjeet Singh for their assistance during my research period. In fact, I owe heartiest thank to every faculty of IISER-Pune.

I am really lucky to have wonderful lab mates. It's my pleasure to thank all the lovable Dr. VGA Lab members Dr. J. Sreedhar

Reddy, Dr. Neelam, Dr. Rashmi, Rakesh, Santosh G., Kiran, Santosh P., Ashok, Madan, Prakhar, Raj Kumar, and Manish as they always maintained a very lively environment inside lab.

My sincere thanks to Dr. Rajesh G. Gonnade (NCL, Pune) for his excellent course on crystallography. Prof. M Ravikanth (IIT B) for cyclic voltammetry facility, Dr. J. Sankar (IISER Bhopal), Dr. Pradeep K. Panda (University of Hyderabad) and Dr. Darba Srinivas (NCL, Pune) for EPR facility.

I thank Dr. V. S. Rao and Santosh Nevse for their precious support and timely help. I thank Dr. Umeshareddy Kacherki (deputy librarian) and Anuradha for library support. I thank IISER, Pune administrative staff members especially Mayuresh, Nayana, Tushar, Mahesh, Nitin, Yatish and Megha for their generous support.

I thank Suresh Prajapat, Syed, Somnath, and Pappu from UG lab IISER Pune. I thank Neeta Deo and Sachin for IT support.

I acknowledge the help from Archana (SCXRD), Pooja Lunawat (NMR), Swati M. Dixit (MALDI), Swathi (HRMS) and Nayana (HRMS) for the instrumental support. Special thanks to Sachin kate (Bruker India) for his kind help during variable temperature NMR experiments.

I must thank my friends, both seniors and juniors specially; Dr. Prakash Sultane, Abishek shukla, Dr. A. V. R. Murthy, Dr. Anurag Sunda, Dr. Amar Mohite, Dr. Sachitanand Mali, Dr. Anupam

Bandyopadhyay, Dr. Arvind Gupta, Dr. Dharma, Dr. Ramya, Sateesh ellipilli, Dnyaneshwar, Abhigyan, Ananthraj, Biplab, Sanjog, Dinesh, Ananth, Rajesh, Ganesh, Sundip, Barun, Rajendra and finally all dear friends from IISER Pune.

I am also thankful to all my friends outside IISER Pune for their support and help. It is indeed difficult to name out them all.

No words can ever convey my sense of gratitude felt for my parents (my father; Mr. Venkateswara Rao and mother; Mrs. Lakshmidevi) and sister (Mrs. Vani).

Finally, I am thankful to Council of Scientific and Industrial Research (CSIR) for Research Fellowship.

Due acknowledgments to them, whose names are unintentionally missed out, despite their unconditional help throughout the last five years.

Gopalakrishna

Contents

Synopsis

The thesis entitled ***"Synthesis, Characterization and Redox Properties of Antiaromatic Expanded Isophlorins"*** decribes the convenience of heterocycles such as thiophene, furan and selenophene in the design of 4nπ macrocycles that resemble the antiaromatic isophlorin framework. In general, antiaromaticity is considered to destabilize the π-delocalization in comparison to aromatic systems. This thesis describes the successfull attempts at the synthesis of stable antiaromatic macrocycles which belong to the class of expanded isophlorins. The 20π Isophlorin was introduced by Woodward as a hypothetical intermediate during the synthesis of porphyrin. Till date, pyrrole based isophlorins are found to be unstable under ambient conditions due to its rapid oxidation to the 18π porphyrin. Substantial efforts were made predominantly by Vogel and co-workers to realize such stable 20π macrocycles from other heterocycles such as thiophene, furan and selenophene. However, few other groups were reasonably successful in the synthesis of 20π macrocycle. Parallely and oblivious of isophlorin, many other groups were attempting to synthesize large macrocycles from thiophene subunits, which also had 4nπ electrons. Such large macromolecules are generally termed as macrocyclic oligothiophenes, which generally do not exhibit effective delocailization. The first chapter provides a quick glimpse to the synthetic chemistry, strcutural charcterization and the inference regarding the antiaromatic character of such π-conjugated macrocycles. This thesis represents the amalgmation of the isophlorin like framework into macrocyclic oligothiophenes, resulting in the synthesis of novel antiaromatic exapanded isophlorins. Apart from syntheses and structural characterization, electronic and redox properties of these macrocycles have been described with suitable support from quantum mechanical calcualtions.

The second chapter describes a simple and straight-forward one-pot synthesis of macrocyclic oligothiophenes from commerically available thiophene and pentafluoro benzaldehyde. Even though this reaction is similar to modified Rothemund's synthesis of porphyrin, the nature of the products isolated from this reaction was much different than observed with pyrrole. A range of π-conjugated macrocycles such as aromatic, antiaromatic, non-aromatic, non-antiaromatic and neutral radicals were isolated in a one-pot reaction. Significantly, a π conjugated macrocycle with five thiophene subunits was isolated from column chromatography. A detailed analysis enabled to confirm this as a neutral 25π electron radical. The radical nature of this macrocycle was further confirmed by one-electron redox

reaction. It could be oxidized to a 24π antiaromatic macrocycle and reduced to a 26π aromatic macrocycle. All the three states of this macrocycle was exhaustively studied by spectroscopic techniques such as ^{1}H NMR, ESR, Uv-Vis absorption, cyclic voltammetry and single crystal X-ray diffraction along with computational studies.

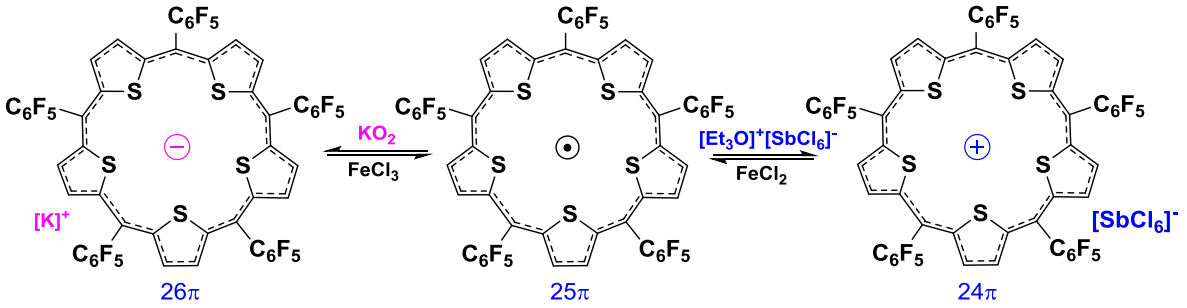

Similar such macrocycles with seven and nine thiophene rings were also identified. Preliminary analysis identifed them as 35 and 45 π-electrons macrocycles with a radical character. In the same reaction, a macrocycle with eight pyrrole rings was also isolated which could be indentified as 40π system. It was found to be planar in the solid state with ring inverted thiophene rings. Its ^{1}H NMR analysis suggested a twisted conformation at lower temperatures. In an effort to arrest the curling of the macrocycle, it was treated with C_{60} fullerene to form non-covalent host-guest complex. However, single crystal X-ray diffraction studies revealed splitting of the macrocycle into two 20π tetrathiophene isophlorin. From these studies it could be understood that the number of thiophene rings was crucial to the electronic properties and the structural features of the macrocycle. Its ability to form neutral and stable macrocyclic radicals is in stark contrast to pyrrole's capability to form only diamagnetic expanded porphyrins.

In continuation on these studies, expanding the conjugation in these macrocycles was imperative to explore the electronic properties of such giant π systems. Adding π-electrons to expand the conjugation could be done either by involving more heterocyclic units or by inserting more carbon bridges inbetween the heterocyclic units. Ethylene bridges are simple and attractive to replace the methine bridges in the macrocycles descibed above. Moreover, they can induce isomerism in such macrocycles with E or Z conformation of the double bond. The details of syntheses, structural features and electronic properties of 32π expanded isophlorins is described in the third chapter of this thesis. Bis-thienyl ethylene was employed as the precursor to have incorporate ethylene bridges in the macrocycles. Genrerally, such macrocyclic oligothiophenes were synthesized by McMurry coupling sutiable dialdehydes of

oligomeric thiophenes. However, an acid catalysed condensation of bis-thienyl ethylene with appropriate diols of thiophene/furan/selenophene was employed to have a combination of both methine and ethylene bridges in a given macrocycles. The macrocyclic products were isolated from column chromatographic seperation and later charctertized by various analytical techniques. It turned out that the single carbon bridges were essential to induce effective π conjugation in the macrocycle. The molecules identifeid from this reaction accounted for 32π and 48π electrons along the conjugated pathway and hence formally antiaroamtic in nature. ^{1}H NMR spectroscopy and estimated NICS values further confirmed the paratropic ring current effects expected of 32π systems. Single crystal X-ray diffraction analysis confirmed that planar structure of the macrocycle. The crystal packing diagram also revealed π-π stacking and unsual F…π interactions along with F…S interactions. However, all the planarity of the macrocycles was dependent on the nature of heterocycles in the macrocycle. Ring inverted structures were also identified in these 32π systems. Interestingly, irrespective of the topology all the 32π systems were found to undergo reversible two-electron oxdiation to form 30π dicationic species. This interconverison was monitored by electronic absorption spectroscopy, while the dications were exclusively charcterized by ^{1}H NMR spectroscopy and single crystal X-ray diffraction analysis. The change in the oxidation state also induced formal changes in the ring current effects. Therefore paratropic ring current effects were observed for 32π systems, while the oxidized 30π systems exhibited diatropic ring current effects. The modified ring currents were also justifed the NICS calcuations respectively. Also, toplogy of the macrocycles were also found to undergo reversible structural changes accompanying the redox process. Specifically, the hexafuran 32π expanded isophlorin exhibited a twisted conformation in the neutral state, while it was found to be planar in its oxidized form. This observation clearly indicated the two-electron ring oxidation of antiaroamtic systems which is generally not observed for aroamatic systems.

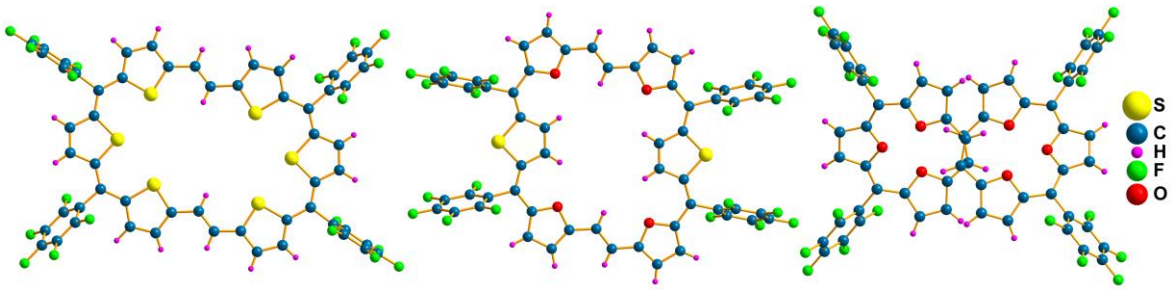

In the same reaction described above, along with the 32π system larger macrocycle with 48π electrons was also identified in the MALDI-TOF mass spectrum. The reaction

conditions were tuned to obtain moderate yields of the 48π macrocycles with nine heterocyclic rings. The composition of the heterocyclic rings could be varied by suitable precursors. Invariably all the macrocycles displayed a planar structure as determined from X-ray diffraction studies on their single crystals. Their crystal packing also revealed unsually strong intermolecualr π-π interactions at disatnce less than 3.4Å. However, only the nine-furan 48π macrocycle was found to adopt a non-planar structure and hence unsymmetrical in nature. NMR spectrum revealed fluxional behaviour of these macrocycles at room temperature, while they could be rigid at much lower temperatures. Similar to 32π systems, these macrocycles also displayed reversible two-electron oxidation to form 46π dications. The reversible nature of the redox process was monitored by electronic absorption spectroscopy. 46π exhibited more then 300 nm red shifts with repsect to the neutral 48π macrocycles. Unlike the 32π systems the oxidation of larger macrocycles yielded paramagnetic dications rather than the expected diamagnetic aromatic species. The two-electron oxidation was confirmed by high resolution mass spectrometry and the oxidized product was found to be EPR active. Magnetic moment measurements revealed paramagentic behaviour at temperatures below 25 K. Such observations are generally identified as dication diradicals. The triplet state being the lowest energy state for diradicals, magnetic measurements indicated a triplet state for the 46π dications at low temperatures. Oxidation of porphyrinoids to dication diradicals are very rare, while 4nπ macrocyclic oliogthiophenes have been known to form dication diradicals. However, these studies indicate the length of the π-conjugation can alter the redox proeprties of the antiaromatic systems. Isophlorin and its expanded derivatives further confirm the altered redox properties. In conclusion, this thesis describes the significant synthesis of π conjugated systems that are predominantly antiaroamtic in nature. The neutral radical and dication radicals are unsual features of porphyrinoids, but find compatiblity with the antiaromatic isophlorin skeleton.

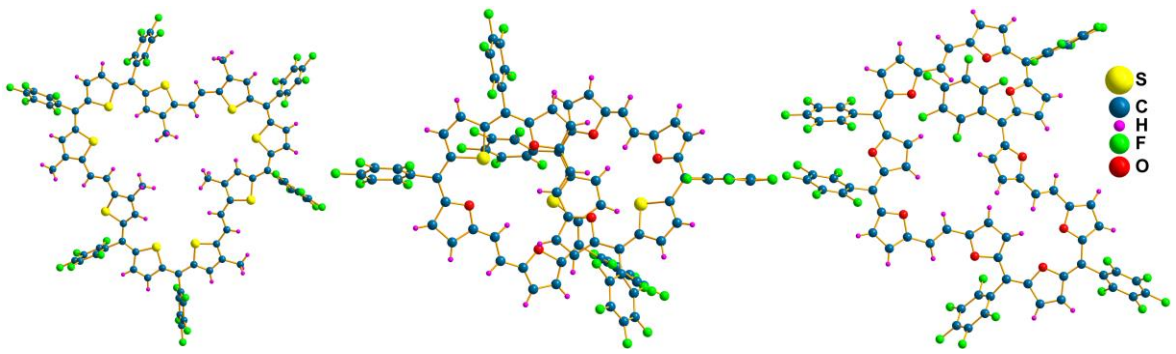

Publications

- **T. Y. Gopalakrishna**, J. S. Reddy, V. G. Anand, *Angew. Chem., Int. Ed.* **2014**, *53*, 10984-10987. An Amphoteric Switch to Aromatic and Antiaromatic States of a Neutral Air-Stable 25π Radical.

- **T. Y. Gopalakrishna**, V. G. Anand, *Angew. Chem. Int. Ed.* **2014**, *53*, 6678-6682. Reversible redox reaction between antiaromatic and aromatic states of 32π-expanded isophlorins.

- **T. Y. Gopalakrishna**, J. S. Reddy, V. G. Anand, *Angew. Chem. Int. Ed.* **2013**, *52*, 1763-1767. Antiaromatic Supramolecules: F···S, F···Se, and F···π Intermolecular Interactions in 32π Expanded Isophlorins.

Chapter I

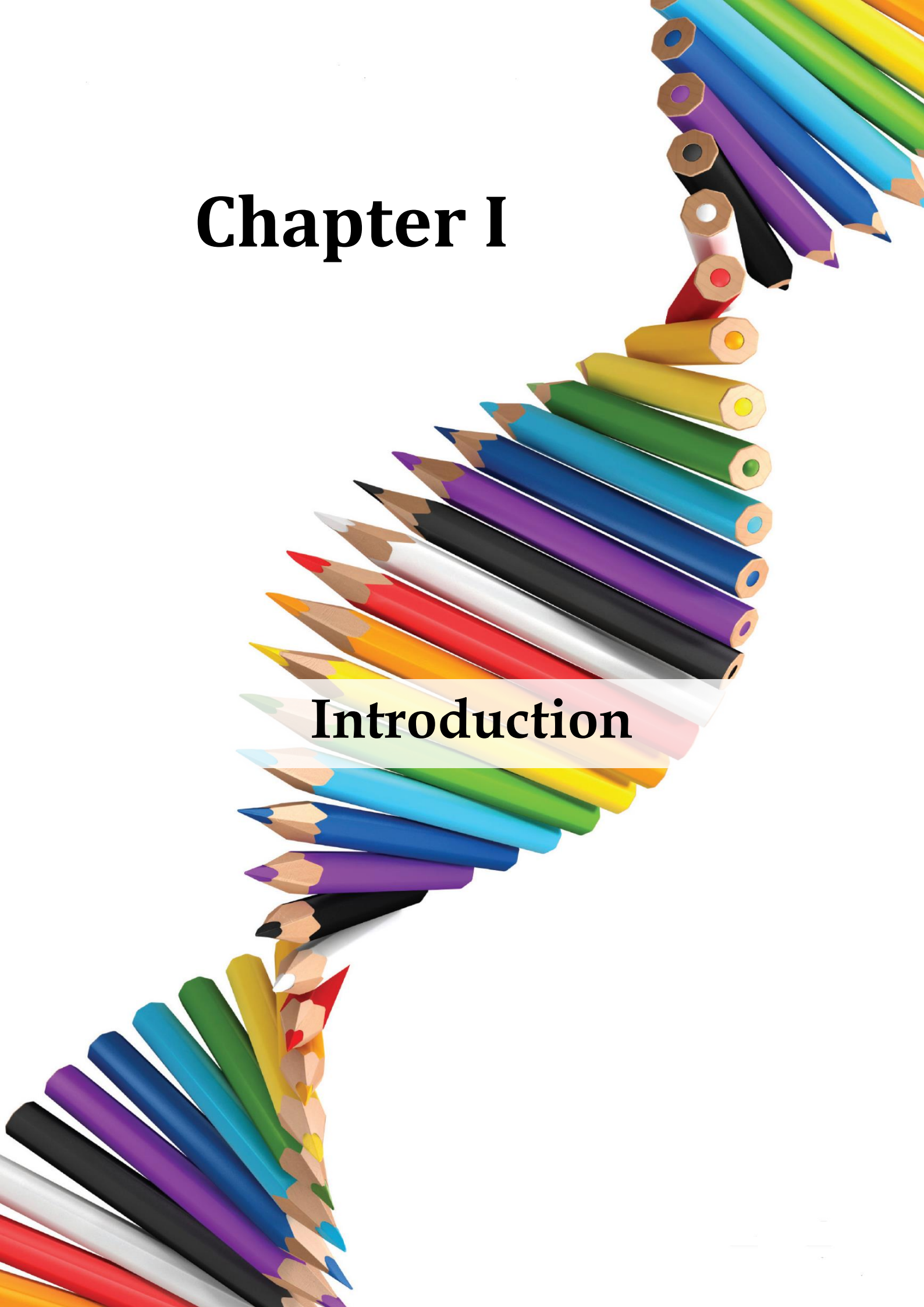

Introduction

π conjugated systems have attracted substantial attention for their photo-physical properties, structural intricacy and synthetic challenges. The effect of π bonds is dependent on the nature of the molecule under consideration. Hence they can be broadly classified as linear and macrocyclic structures. In a circular type conjugation, the delocalization of π electrons induces additional electronic properties such as ring currents for flat molecules. Hückel's rule generalizes planar π conjugated molecules as aromatic if they contain (4n+2) number of π electrons along the conjugated pathway[1]. A variety of aromatic molecules and their oligomeric systems have been synthesized and studied for their opto-electronic properties. Loss of planarity in π conjugated molecules renders them non-aromatic due to diminished ring current effects. On the other hand, macrocyclic structures that bear 4n number of π electrons along a conjugated pathway have ring current effects opposite to that as observed for (4n+2) π molecules. Hence, the term "anti-aromatic" was coined for planar molecules bearing 4n π electrons with uninterrupted conjugation[2]. However, anti-aromatic systems are relatively less explored due to the inherent instability derived from conjugation[3]. Nevertheless, the search for stable anti-aromatic molecules has been continuous but feeble.

In an attempted synthesis of Vit B_{12}, Woodward suggested the formation of an 18π porphyrin ring **I.2** through the oxidation of an unstable antiaromatic 20π intermediate, termed as "isophlorin"**I.1**[4]. Ever since, there have been constant efforts to isolate the unstable 20π intermediate.

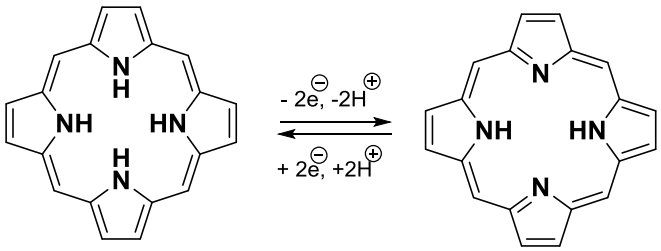

I.1 **I.2**

Vogel and co-workers pioneered the synthesis of macrocycles derived from thiophene/furan/selenophene by replacing all the pyrrole rings of a porphyrin [5]. These molecules resemble the cyclic structure of porphyrin and were expected to stabilize a 20π electrons conjugated system in their neutral state. However, they undergo quick two-electron oxidation to form an 18π porphyrin dication[5b]. Vogel and co-workers reported porphyrin analogs of tetrathia-porphyrin, **I.3**, dication having a carbon bridge in between the thiophene

units[5c]. The synthesis of the tetraoxa dicationic **I.4** species was achieved in three steps starting from furfuryl alcohol. The molecular structure elucidated by single crystal X-ray diffraction analysis displayed displacement of the thiophene rings from the mean plane of the macrocycle, whereas tetraoxa-porphyrin dication **I.4** adopted a planar structure.

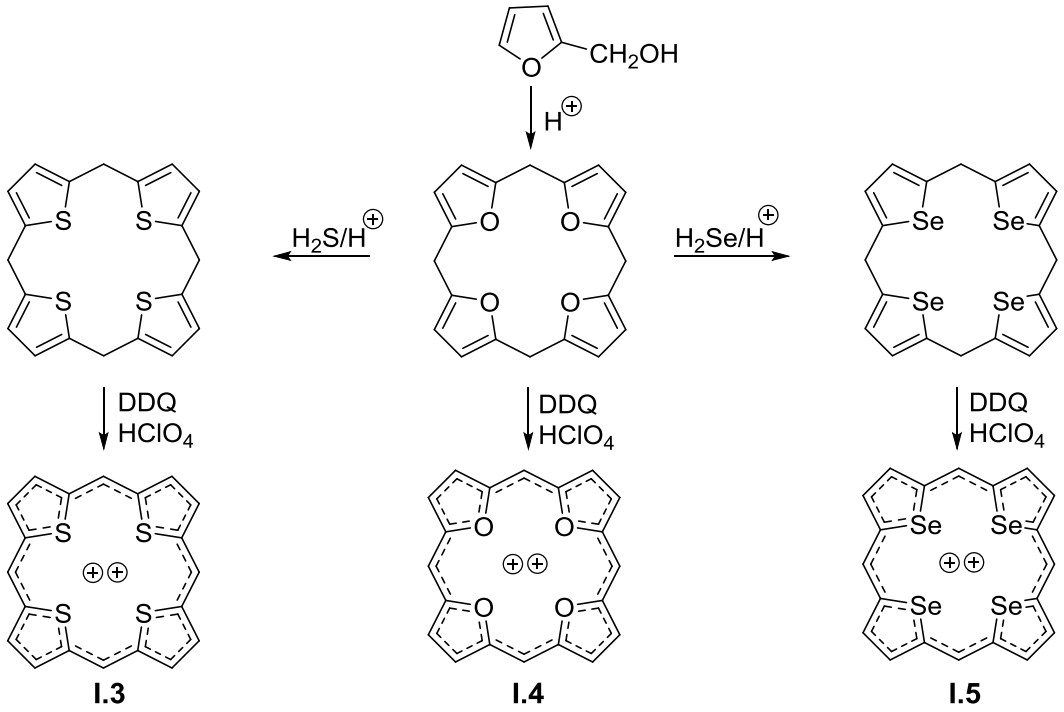

This was attributed to relatively large Van der Waal radius of sulphur when compared to oxygen. In spite of its deviation from planar structure, ^{1}H NMR spectra displayed diatropic ring currents, suggestive of global delocalization. Notwithstanding the unstable nature of beta substituted tetra-thia/oxa/selena isophlorin, the synthesis of an unsubstituted tetraoxaisophlorin **I.6** was achieved by two-electron reduction of corresponding dication **I.4** using potassium in THF[5e].

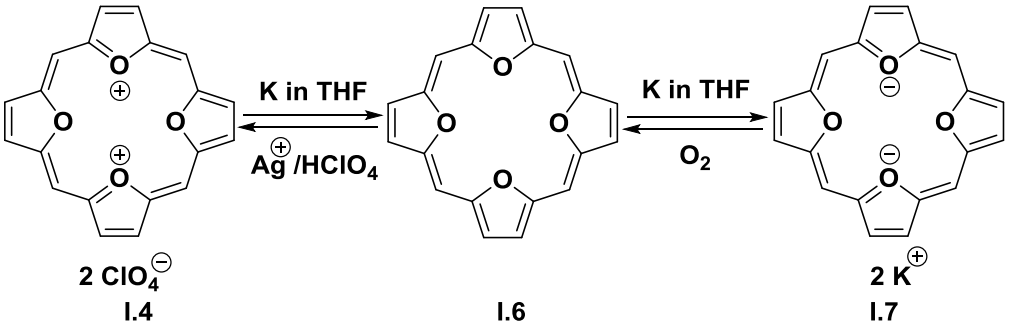

The reaction proceeds further, leading to the formation of tetraoxaporphyrin dianion **I.7**. Neutral tetraoxaisophlorin was isolated as air sensitive black crystals (could be stored at -78

°C) by two-electron oxidation of the dianion using molecular oxygen at low temperature. The *meso* proton was found to resonate at -0.3 ppm in its ^{1}H NMR spectrum suggesting a strong paratropic ring current effect. Even though its molecular structure determined by single crystal X-ray crystallographic analysis confirmed a planar structure, the nature of bonding along the C_{20}-perimeter was inconclusive due to static and possible dynamic disorder.

Attempts were made to synthesize octaethyltetrathia isophlorin[5f]. The acid catalyzed cyclo condensation of 3,4-diethyl-2-(hydroxymethyl) thiophene led to the formation of tetrathia-porphyrinogen **I.8** along with pentathia-porphyrinogen **I.10**. Oxidation of octaethyl tetrathia-porphyrinogen with 2,3-dichloro-5,6-dicyano-1,4-benzoquinone (DDQ) in acetic acid and 70% perchloric acid led to the formation of octaethyltetrathiaporphyrin dication **I.9**. Oxidation of decaethylpentathiaporphyrinogen with antimony pentachloride in dichloromethane yielded 22π aromatic decaethylpentathia porphyrin trication **I.11**[5f].

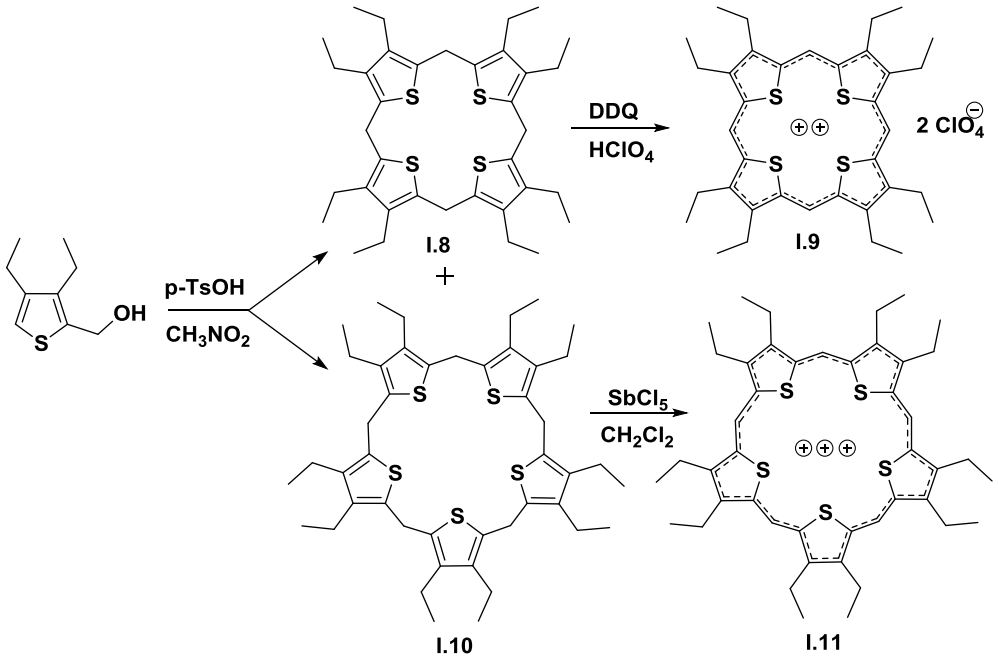

In continuation, the octaethyl derivative of neutral N,N',N",N'"-tetramethylisophlorin **I.13** was synthesized by a two-electron reduction of N,N',N",N'"-tetramethyl-octaethylporphyrin dication **I.11** using sodium in THF [5d]. In contrast to the highly reactive tetraoxaisophlorin, it was found to be moderately stable when exposed to air. The *meso* proton resonated at 4.95 ppm in its ^{1}H NMR spectrum, and down field shifted by 5.3 ppm in comparison to tetraoxaisophlorin. This shift indicated the structure induced loss of paratropism. In the solid state, this molecule was found to adopt a saddle shaped conformation with *syn, anti, syn, anti* arrangements of N-methyl groups.

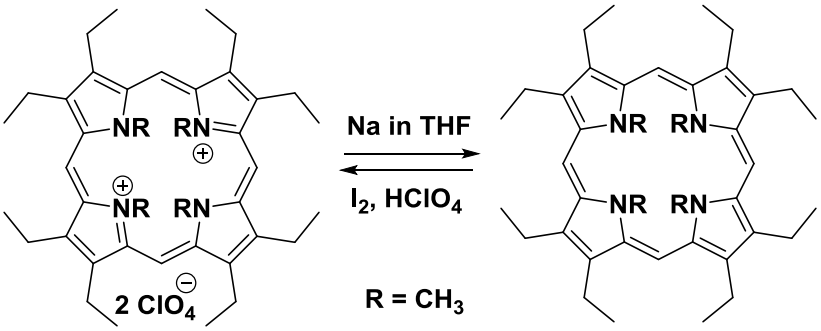

I.12 I.13

However, the synthesis of pyrrole based stable isophlorins remains a synthetic challenge till date. In 2005, Vaid and co-workers synthesized silicon (IV) isophlorin **I.14** complex [Si(TPP)$(L)_{2;}$ L = THF or pyridine] by the reduction of Si(TPP)Cl_2 with two equivalents of Na/Hg in THF[6]. This compound was found sensitive to ambient conditions. Single crystal X-ray diffraction analysis confirmed a ruffled structure with nearly equal Si-N bond lengths. Even though it can be expected that Si(IV) can be complexed by an isophlorin, this molecule suggested macrocycle's susceptibility to distort upon complexation. More studies are required to explore the ability of isophlorin to ligate metal ions and metalloids.

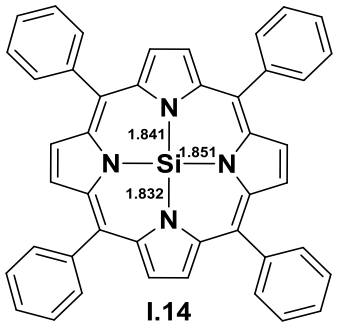

I.14

In 2007 Chen and co-workers established a strategy to synthesize relatively stable tetra pyrrole isophlorin by substituting four β-hydrogens with electron withdrawing trifluoromethyl substituents[7]. The final step in the synthesis was the reduction of a Cu(II)β-tetrakis(trifluoromethyl)-meso-tetraphenyl porphyrin **I.15** with activated zinc powder in DMSO solution. This procedure highlighted a harder reduction of an aromatic 18π porphyrin to anti-aromatic 20π isophlorin. Although it is a 20π conjugated system, it did not display significant paratropic ring currents in its ^{1}H NMR spectrum. The non-planar, saddle conformation of this isophlorin was confirmed by single crystal X-ray diffraction analysis.

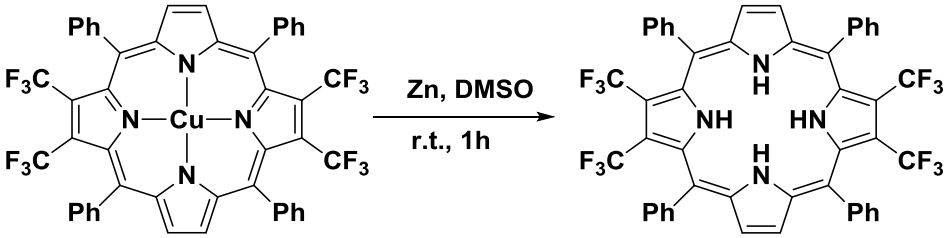

I.15 I.16

P. Brothers & co-workers have synthesized a diboron complex of porphyrin leading to a macrocyclic product at the cross road of aromatic and antiaromatic behaviour [8].

In 2008 Reddy and Anand reported the synthesis of stable tetraoxa and dioxa dithia 20π isophlorins, **I.18** and **I.17,** by substituting strong electron withdrawing pentafluoro groups on the *meso* carbons[9]. Strong paratropic ring current effect was observed in their respective ^{1}H NMR spectrum. Single crystal X-ray crystallography analysis conformed planar structures for these core modified isophlorins.

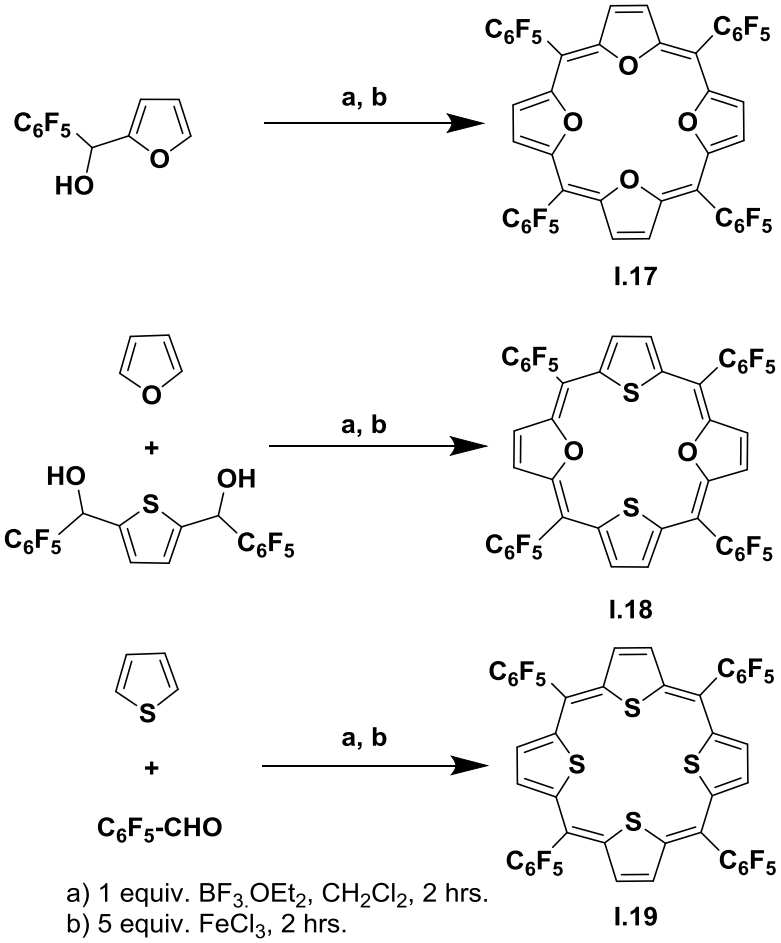

It was observed that these molecules were highly stable, in spite of being antiaromatic in nature. These molecules represent the first examples of stable 4nπ system that resist oxidation

to 18π aromatic dications even with strong oxidizing agents such as perchloric acid. A similar synthetic protocol was employed to synthesize tetrathia isophlorin **I.19** by acid catalyzed cyclo condensation of 2-(1-hydroxy-1-pentafluorophenylmethyl) thiophene. In contrast to tetraoxa isophlorin, its ^{1}H NMR spectrum did not show significant paratropic ring current effects which was later attributed to its non planar structure as determined from its single crystal X-ray diffraction analysis[10].

In the same year Imahori and co-workers reported 20π isophlorin-metal complexes, **I.21**, by redox-coupled complexation of P,S,N_2-hybrid porphyrin **I.20** with group-10 metals [11]. No significant ring currents were observed in their respective ^{1}H NMR spectra. The single crystal X-ray diffraction analysis revealed the non-planar conformation in which the phosphorus and sulfur atoms were displaced by 0.95 and 0.93 Å, respectively, from the mean π plane composed of the peripheral 20 carbon atoms due to the coordination to Pd metal centre, by square planar geometry.

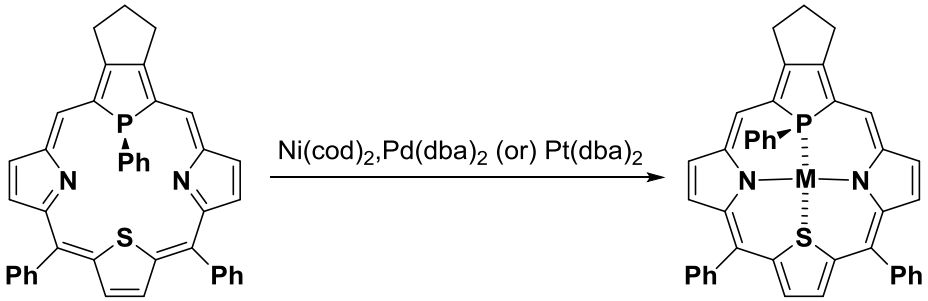

1.20 **1.21**

Apart from these 20π isophlorins, a series of 30π expanded isophlorins with varying number of heterocyclic units such as furan/thiophene/selenophene were synthesized and characterized by Reddy and Anand in 2009[12]. These molecules displayed diverse structural features based on the number of ring inversion and the topology of the macrocycles. The diatropic ring current effect observed in their respective ^{1}H NMR spectrum was suggestive of their aromatic behavior. The molecular structure of cyclo-hexa thiophene [1.1.1.1.1.1] **I.22** was found to adopt a rectangular shape with two diagonally inverted thiophene rings. While, the NMR spectrum of cyclo-hexa furan [1.1.1.1.1.1] **I.23** suggested ring inversion of alternate furan rings[12].

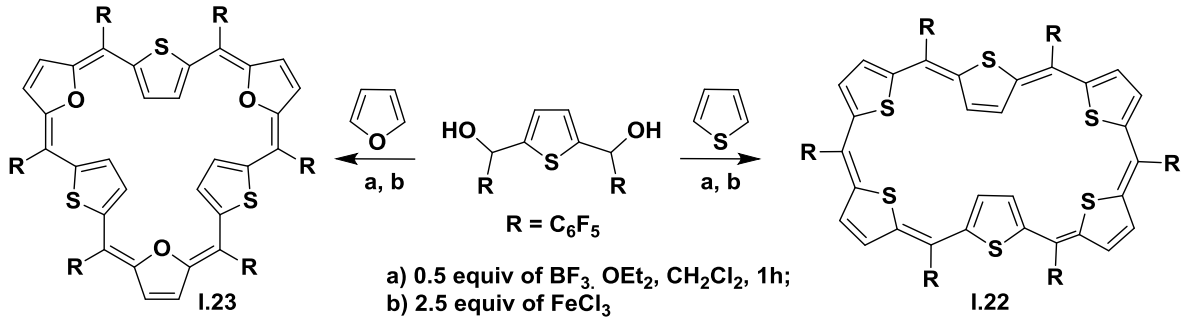

In a comparison to similar macrocycles derived from cyclic polythiophenes, it could be noted that electronic properties indicated lack of effective π conjugation in macrocyclic oligothiophenes[13]. Polythiophenes and their corresponding α-conjugated oligothiophenes have attracted considerable attention because of their potential in organic electronics based applications[14]. They exhibit unique optical and electrochemical properties. A variety of macrocyclic oligothiophenes and their π-extended derivatives have been reported[15]. Till date direct coupling between alpha-alpha carbons between adjacent thiophene units and also by connecting thiophene sub-units through either acetylene or ethylene bridges, appears to be an attractive strategy to synthesize macrocyclic oligothiophenes[16].

α-Conjugated Macrocyclic Oligothiophenes:

A series of α-conjugated cyclothiophenes bearing twelve, fourteen and sixteen thiophene units have been reported by Bäuerle and coworkers. In the first step of macrocyclization, the terminally bis-ethynylated oligothiophenes are subjected to reaction under modified Eglington-Glaser conditions this was followed by cyclization of acetylene bridges into thiophene ring, by treating with sodium sulfide to give the fully π-conjugated cyclo(n)thiophenes. Even though the reaction was useful to synthesize size specific macrocycles, it has been hampered by moderate to low yields[16].

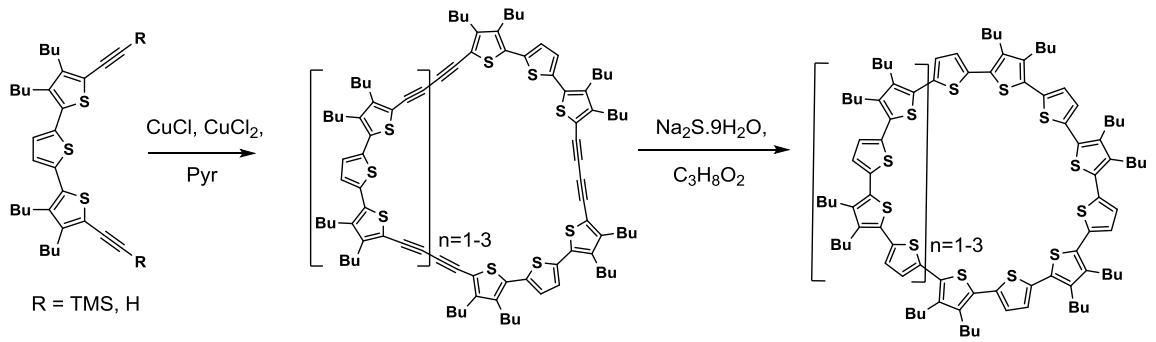

I.24 -I.26

All the macrocycles **I.24-I.26** could be considered as 4nπ [48]-, [64]- and [72] anti-aromatics but no obvious ring current shifts were observed[17] in their ^{1}H NMR spectrum therefore they are considered as benzeniod in character rather than annulenoids. To improve the yields of molecule specific synthesis, an effective protocol was developed by Bäuerle and co-workers in which bis-ethynylated building blocks and transition metal precursor complexes self-assemble to form a stable metalla-macrocycle. The transition metal units were expelled with simultaneous C-C bond formation through reductive elimination leading to the formation of targeted conjugated macrocycles[13b, 18].

Macrocyclic Oligothiophenes with ethylene bridges: Earlier to these reports, a heterocyclic derivative of [18] annulene with three sulfur bridges was obtained in a low-yielding multi-step synthesis[19]. Efficient synthesis of this compound was achieved by Cava and co-workers by employing McMurry coupling of 2,5-thiophenedicarboxaldehyde[19-20]. In spite of being a Hückel type (4n+2)π system, no significant diatropic ring current effect could be detected in its ^{1}H NMR spectrum. The protons were found to resonate as independent thiophene and vinylene units rather than as a conjugated annulene. Single crystal X-ray diffraction analysis confirmed its non-planar structure with all the three thiophene units being deviated totally out of the macrocyclic plane. Along with this 18π macrocycle **I.27**, a higher congener tetrasulfide (24π) **I.28** was also isolated which was devoid of ring current effects expected for antiaromatic macrocycles.

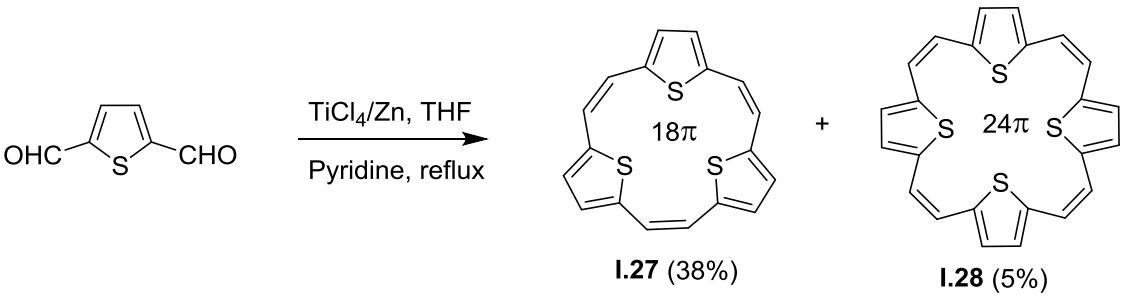

In a similar procedure, McMurry coupling of 2,2'-bithiophene-5,5'dicarboxaldehyde under high dilution condition lead to the formation of a (4n)π tetrathia[20]annulene [2,0,2,0] **I.29**, and a (4*n*+2)π hexathia[30]annulene (2,0,2,0,2,0) **I.30** annulenes[20a]. Even though both these annulenes were found to be fairly stable, no ring current effects were observed in their respective ^{1}H NMR spectra. The non-planarity of both these macrocycles was confirmed from single crystal X-ray analysis.

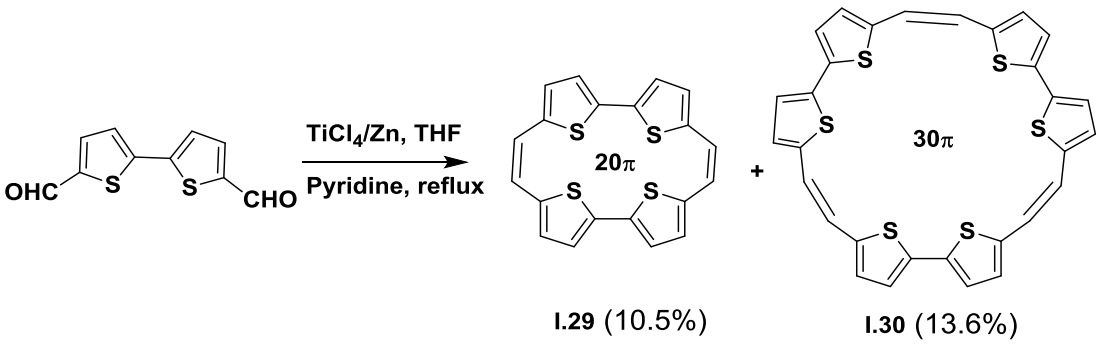

I.29 (10.5%) **I.30** (13.6%)

The hexathia homoporphycene **I.31** was isolated as the only higher homologue of tetrathiaporphycene in the McMurry coupling of 5,5'-terthiophenedicarboxaldehyde[21]. Even in this macrocycle, no ring current effects could be observed in its ^{1}H NMR spectrum in spite being a 28π (4nπ) macrocycle, suggesting lack of effective delocalization of π electrons.

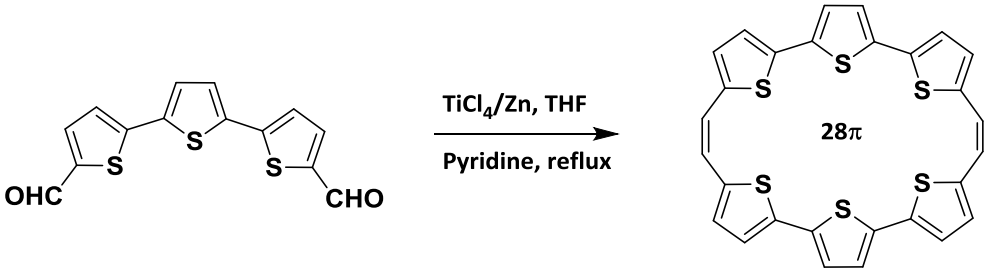

I.31 (64%)

Tetraepoxy Annulenes:

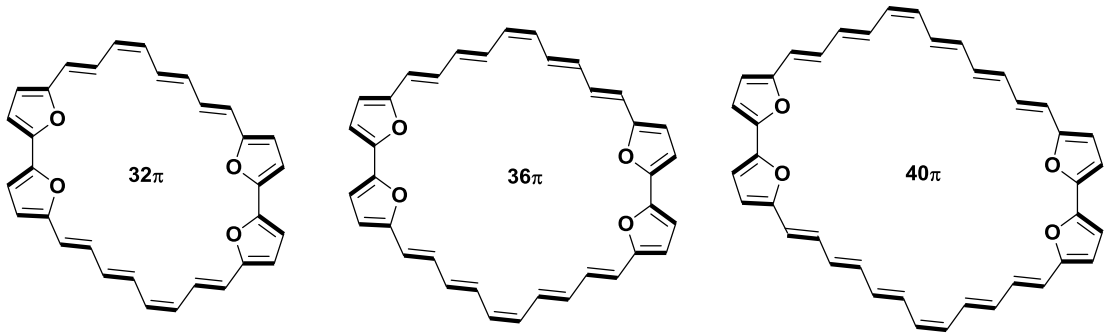

I.32 **I.33** **I.34**

Analogous to the macrocyclic thiophene, a series of tetra furan based tetraepoxy Annulenes were reported by Märkl[22]. In fact they were identified as annulenes and the nomenclature was based on the number of π electrons in the cyclic structure as; tetraepoxy[32]annulene(8.0.8.0),[23] **I.32**, tetraepoxy[36]annulene(10.0.10.0)[24], **I.33**, and tetraepoxy[40]annulene (12.0.12.0) **I.34**. They have varying number of ethylene linkages generated by a double Wittig type cyclization of appropriately designed precursors. All these

three molecules formally represent 4nπ systems. The ^{1}H NMR analyses confirmed a steady decrease in paratropic ring currents from **I.32 -I.34**. An increase in size of these macrocycles correspondingly increased the conformational flexibility leading to deviation from planar structures. However poor solubility hindered the ^{1}H NMR analysis of **I.34.** Tetraepoxy[32]annulene (6.2.6.2) **I.35** and Tetraepoxy[32]annulene (4.4.4.4)[25] **I.36** represent structural isomers of **I.32**, which were synthesized by varying the number of ethylene bridges between the furan sub-units[26]. Even though **I.36** displayed paratropic ring current effects in its ^{1}H NMR spectrum, it was also identified that it can exist as three different conformational isomers in solution, which hindered unambiguous characterization of its structure in the solution state[27].

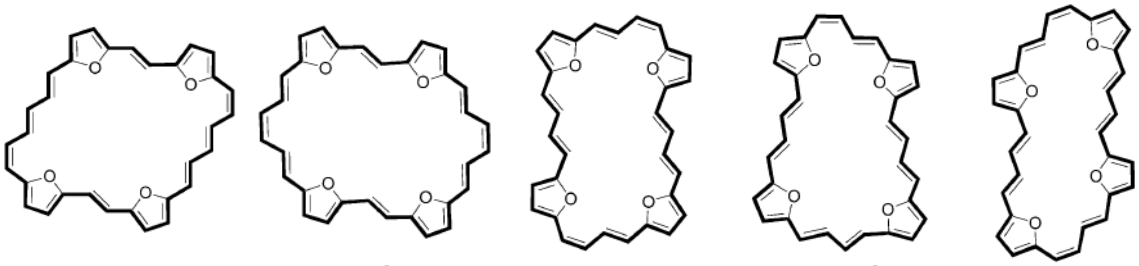

I.35a **I.35b** **I.36a** **I.36b** **I.36c**

Oxidation of **I.32 -I.36** with 2,3-dichloro-5,6-dicyano-1,4-benzoquinone (DDQ) yielded the corresponding dicationic species which displayed diatropic ring current effects in their respective ^{1}H NMR spectrum, indicating their aromatic nature. The change in the chemical shift value (Δδ) between inner and outer protons of the ethylene carbons was found to be 25 ppm. Further, the observation of a sharp soret type band accompanied by two Q-type bands in the electronic absorption spectrum confirmed the aromatic behaviour of these of dicationic species.

In another report, Iyoda and co-workers have reported the synthesis of macrocycles composed of thienylene, ethenylene and ethynylene units by employing McMurry coupling as the key reaction[28]. Subjecting a penta oligo- (thienylene-ethynylene) dialdehyde **I.37**, synthesized from thiophene in twelve steps, to McMurry coupling resulted in macrocycles with ten, fifteen, twenty, twenty-five and thirty thiophene units[28b]. The major product, a cyclodimer with ten thiophene sub units **I.38**, was isolated in 30% yields which consisted of the three possible isomers *E/E*, *E/Z* and *Z/Z* in the ratio 18:1:3. These macrocyclic oligothiophenes displayed a tendency to attain saturation with respect to the energy of

absorption, in spite of increase in the number of heterocyclic units, which suggested lack of effective conjugation between the adjacent thiophene units[29].

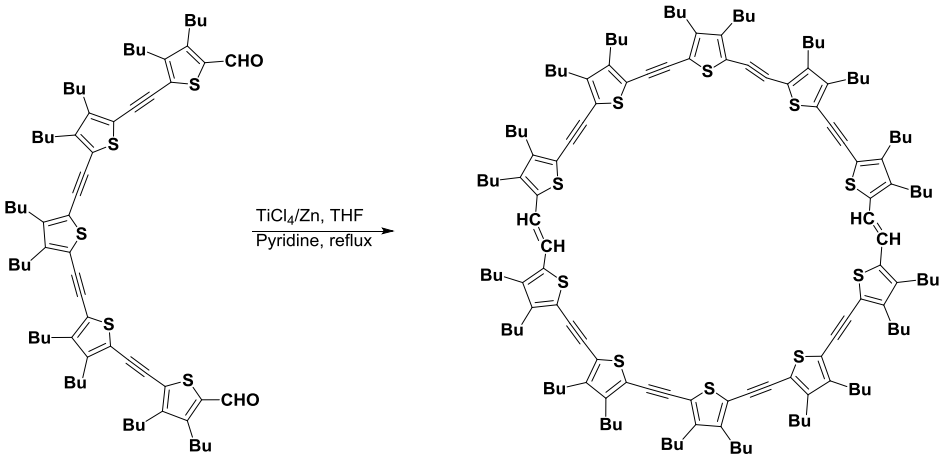

I.37 I.38

Apart from the above mentioned macrocycles, porphyrinoids have also been explored for the realization of anti-aromatic macrocycles[30]. They have also been in the focus of topology based Hückel (planar) and Möbius (twisted) aromaticity. In this thesis, the role of thiophene and similar heterocycles such as furan or selenophene will be highlighted as sub-units to synthesize planar & stable anti-aromatic molecules. The thiophene based macrocycles that lack any ring current effects can be explained based on the ineffective linkers that do not perturb the π delocalization of a heterocyclic unit[31]. However, the molecules synthesized by Vogel and co-workers clearly suggest that an odd number of carbon bridges between the adjacent thiophene units can induce global π delocalization for a macrocyclic product[32]. This has been confirmed from the synthesis and the spectroscopic evidence for tetra-thia/oxa/selena porphyrin dications and also from the stable 20π isophlorin derivatives of furan and thiophene.

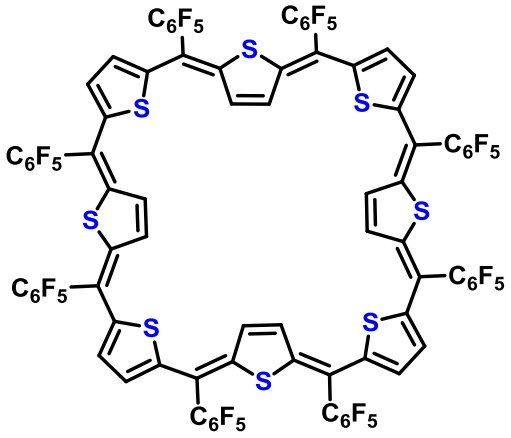

The expansion of an isophlorin conjugation can be explored to realize large anti-aromatic macrocycles[33]. The absence of nitrogen based pyrroles can prevent the imine-amine inter-conversion thereby stabilizing a π network that supports an annulene like macrocycle. A 40π octa-furan expanded isophlorin **I.39** has been characterized in solution and solid state as the largest anti-aromatic macrocycle till date[33]. The strategy employed in the synthesis of stable 20π isophlorin offers a novel means to realize a variety of 4nπ systems and study their properties. In pyrrole based macrocycles, proton-coupled electron transfer reaction was recently reported by Sessler and co-workers[34]. The 24π planar rosarin **I.40** can be reduced to an aromatic 26π system **I.42** through a unstable 25π cationic radical **I.41**, which in turn can be oxidized back to the parent antiaromatic macrocycle.

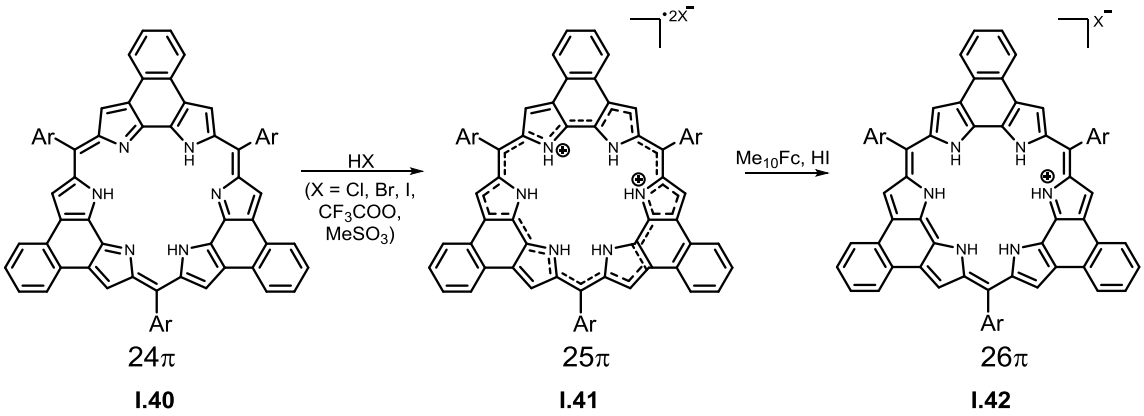

Similary Osuka and co-workers have described the inter-conversion of hexaphyrins between aromatic (26π) **I.43** and antiaromatic (28π) **I.44** states by employing suitable redox agents. In both these cases the π-conjugation path way is altered due to the addtion of the protons upon reducing the oxidized macrocycle. In such porphyrinoids, the pyrrolic nitrogen's ability to oscillate between the imine and amine forms is crucial to regulate the conjugated pathway for facilitating such an alteration[35].

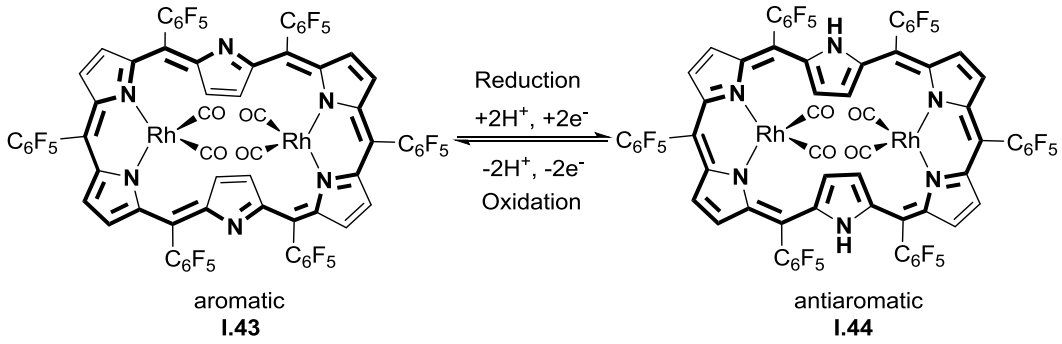

Apart from these proton coupled redox reactions, the flexible nature of expanded porphyrinoids enable them to switch topology (Hückel and Möbius) between aromatic and

antiaromatic states with the same number of protons and π-electrons. Latos-Grażyński and co-workers reported solvent and temperature-dependent conformational changes between Hückel antiaromatic and Mobius aromatic conformations of *p*-benzi[28]hexaphyrin (1.1.1.1.1.1) **I.45 (left)** in solution state. The two conformers differ in the relative orientation of the phenylene rings. In the Hückel structure **I.45 (right)**, the rings are cofacial, whereas they are oriented edge-to-face in the Möbius form[36].

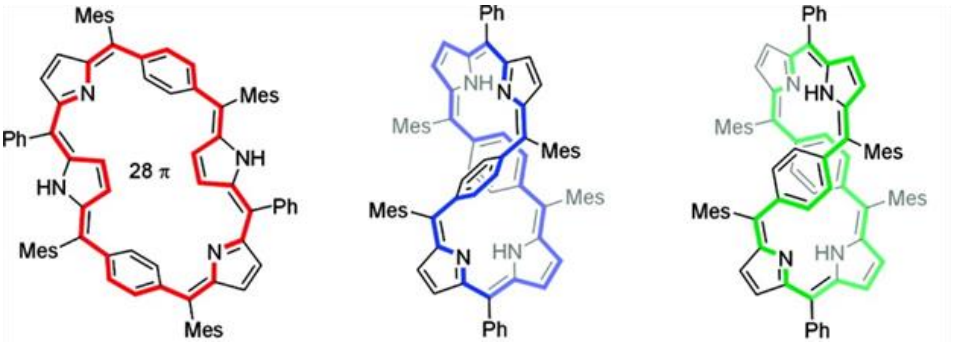

I.45

Similar temperature dependent conformational changes observed for [28]hexaphyrins (1.1.1.1.1.1) with different meso substitutions was reported by Osuka and co-workers. [28]hexaphyrins(1.1.1.1.1.1) exists in equilibrium among several rapidly interconverting Möbius conformations, in solution at 25°C. Upon decreasing temperature to −100 °C in THF, these rapid interconversions among Möbius conformations are frozen, allowing the detection of a single [28]hexaphyrin(1.1.1.1.1.1) species having a Möbius conformation. But in solid state it adopts either planar **I.46** or Möbius-twisted conformations **I.47**, depending upon the *meso*-aryl substituents and crystallization conditions[37].

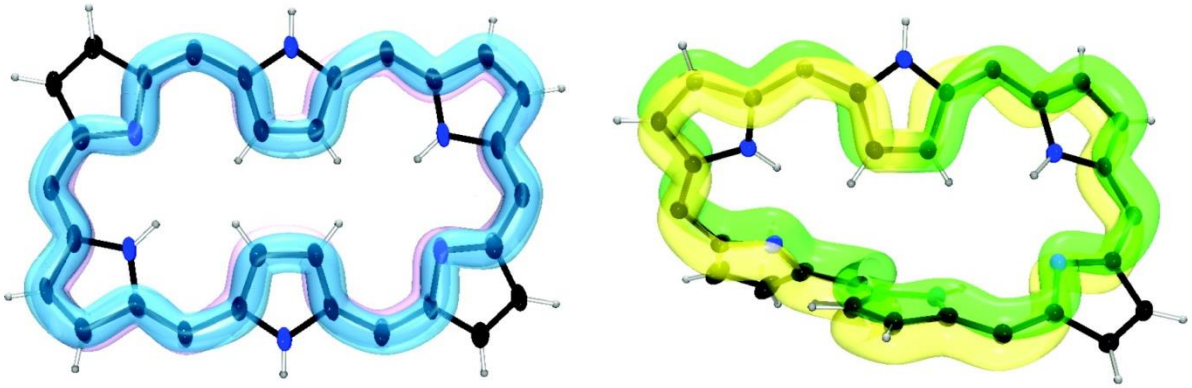

I.46 **I.47**

In summary, π conjugation in macrocyclic structures can vary depending on the nature of the sub-units and the effective overlap of π orbitals between adjacent heterocyclic units. It can be inferred that, odd number of sp^2 carbon atoms connecting the heterocyclic units can induce effective π conjugation as observed in the porphyrinoids. Lack of sp^2 carbon bridges or even number of such bridges in between the heterocyclic units as observed in macrocyclic oligothiophenes do not encourage annulenoid forms of π conjugated macrocycles. A combination of odd and even number of sp^2 hybridized carbon bridges can be explored to synthesize a variety of antiaromatic macrocycles. Alternatively, the effect of non-pyrrolic heterocyclic units such as thiophene/furan/selenophene can be crucial to study the effect of protonation and the corresponding electronic changes in such macrocyclic systems. In this thesis, the synthesis, characterization and electronic properties of macrocycles derived from thiophene sub-units will be described in detail. Particularly, emphasis is devoted to relatively simple synthetic methodology and study of redox properties in such macrocyclic systems.

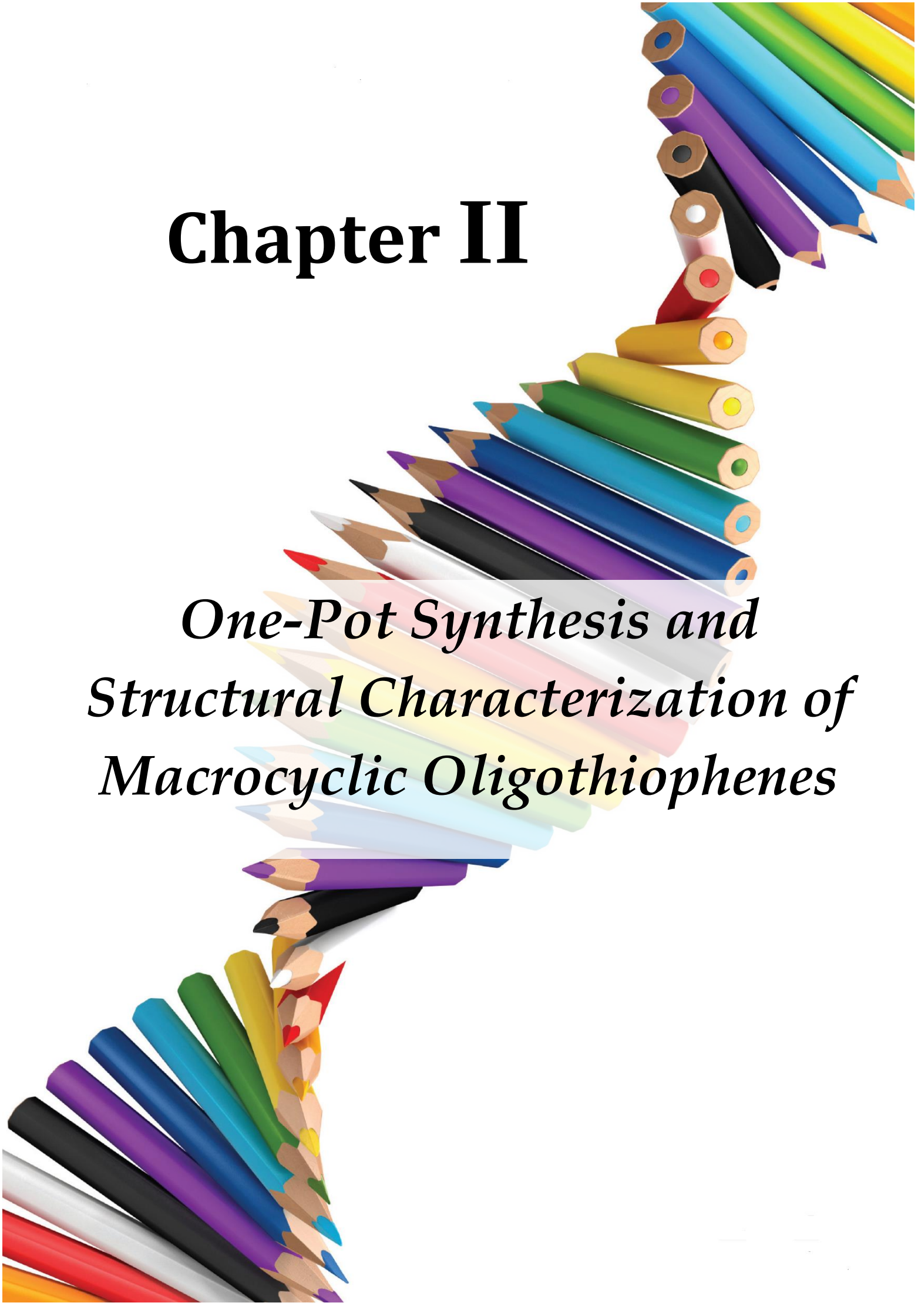

Chapter II

One-Pot Synthesis and Structural Characterization of Macrocyclic Oligothiophenes

II.1. Introduction:

Porphyrins and expanded porphyrins represent fine examples to study π-conjugation. These molecules find important applications in variety of fields such as molecular recognition, medicine and organic electronics[38]. Porphyrins with different substituents on *meso* and β positions can be synthesized in a one-pot synthesis by employing Lindsey conditions[39]. In this modified Rothemund reaction[40], pyrrole undergoes acid catalyzed cyclo-condensation with an aldehyde followed by oxidation with DDQ or Chloranil. This method has found applicability for synthesizing a range of *meso*-substituted porphyrins **(Scheme-II.1)** and its core-modified derivatives.

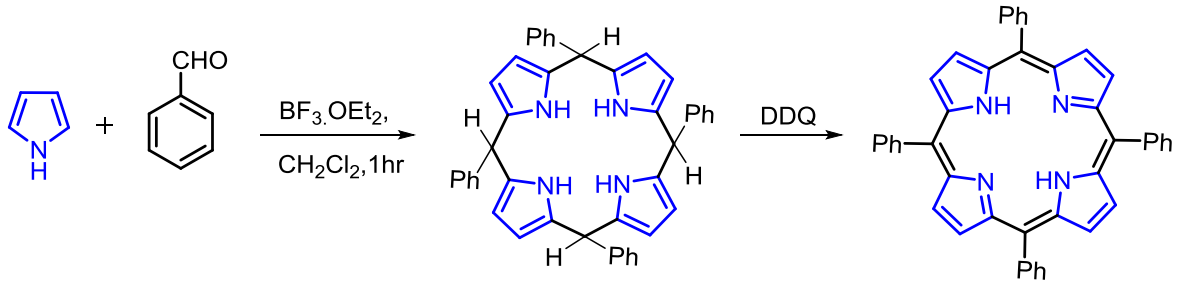

Scheme-II.1: Acid catalyzed condensation of pyrrole and benzaldehyde

It was observed that pyrrole reacts with electron deficient pentafluoro benzaldehyde to yield hexa pyrrolic expanded porphyrins[41]. Osuka and co-workers are employed similar reaction conditions to synthesize a series of expanded porphyrins having five to twelve pyrroles with equal number of *meso* bridges **(Scheme-II.2)**. The extension of conjugation in all these macrocycles was reflected by the significantly red-shifted absorbance and the marked change in the color of their respective solutions[42].

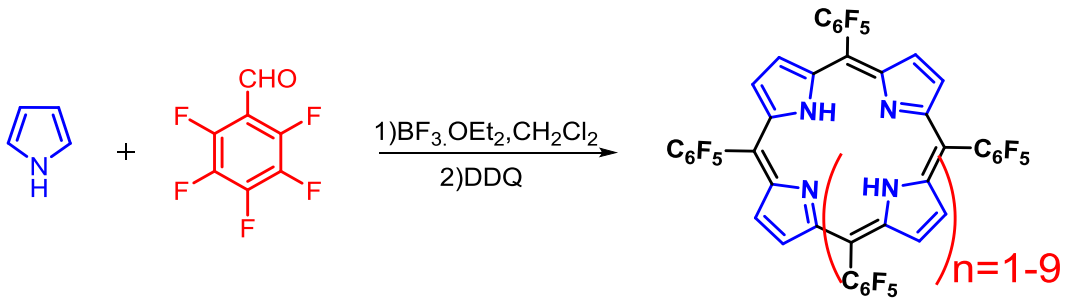

Scheme-II.2: One pot synthesis of expanded porphyrins.

II.2: Synthesis:

Anticipating analogous macrocycles under identical reaction conditions, catalytic amount of boron trifluoride etherate was added to an equimolar ratio of thiophene and pentafluoro benzaldehyde in dichloromethane **(Scheme-II.3)**. After stirring this solution under dark for an hour, the reaction mixture was exposed to air and Ferric chloride ($FeCl_3$) was added with stirring continued for additional one hour. The MALDI-TOF mass spectrum of this reaction mixture **(Figure-II.1)** revealed macrocycles containing four to ten thiophene sub-units.

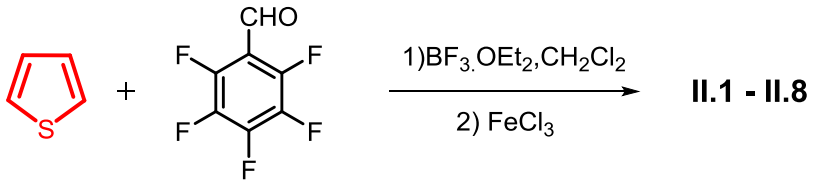

Scheme-II.3: One pot synthesis of expanded isophlorins.

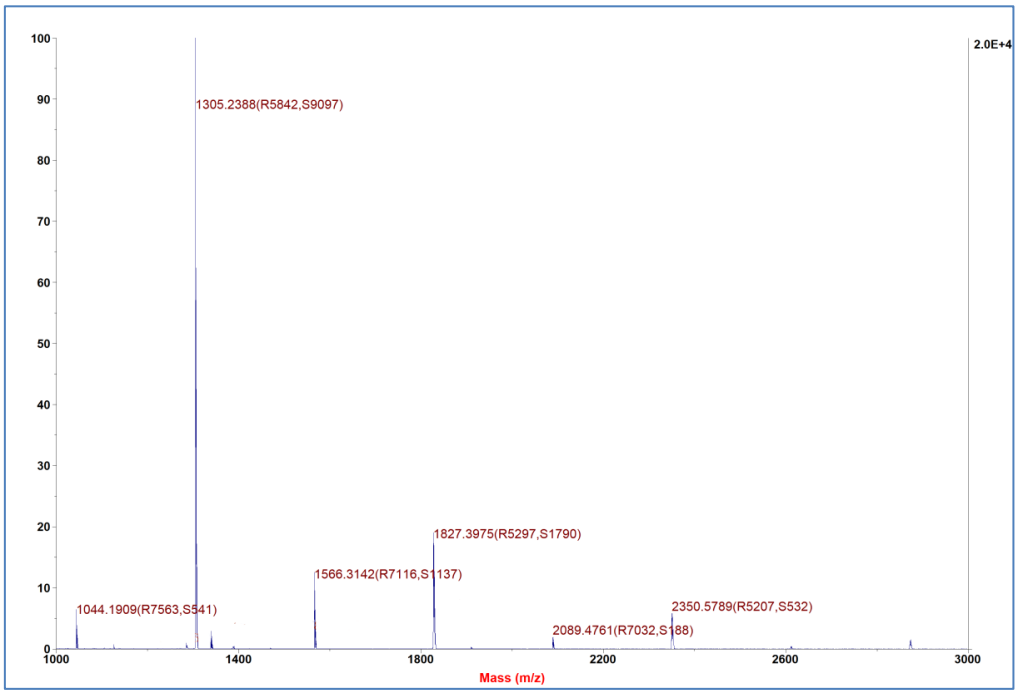

Figure-II.1: MALDI-TOF mass spectrum of reaction mixture (scheme II.3).

II.3: Isolation and Characterization of pentathiophene radical (II.2):

After routine workup, column chromatographic separation of the reaction mixture led to isolation of individual macrocycles. The 20π tetrathiaisophlorin (**II.1**) and 30π hexathia hexaphyrin (**II.3**) were isolated as similar to earlier reports. Macrocycle with five, seven and

nine thiophene sub units were expected to be semi-conjugated due to odd number of carbon atoms in conjugated pathway. A green colored fraction that eluted with CH_2Cl_2 / Petroleum ether (1:10) displayed a sharp and an intense absorption at 470 nm (ε = 195,000). It corresponded to an *m*/*z* value of 1304.8992 in its high-resolution mass spectra **(Figure-II.2)**. This was found to be one mass unit less than the expected *m*/*z* value of a semi-conjugated macrocycle **(Scheme-II.4) II.2a** ($C_{55}H_{11}F_{25}S_5$: Calcd. 1305.9065) suggesting the loss of a hydrogen atom in the macrocycle ($C_{55}H_{10}F_{25}S_5$: Calcd. 1304.8987).

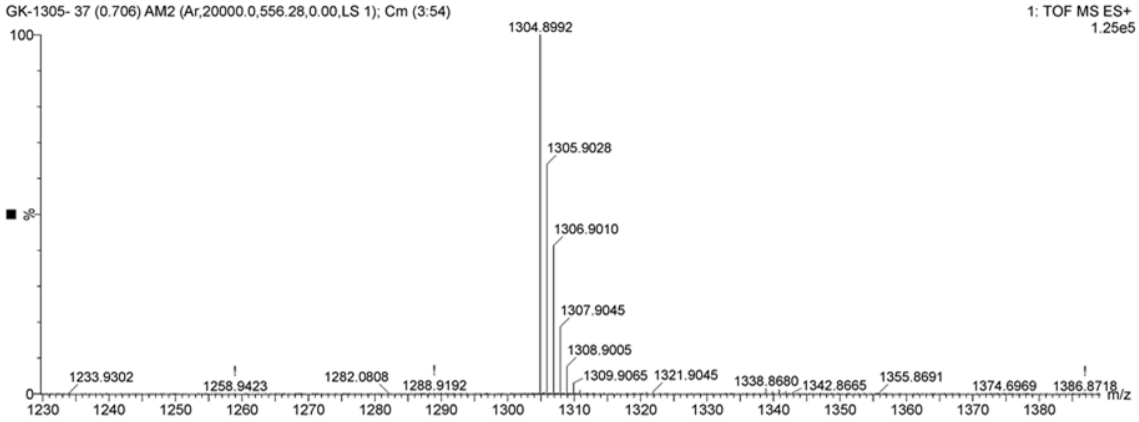

Figure-II.2: High-resolution mass spectra of **II.2**.

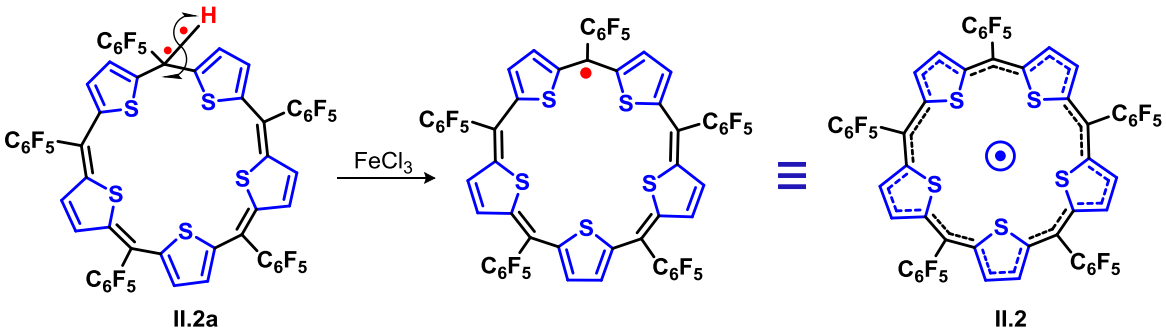

Scheme-II.4: Plausible formation of radical from **II.2a.**

Its ^{1}H NMR spectrum did not display any signal corresponding to the macrocycle, either at room temperature or at low temperature. Electron Paramagnetic Resonance (EPR) spectrum recorded at room temperature and at 77 K **(Figure-II.3)** displayed a singlet with g = 2.0026, characteristic of organic radical due to an unpaired electron (S=1/2). It was found to be stable even upon exposure to ambient atmosphere for several months. Its thermogravimetric analysis (TGA) suggested high thermal stability up to 300ºC.

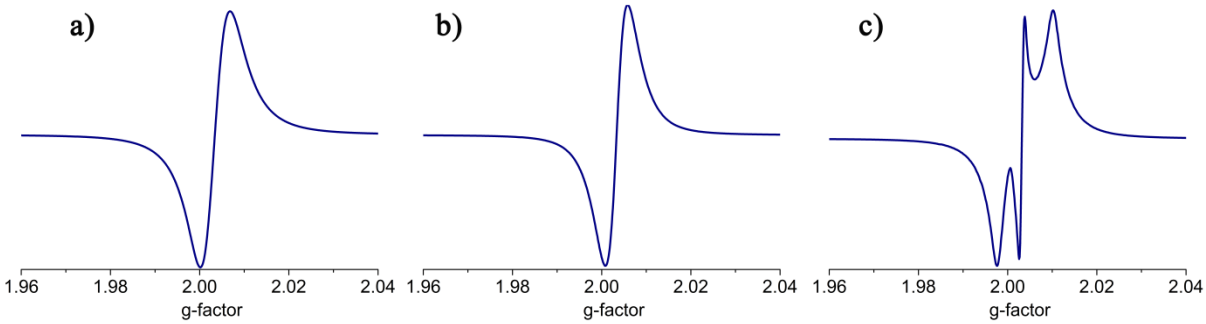

Figure-II.3: EPR spectra of **II.2** **(a)** at 298 K in the solid state, **(b)** at 77 K in Chloroform solution and **(c)** at 77 K in the solid state.

To confirm the molecular structure of **II.2**, good quality single crystals were grown by using solvent diffusion method. It crystallized in monoclinic system with P21/c space group and exhibited an unprecedented planar conformation with respect to the five-thiophenes. Sulfur atoms of all the five thiophenes pointed towards the center of the macrocycle. This structure represents the first example belonging to planar *meso* phenyl pentaphyrin class of macrocycles that lack inversion of the heterocyclic units **(Figure-II.4)**. It also emphasized the effective delocalization of the π-electrons for the additional stability of the radical. Similar macrocycles with pentapyrrole derivatives undergo ring inversion followed by fusion, leading to non-planar conformation[43]. The near orthogonal orientation of the pentafluorophenyl rings with respect to the plane of the macrocycle in **II.2** facilitates the steric hindrance induced prevention of π stacking, to diminish the possible intermolecular interaction through the unpaired electrons. A formal count of 25π electrons along its conjugated pathway classified it as neither as aromatic [(4n+2)π] nor as antiaromatic [(4n)π] in nature

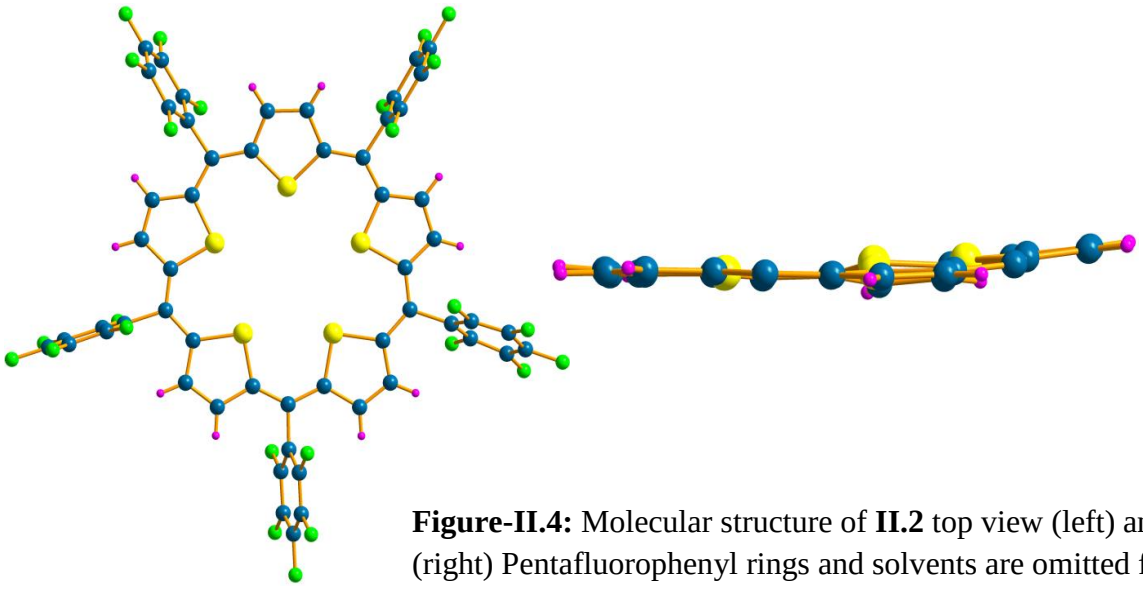

Figure-II.4: Molecular structure of **II.2** top view (left) and side view (right) Pentafluorophenyl rings and solvents are omitted for clarity.

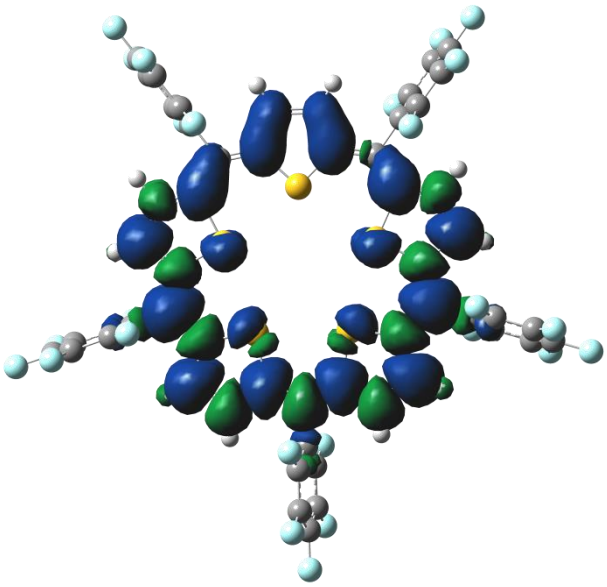

Figure-II.5: Spin density distribution of **II.2** calculated at UB3LYP/6-31G (d,p).

Unrestricted DFT calculations (UB3LYP/6-31G(d,p)) were performed in an effort to understand the unusual high stability of this open-shell species, **II.2**. The calculations implied the unpaired electron density to be encompassed over the cyclic framework of **II.2 (Figure-II.5)**

II.4: Isolation and Characterization of Hepta thiophene radical (II.4):

Apart from the green colored fraction **II.2**, a brown colored fraction was also isolated from column chromatographic purification. This fraction exhibited an *m*/*z* value of 1827.99 in its MALDI-TOF mass spectrum **(Figure-II.6)** suggesting the formation of a heptathiophene macrocycle (**II.4**). The color of the solution and the broad absorption with λ_{max} at 491 nm suggested the delocalized nature of π electrons in this macrocycle. Similar to **II.4,** no signals were observed in its ^{1}H NMR spectrum. EPR spectrum recorded at room temperature displayed a singlet with g = 2.001, characteristic of a radical due to an unpaired electron (S=1/2). Through preliminary EPR, absorption spectroscopy and Mass spectrometric analysis the **II.4** macrocycle could be identified as a neutral radical with 35π electrons.

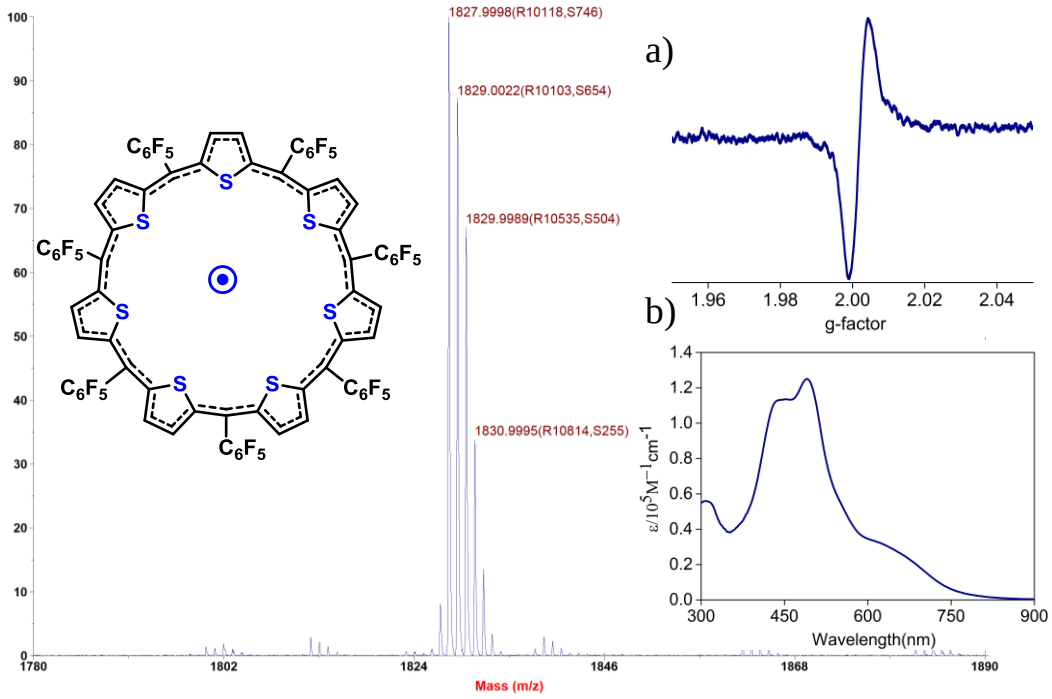

Figure-II.6: MALDI-TOF mass spectrum of **II.4** [Inset a) EPR b) electronic absorption spectrum recorded in CH_2Cl_2].

II.5: Isolation and Characterization of Nona thiophene radical (II.6):

Along with the **II.2** and **II.4**, a second green colored fraction was identified in the column chromatographic separation. It displayed an *m*/*z* value of 2350.09 in its MALDI-TOF mass spectrum suggestive of nonathiophene macrocycle **II.6 (Figure-II.7)**. Similar to **II.4** this compound also displayed a broad absorption with λ_{max} at 488nm **(Figure-II.7)** and no signals were observed in its ^{1}H NMR spectrum. EPR spectrum recorded at room temperature displayed a singlet with g = 2.002, **(Figure-II.7)** characteristic of an organic radical. From preliminary investigations, it could be identified as nonathiophene macrocyclic neutral radical **II.6** with 45π electrons. All efforts to determine the molecular structure of **II.4** and **II.6** could not be successful due to lack of crystals suitable for single crystal X-ray diffraction. However, both **II.4** and **II.6** were found to be stable for long periods of time under ambient conditions.

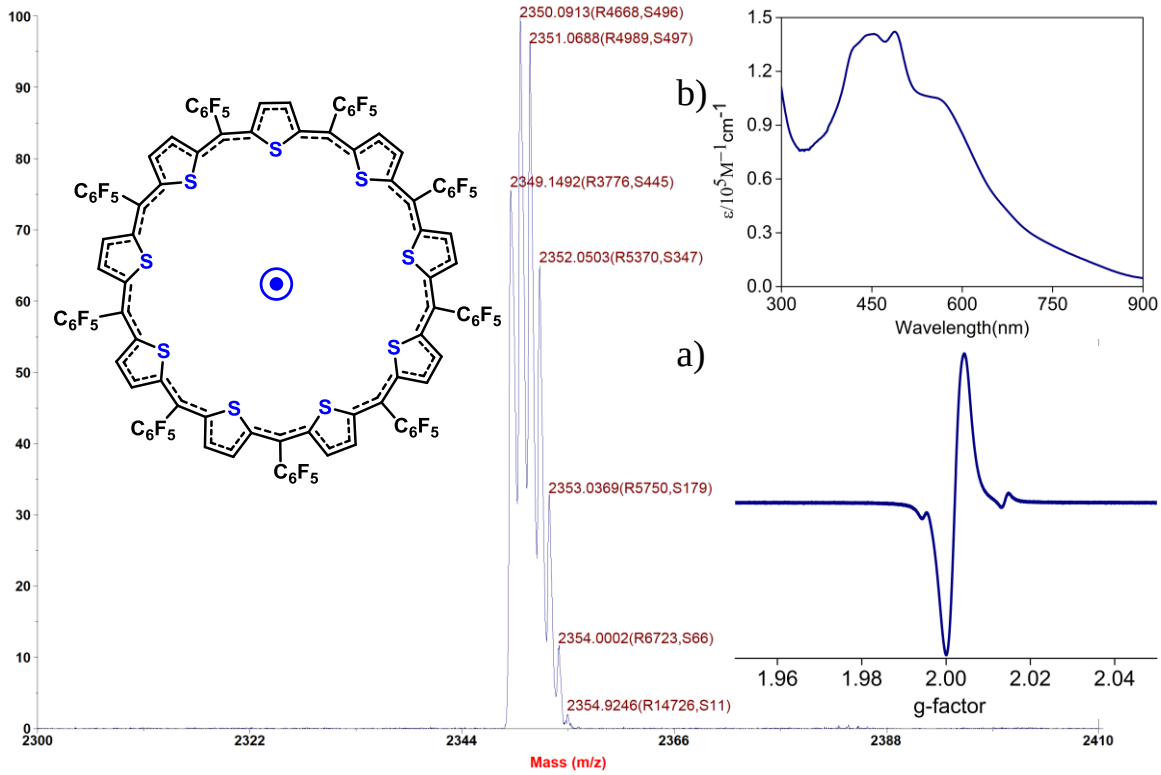

Figure-II.7: MALDI-TOF mass spectrum of **II.6** [Inset a) EPR b) electronic absorption spectrum recorded in CH_2Cl_2].

II.6: Redox properties of (4n+1)π neutral radicals:

All these stable neutral radicals **II.2**, **II.4** and **II.6** were characterized as (4n+1)π systems with 25, 35 and 45π-electrons respectively. This (4n+1)π open-shell configuration is an unusual state between aromatic (4n+2)π and antiaromatic (4n)π electronic circuits. Suitable redox reagents can be employed to reduce this (4n+1)π system into an aromatic mono anion or oxidize into an antiaromatic mono cation state. Preliminary cyclic voltammetric studies for **II.2** to exhibited one reduction wave at -0.05 V and four oxidation waves in the region between 0.6 - 1.5 V **(Figure-II.8)**. A low value of reduction potential suggested the relative ease for formation of aromatic anion when compared to antiaromatic cation.

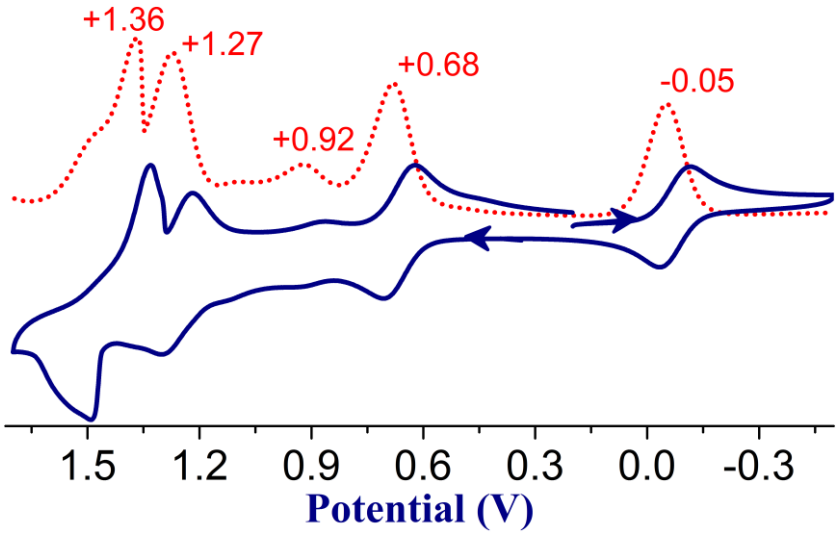

Figure-II.8: Cyclic (blue) and Differential Pulse (red) voltammograms of **II.**2 in dichloromethane containing 0.1 M tetrabutylammonium perchlorate as the Supporting electrolyte recorded at a 50 mV s^{-1} scan rate.

The E^{sum} obtained from the numerical sum of first E^{ox} and E^{red} attributes the amphoteric characteristic of a hydrocarbon[44]. An estimated E^{sum} value of 0.73 V from the first reduction potential (-0.05 V) and oxidation potential (+0.68 V) proved the facile amphoteric nature of this radical. It represents one of the least values compared to previous reports for neutral radicals[45] **II.10-II.12 (Scheme-II.5)**. Inspired by this amphoteric behaviour of **II.2** we attempted the chemical synthesis of the antiaromatic monocation and aromatic monoanion by employing suitable one electron redox reagents.

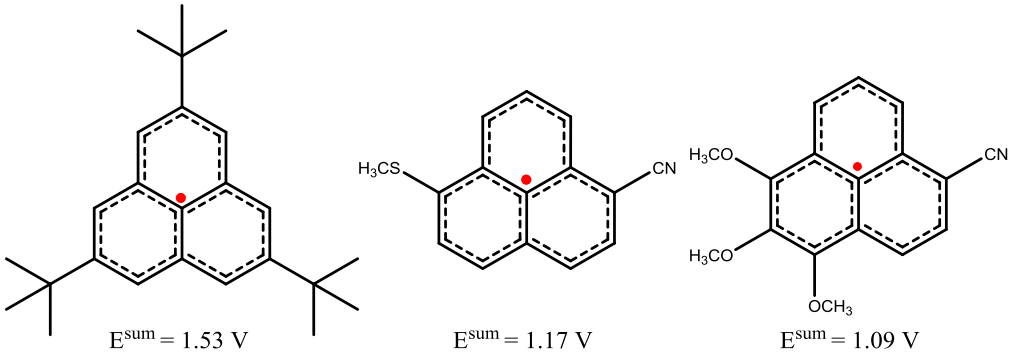

E^{sum} = 1.53 V — **II.10**

E^{sum} = 1.17 V — **II.11**

E^{sum} = 1.09 V — **II.12**

Scheme-II.5: E^{sum} values of some of the persistent radicals.

II.7: One electron oxidation of II.2:

Meerwein's salts such as $[Et_3O]^+[SbCl_6]^-$ acts as an effective one electron-oxidizing agent for π-conjugated systems[46]. Addition of this Meerwein's salt to **II.2** in dichloromethane **(Scheme-II.6)** immediately induced a color change from green to brownish colored solution. This brownish solution displayed a red shifted absorption at 513 nm (150,000) with relatively reduced intensity, followed by characteristic weak and broad absorption **(Figure-II.9)**, in the region between 900-1000 nm, suggesting the antiaromatic character of cationic species.

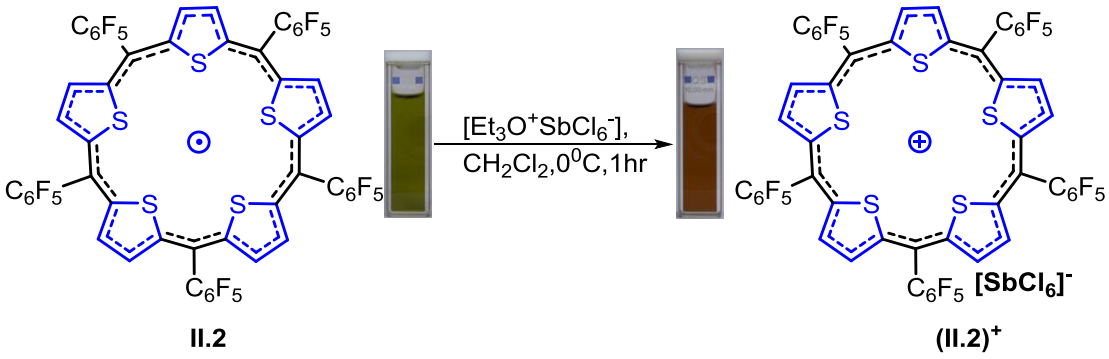

Scheme-II.6: One electron oxidation of **II.2.**

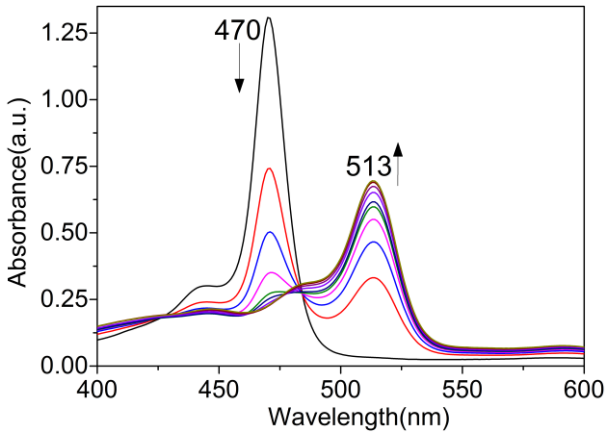

Figure-II.9: Absorption changes observed upon the addition of Meerwein's salt to **II.2** in dichloromethane.

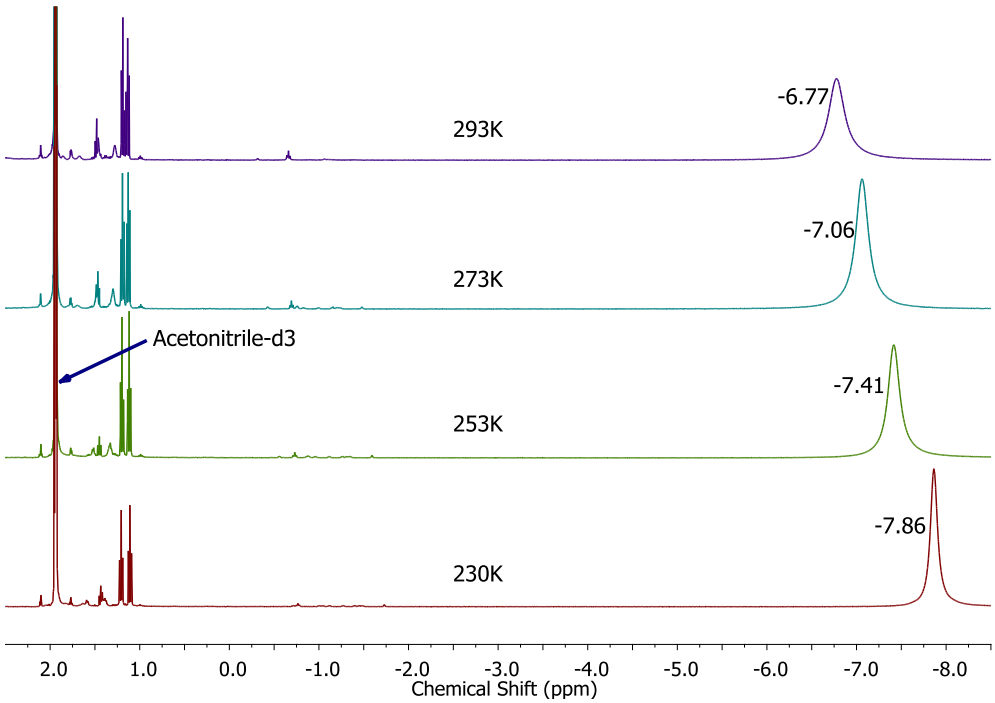

Figure-II.10: Variable temperature ^{1}H NMR spectrum of **II.2**$^{+}$.

Addition of the brownish solution to cooled diethyl ether yielded dark colored crystals. ^{1}H NMR spectrum obtained by dissolving these crystals of (**II.2**)$^{+}$ in CD_3CN displayed a singlet at δ = -6.77 ppm at 293K, while it was further upfield shifted to -7.86 ppm at 230K **(Figure-II.10)**. A singlet also confirmed the high symmetry of the macrocycle due to its planar structure and lack of ring inversions. The remarkable paratropic ring current effect expected of 24π antiaromatic cation confirmed the one-electron oxidation of the radical. Such a strong up field chemical shift is the highest ever to be recorded for any 4nπ macrocycle to date, which further validated a planar confirmation of cation in state. The molecular structure of 24π antiaromatic cation was established by single crystal X-ray diffraction analysis. Good quality single crystals of the (**II.2**)$^{+}$ could be grown from its acetonitrile solution. The antiaromatic cation also exhibited a flat structure, similar to that of **II.2** in the solid state. Hexachloro antimonate was found to be associated with the cationic macrocycle as the counter anion **(Figure-II.11)** to justify the adduct nature of the oxidized macrocycle.

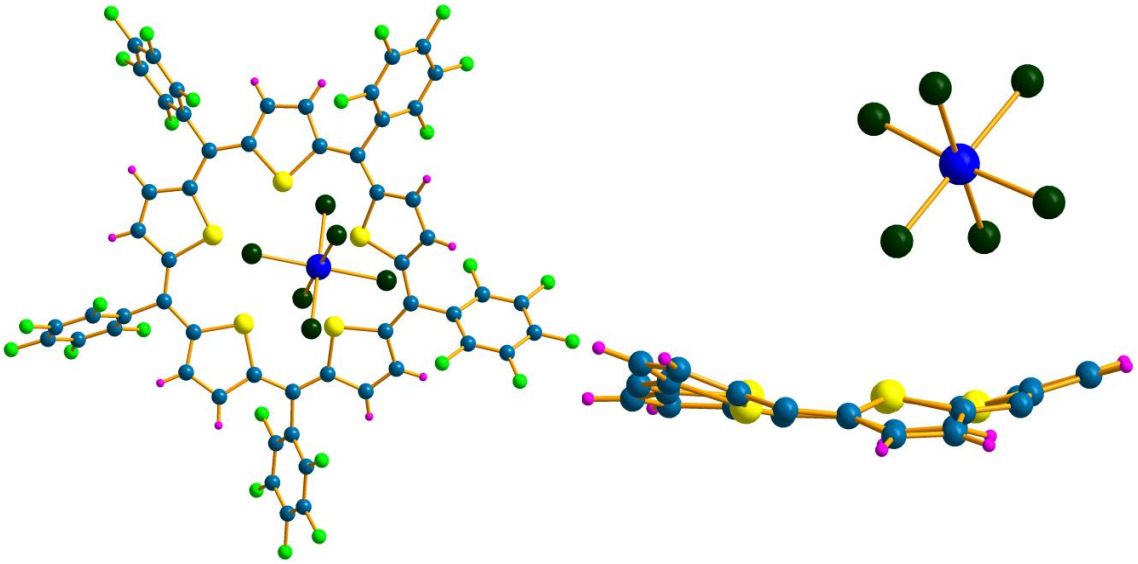

Figure-II.11: Molecular structure of **II.2**$^{+}$top view (left) and side view (right). Phenyl rings are omitted for clarity in the side view.

II.8: One electron reduction of II.2:

II.2 was subjected to one-electron reduction by potassium superoxide (KO_2) in the presence of 18-crown-6 (18C6). Addition of KO_2 to a solution of **II.2** in DMSO **(Scheme-II.6)** induced a quick change in the color of the solution from green to pink. The pink colored solution of (**II.2**)$^{-}$ displayed an intense and a red shifted absorption **(Figure-II.12)** at 542 nm (270,000) with a Q-like band at 730 nm (24,000) signifying the aromatic characteristics of the reduced radical.

Scheme-II.7: One electron reduction of **II.2**.

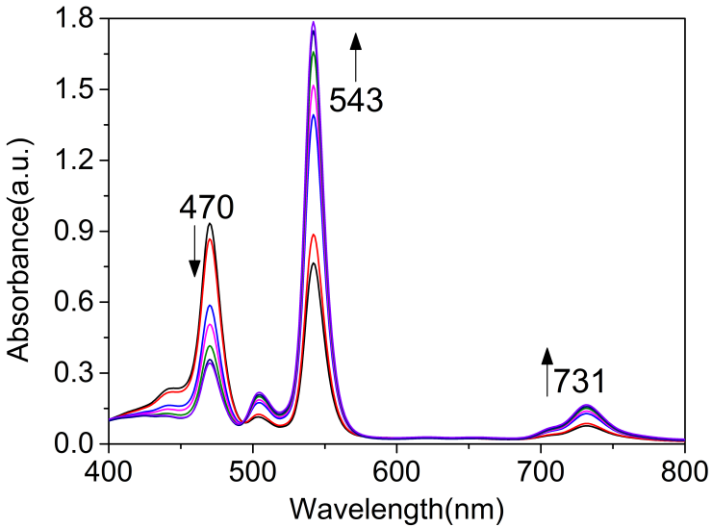

Figure-II.12: Absorption changes observed upon the addition of KO_2 to **II.2**. in DMSO

^{1}H NMR spectrum obtained by mixing **II.2** with KO_2 and 18-crown-6 in deuterated DMSO displayed a singlet at 11.15 ppm **(Figure-II.13)**. Again, the ^{1}H NMR spectrum signified the high symmetry of the macrocycle even upon its reduction to an anion. Such a downfield shift confirmed the diatropic ring current effect expected of a 26π aromatic anion obtained by the one-electron reduction of the radical. The independent chemical transformation of the radical into antiaromatic cation and aromatic anion could be demonstrated by contrasting ring current effects in their respective ^{1}H NMR spectrum.

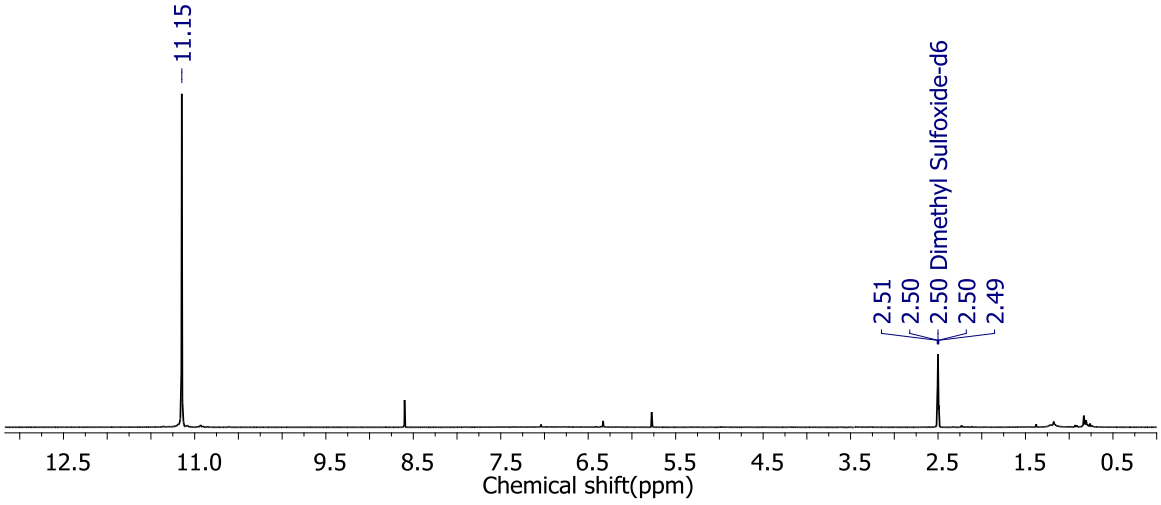

Figure-II.13: ^{1}H NMR spectrum of **II.2**$^-$.

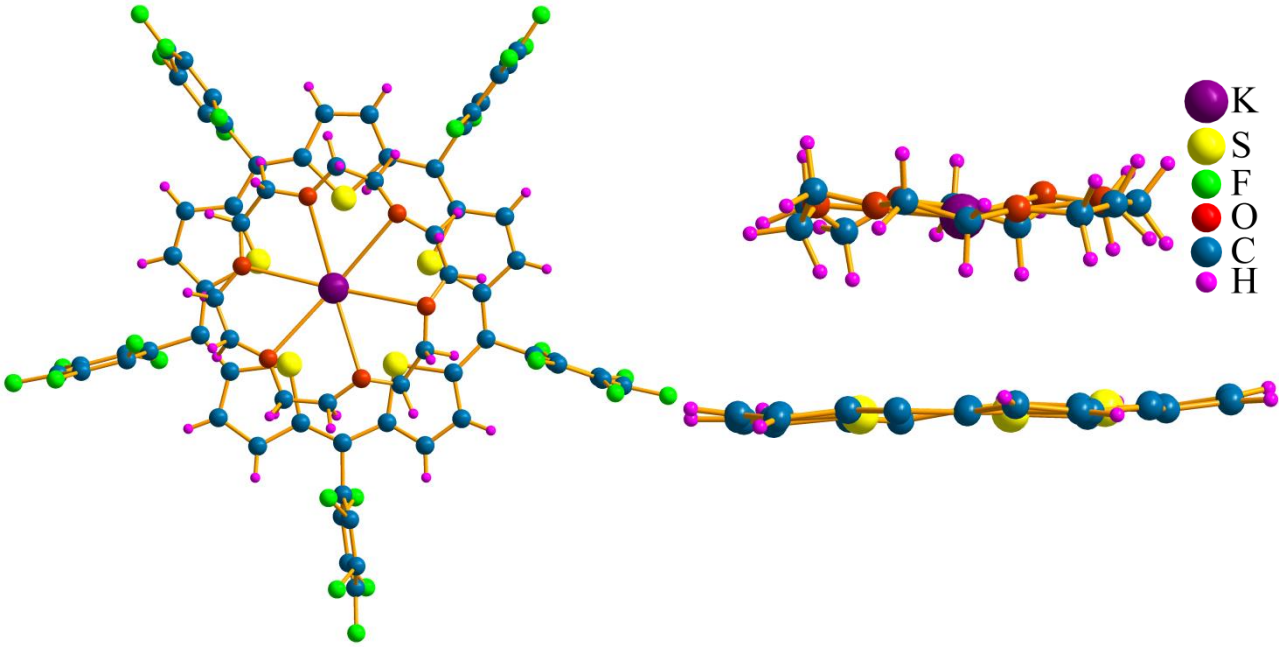

Figure-II.14: Molecular structure of **II.2**$^{-}$ top view (left) and side view (right). Phenyl rings are omitted for clarity in side view.

Molecular structure of aromatic anion was determined by single crystal X-ray diffraction analysis of its single crystals **(Figure-II.14)** grown from DMSO. It was found to possess a planar structure with potassium bound by 18-Crown-6 as the counter cation. This supported the strong diatropic ring current effects of anion as observed in its ^{1}H NMR spectrum. A distance of 3.89Å was determined from the macrocyclic plane to potassium atom in the crown ether complex.

II.9: Chemical reversibility:

The oxidation of anion (**II.2**)$^{-}$ to the neutral macrocycle **II.2** was achieved by reacting with Iron (III) chloride. The color of the solution changes from pink to green color. The change in the absorption of Soret-like band from 543 nm to 470 nm confirmed the formation of neutral radical **(Figure-II.15)**. Similarly reduction of (**II.2**)$^{+}$ to the neutral **II.2** was achieved using Iron (II) chloride. This redox processes was also monitored by absorption spectroscopy.

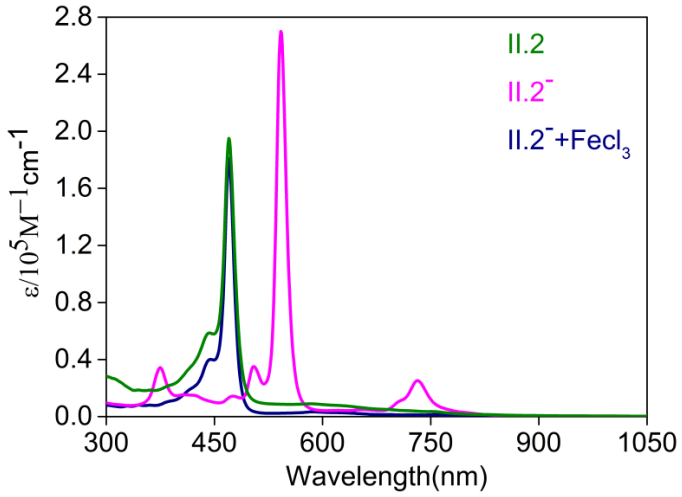

Figure-II.15: Absorption changes upon the addition of $FeCl_3$ to**II.2**$^-$.

II.10: Comproportionation reaction:

The addition of (**II.2**)$^-$ to (**II.2**)$^+$ lead to the neutralization of the charges and produced the neutral radical species as observed by the absorption corresponding to **II.2**. This reaction resembles a comproportionation reaction, demonstrating the ability of (**II.2**)$^-$ and (**II.2**)$^+$ to act as a mutual redox couple. The mutual neutralization of the ionic species supports the high stability of the neutral radical.

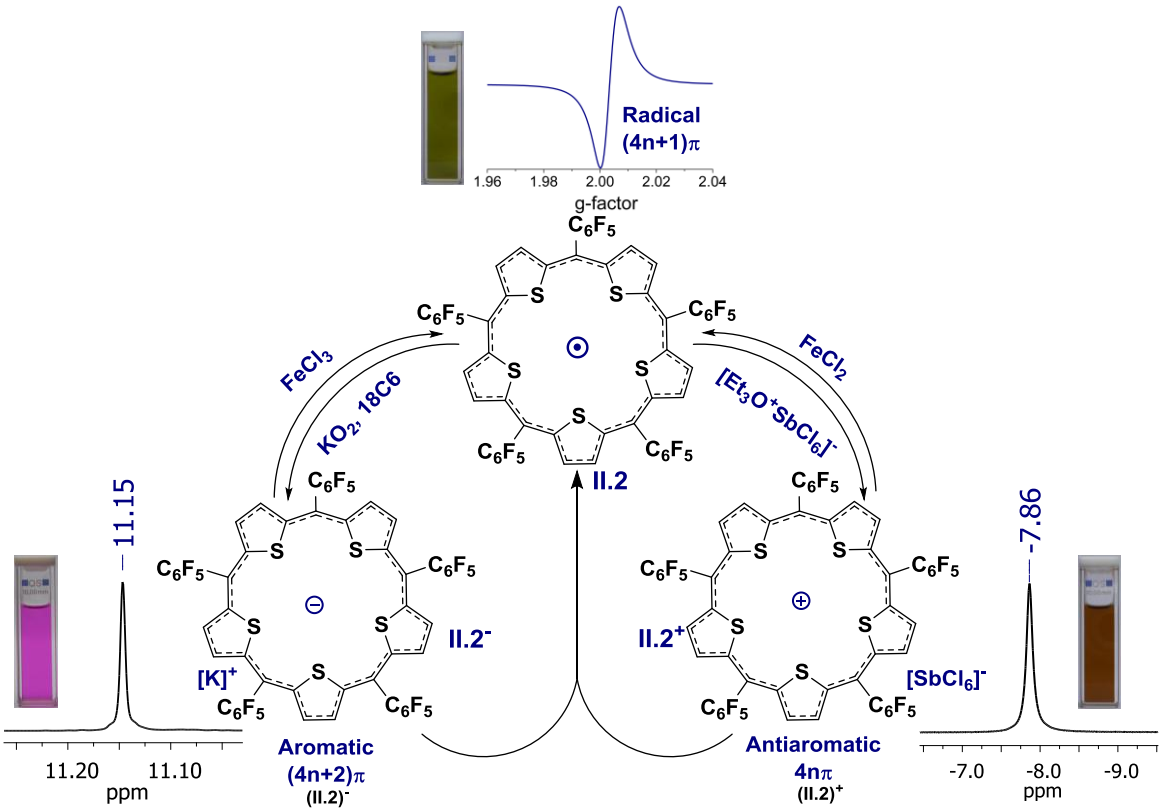

Scheme-II.8: Comproportionation reaction between **II.2**$^-$ and **II.2**$^+$.

II.11: Quantum mechanical calculations:

To get further insight into molecular orbitals and to quantify the aromaticity of three oxidation states of **II.2**, Quantum mechanical calculations were performed with the Gaussian09 rev D program suite[47]. All calculations were carried out by Density Functional Theory (DFT) with Becke's three-parameter hybrid exchange functional and the Lee-Yang-Parr correlation functional (B3LYP) and 6-31G(d,p) basis set for all the atoms that were employed in the calculations. The molecular structures derived from single crystal analysis were used to obtain the geometry-optimized structures. Among several methods are explored to quantify the aromaticity of conjugated systems[48], Nucleus Independent Chemical Shift (NICS)[49] is one of the successful indices to quantify the aromaticity. Schleyer introduced this magnetic criterion as a measure of aromaticity and antiaromaticity (or non-aromaticity). He defined it as "Absolute magnetic shieldings, computed at *ring center* (non-weighted mean of the heavy atom coordinates) or at another interested point of molecule. To correspond to the familiar NMR chemical shift convention, the signs of the computed values are reversed".

NICS	Magnetism	Ring Current	Aromaticity
Significantly Negative	Magnetically Shielded	Diatropic	Aromatic
Positive	Magnetically Deshielded	Paratropic	Anti-aromatic
Around Zero			Non-Aromatic

Table-II.1: NICS and ring currents.

NICS values were obtained with gauge independent atomic orbital (GIAO) method based on the optimized geometries. The global ring centers for the NICS (0) values were designated at the non-weighted mean centers of the macrocycles. In spite of its radical nature, a positive NICS (0) value of **+14.66** ppm was estimated for **II.2,** suggesting the strong delocalized nature of unpaired electron. The NICS (0) value of **+37.50** ppm for the **(II.2)**$^{+}$ is the highest ever computed value for antiaromatic species, equally matched by a strong paratropic ring current effect in its ^{1}H NMR spectrum. A negative NICS (0) value of **-14.96** ppm **(Table-II.1)**, confirmed the aromatic property of (**II.2**)$^{-}$.

The Anisotropy of the Current-Induced Density (ACID)[50] was also plotted to visualize the ring current due to delocalized π electrons. The AICD plots can directly display the magnitude and direction of the induced ring current when an external magnetic field is applied orthogonal to the macrocycle plane. Current density plots were obtained by employing the continuous set of gauge transformations (CSGT) method to calculate the current densities, and the results were plotted using POVRAY 3.7 for Windows. Similar to NICS method, clockwise ring currents represent aromatic molecules whereas anticlockwise ring currents are representative of antiaromatic molecules. Apart from the direction of ring currents, it also aids in determining the path of the delocalized π-electrons. **II.2** and its cationic derivative **(II.2)**$^{+}$ exhibited anti-clockwise ring currents suggesting the delocalization of π-electrons **(Figure-II.16)** in antiaromatic state, whereas anionic form **(II.2)**$^{-}$ clearly displayed clockwise delocalization[50]. In both anion and cation, the electron flow was observed only through the carbon perimeter.

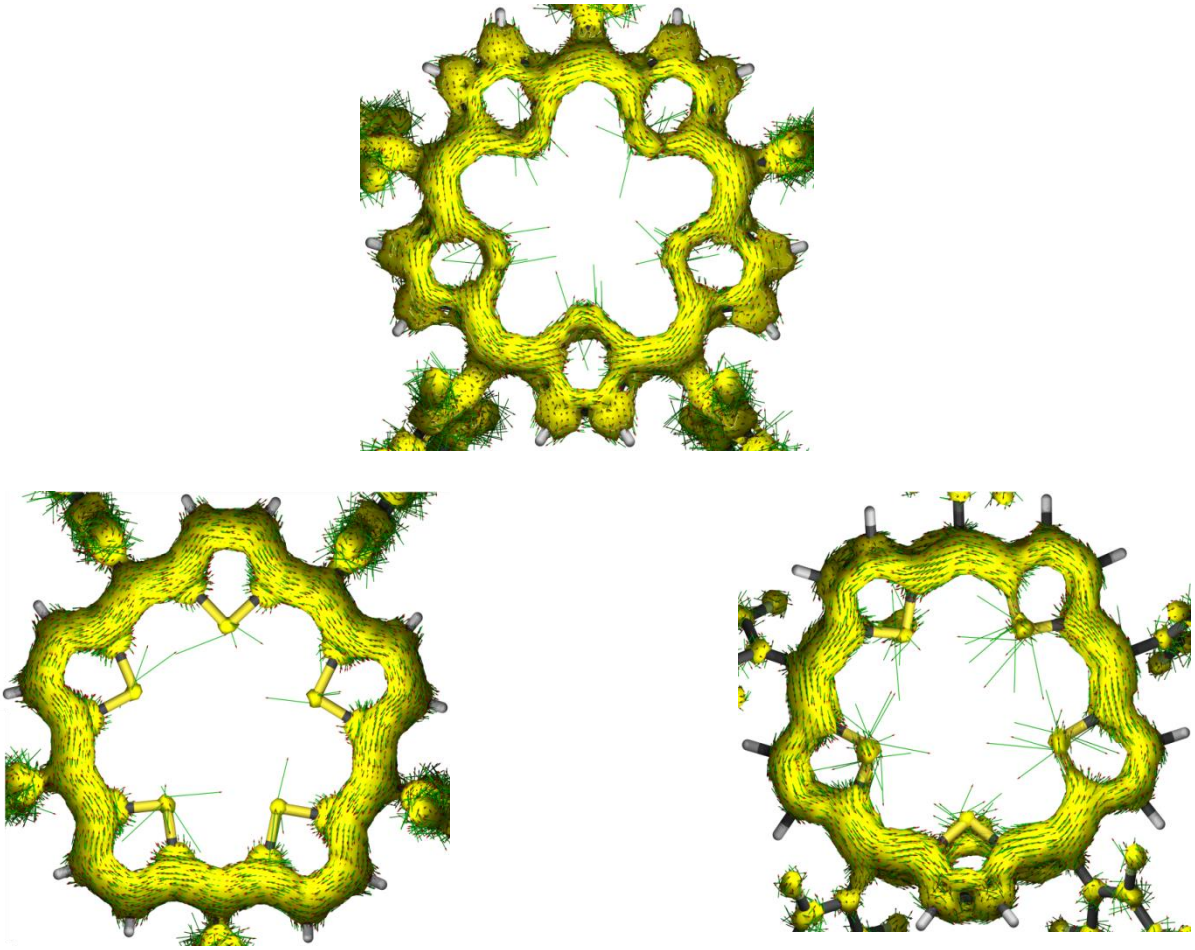

Figure-II.16: AICD plot of **II.2** (top), **(II.2)**$^{-}$(bottom left) and **(II.2)**$^{+}$ **(**bottom right**).**

To simulate the steady-state absorption spectra, time-dependent TD-DFT calculations were employed on the optimized structures. Simulated absorption spectra for all the three oxidations states of **II.2** matched the experimental results. The smallest HOMO-LUMO gap of 1.04 eV and optically dark NIR states at 2520 nm supported the antiaromatic character[51] of cationic state **(Figure-II.17)**. A relatively higher HOMO-LUMO gap of 2.24 eV supported the aromatic nature of anionic state.

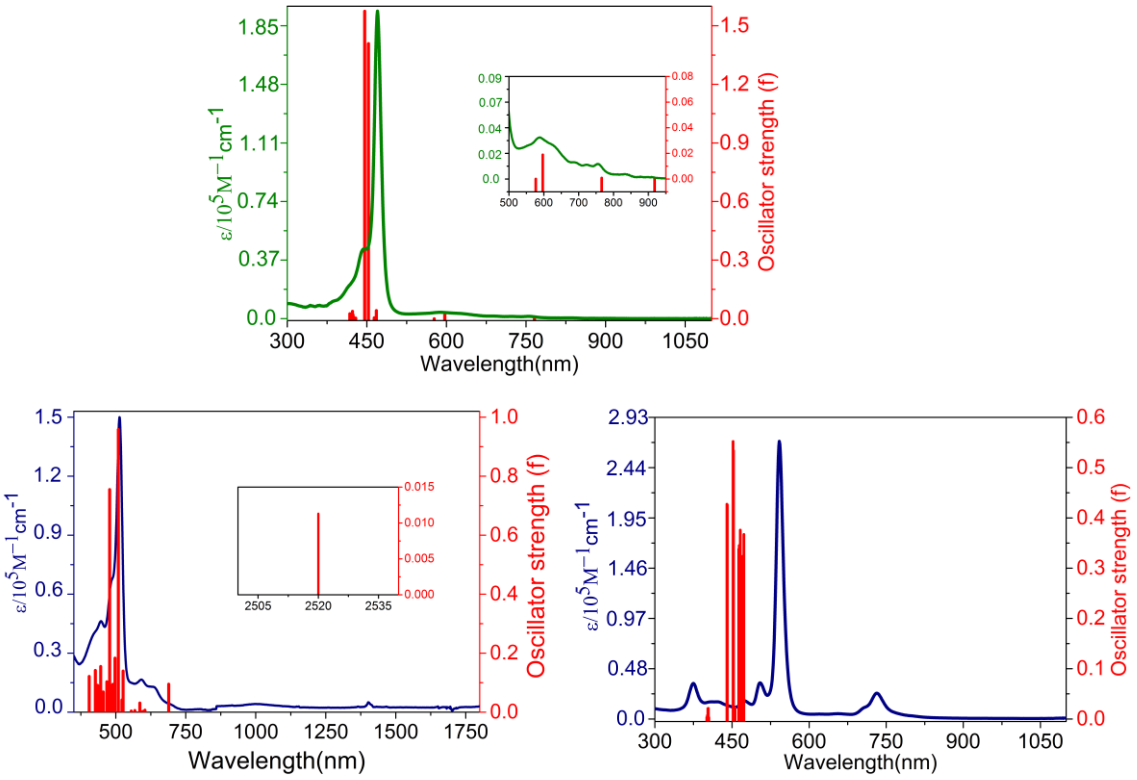

Figure-II.17: The steady state absorption spectras along with the theoretical vertical excitation energies (red bar) obtained from TD-DFT calculations carried out at the B3LYP/6-31G(d,p) level top (**II.2),** bottom left **(II.2)**$^{+}$ bottom right **(II.2)**$^{-}$**.**

II.12: Synthesis and Characterization of β-phenyl substituted pentathiophene (II.7):

In order to study the effect of substitution, one of the **β**-hydrogen on the thiophene was replaced by a phenyl group. Synthesis of **β**-phenyl substituted macrocyclic oligothiophenes was achieved in two steps starting from 4-phenylthiophene-2-carbaldehyde. In contrast to one-pot synthesis from thiophene and pentafluoro benzaldehyde, the MALDI-TOF mass spectrum of this reaction mixture displayed pentathiophene macrocycle as the major product

along with the tetrathiophene macrocycle. However, no higher macrocycles were observed in this reaction.

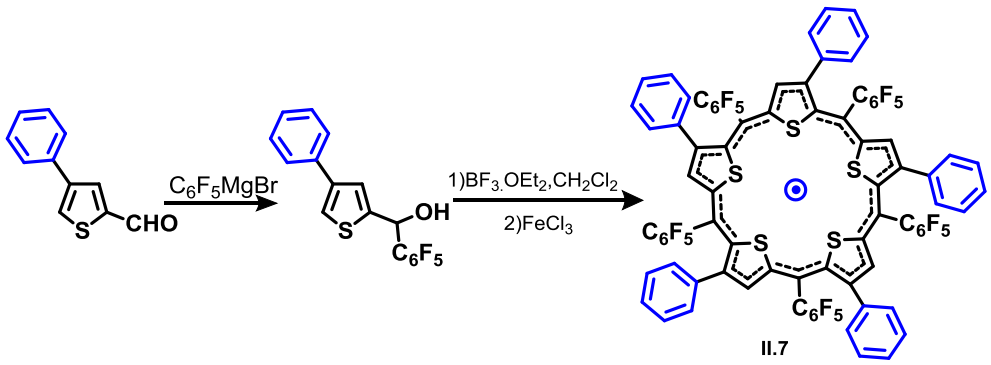

Scheme-II.9: Synthesis of **II.7**.

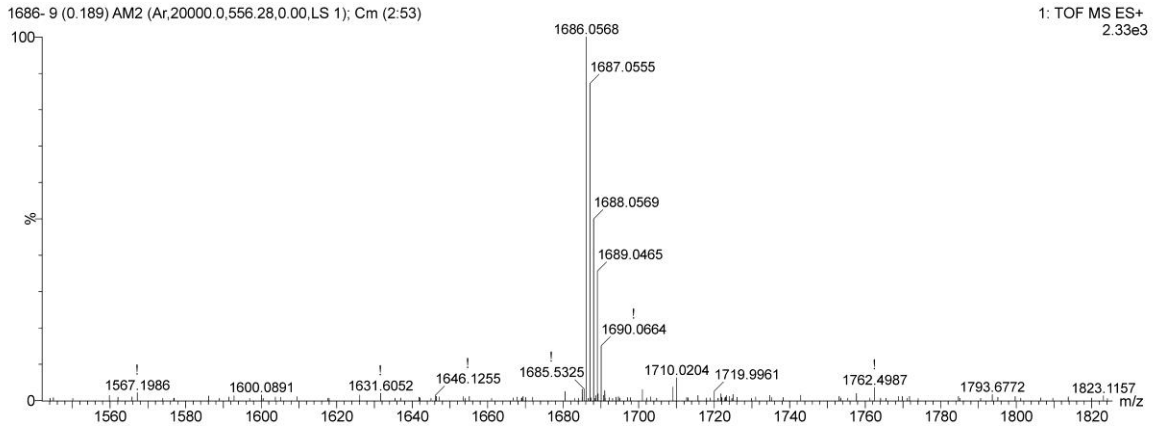

Figure-II.18: High resolution mass spectra of **II.7**.

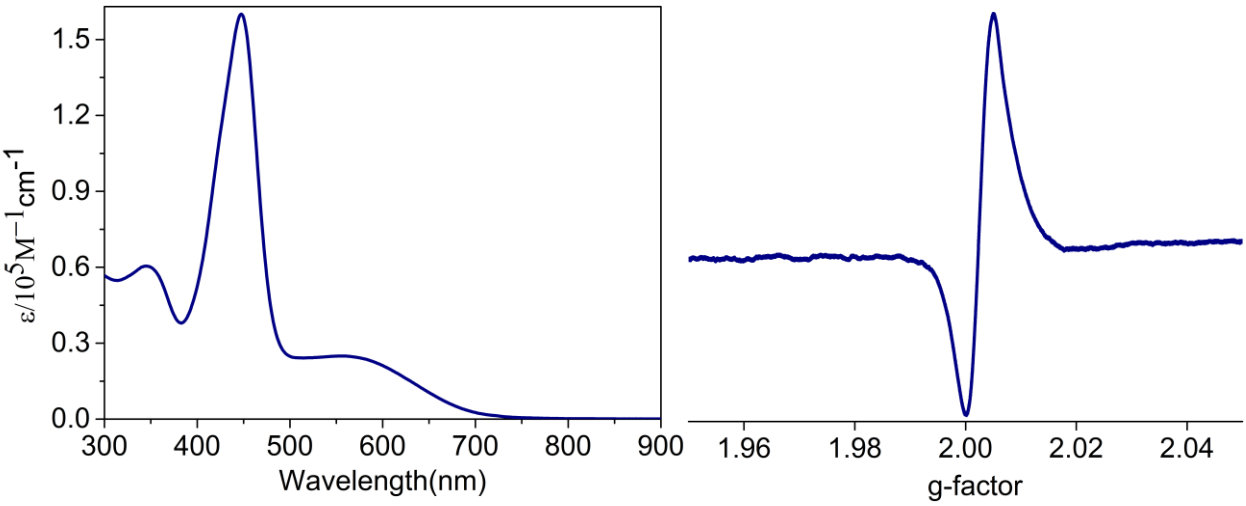

Figure-II.19: UV-Visible (left) and EPR spectra (right) of **II.7**.

Column chromatographic separation of reaction mixture yielded a brown colored solution which exhibited a λ_{max} at 448 nm (160,000) in CH_2Cl_2. It's high-resolution mass spectrum displayed an *m*/*z* value of 1686.0568 (**Figure-II.18)** in agreement with the expected value for **II.7.** Similar to **II.2,** no signals were observed in ^{1}H NMR spectrum of **II.7** suggesting the presence of paramagnetic species. Its EPR spectrum exhibited a resonance with g = 2.0023, confirming the expected radical **(Figure-II.19)** and was found to absorb at 447 nm. The molecular structure of the **β**-phenyl substituted pentathiophene, **II.7**, was established by single crystal X-ray diffraction analysis. Its single crystals were grown by solvent diffusion method using DMSO. It crystallized in Triclinic system with P-1 space group. Similar to **II.2** sulphur atoms of all the five thiophenes pointed towards the macrocyclic center. However, this molecule was found to deviate from a planar structure due to the steric crowding of phenyl and pentafluoro groups **(Figure-II.20)**.

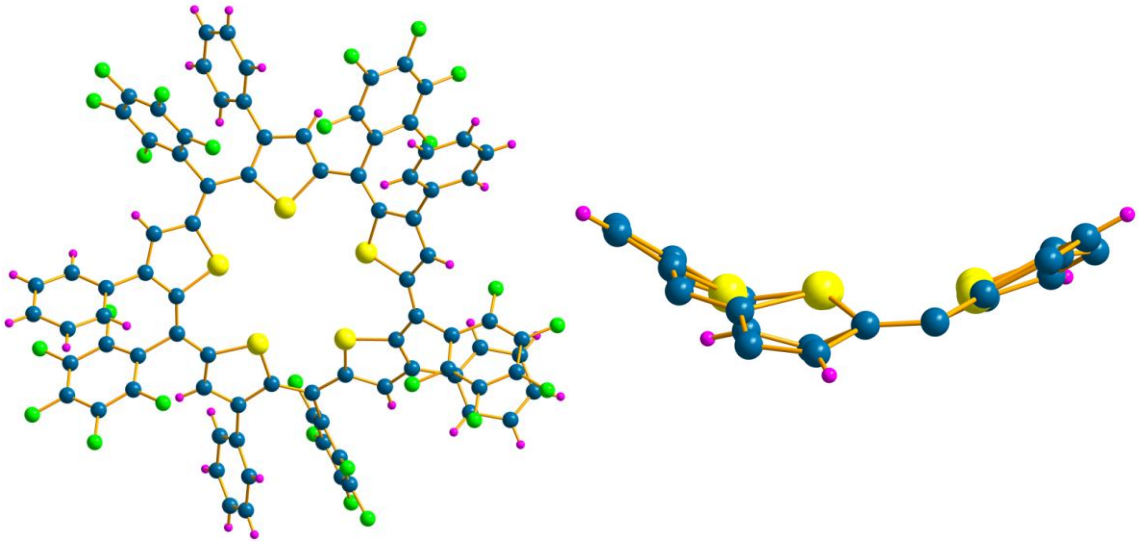

Figure-II.20: Molecular structure of **II.7** top view (left) and side view (right). Phenyl rings are omitted for clarity in the side view.

II.13: One electron reduction of II.7:

In spite of its non planar nature, **II.7** underwent a one-electron redox process similar to that of **II.2.** Addition of KO_2 to a solution of **II.7** in DMSO induced a quick change in the color of the solution from brownish to green **(Scheme-II.10)**. The green colored solution of $(\mathbf{II.7})^-$ exhibited an intense red shifted absorption at 605 nm (200,000) with a Q-like band at 806 nm (24,000) signifying the aromatic characteristics of the reduced radical **(Figure-II.20)**. The magnitude of the observed bathochromic shift of 157 nm was found to be more than twice as that observed for **II.2.**

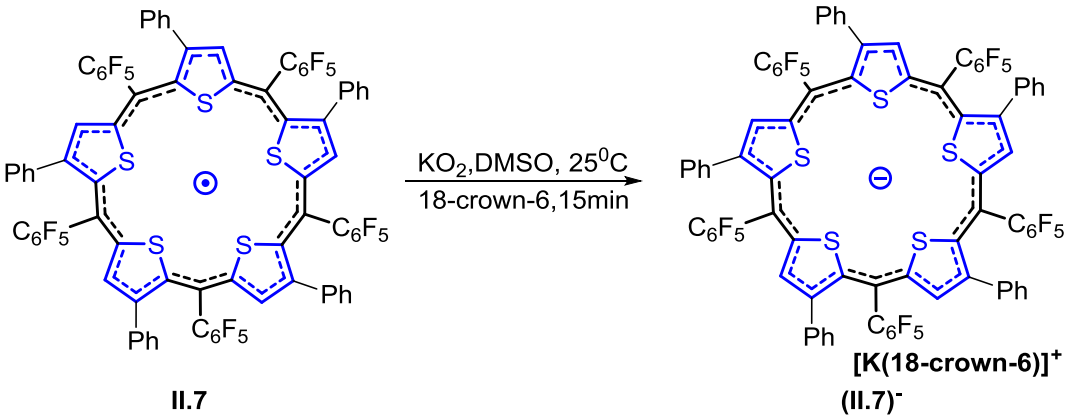

Scheme-II.10: One electron reduction of **II.7**.

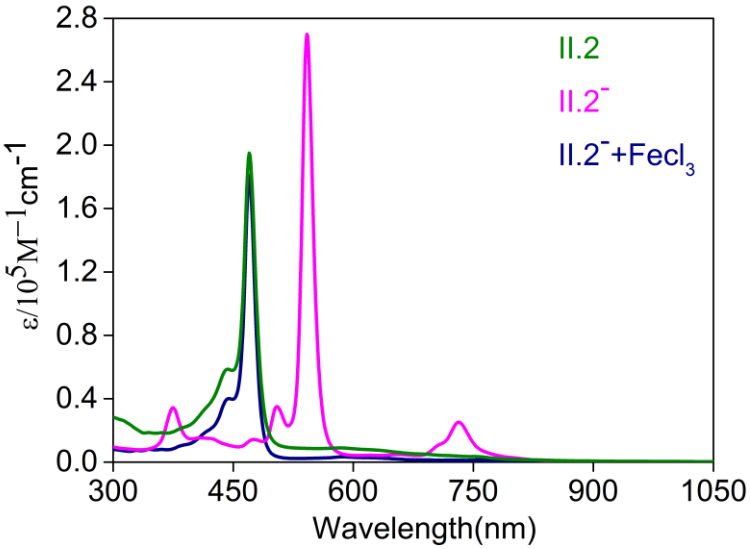

Figure-II.20: Absorption spectral changes upon the addition of KO_2 to **II.7** in DMSO.

The ^{1}H NMR spectrum obtained by addition of KO_2 and 18-crown-6 to **II.7**, in deuterated DMSO displayed a singlet at 9.96 ppm (**Figure-II.21)** corresponding to thiophene protons. Such a downfield shift confirmed the diatropic ring current effect of the 26π aromatic anion obtained by the one-electron reduction of the radical. The reduced diatropic ring currents compared to **II.2** could be attributed to the deviation from planar topology in spite of similar symmetry.

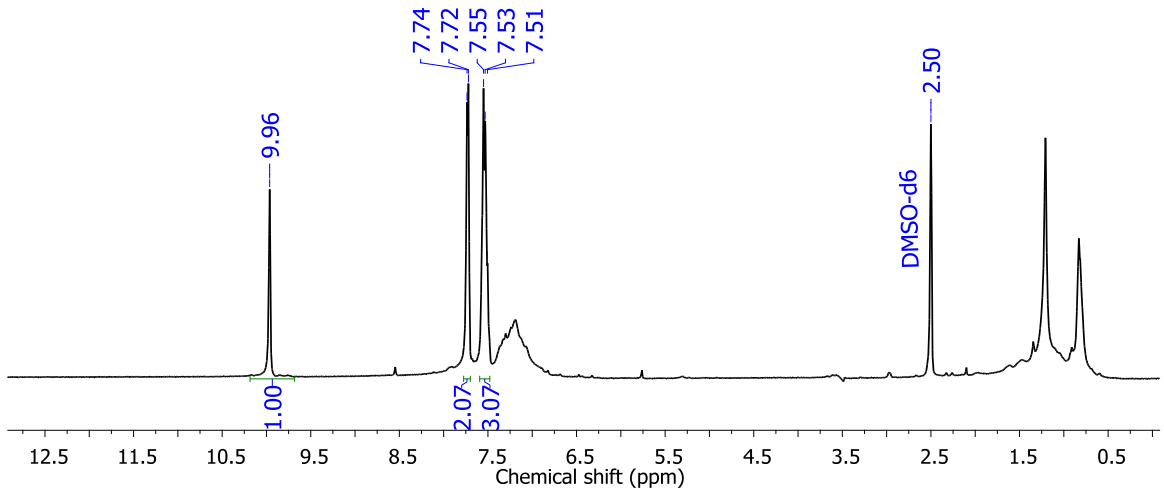

Figure-II.21: ^{1}H NMR spectra of **II.7**$^{-}$.

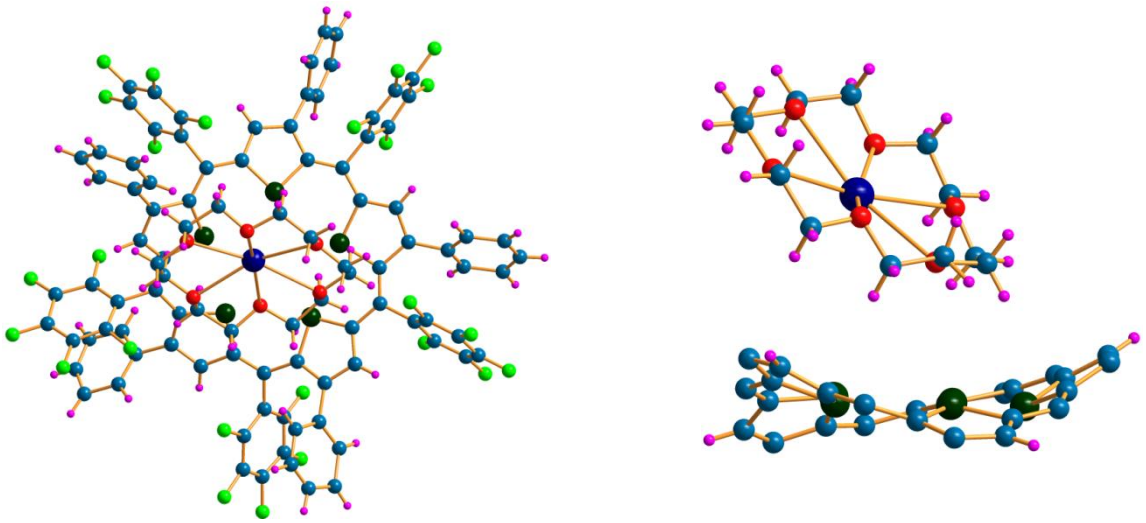

Figure-II.21: Molecular structure of **II.7**$^{-}$ top view (left) and side view (right).

Its single crystals were grown by slow evaporation of DMSO solution over few days. It crystallized in triclinic crystal system with P-1 space group. It was observed that the molecular structure of this macrocycle deviated from planarity similar to **II.7.** Potassium bound by 18C6 was observed as the counter cation in the crystal packing diagram. It was observed that this potassium crown-ether cation is not parallel to the macrocyclic plane due to steric crowding from the phenyl groups **(Figure-II.21)**.

II.14: Isolation and Characterization of octathiophene macrocycle (II.5):

Along with the products described above **(Scheme-II.3)**, a pink colored fraction was also isolated from column chromatographic separation. It displayed an *m*/*z* value of 2087.7598 in its high-resolution mass spectrum **(Figure-II.22)** confirming the composition of an

octathiophene macrocycle. This macrocycle accounts for 40π electrons along its conjugated pathway and due to this extended conjugation its λ_{max} was found to be at 546 nm (130,000). The octathiophene macrocycle **(II.5**) had a smaller molar extinction co-efficient compared to previously reported furan analogue (**II.8**) 535 nm (340,000) indicative of a different structural feature for the same number of π electrons[33].

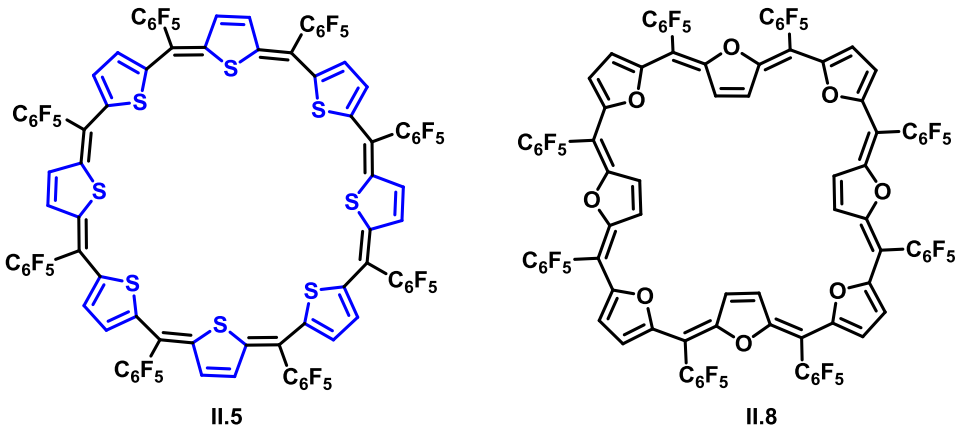

Scheme-II.11: Chemical structures of **II.5** and **II.8**.

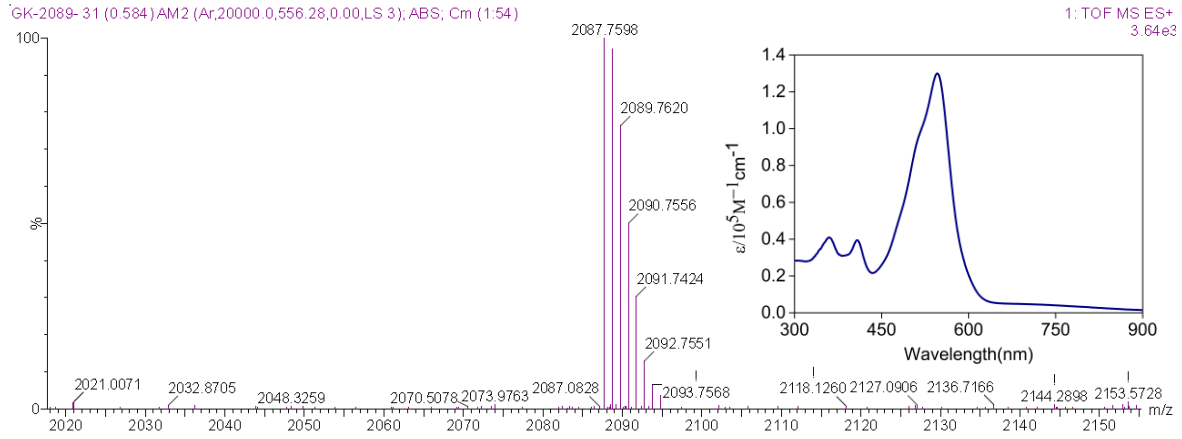

Figure-II.22: High resolution mass [Inset: UV-Visible spectrum of **II.5** in CH_2Cl_2.

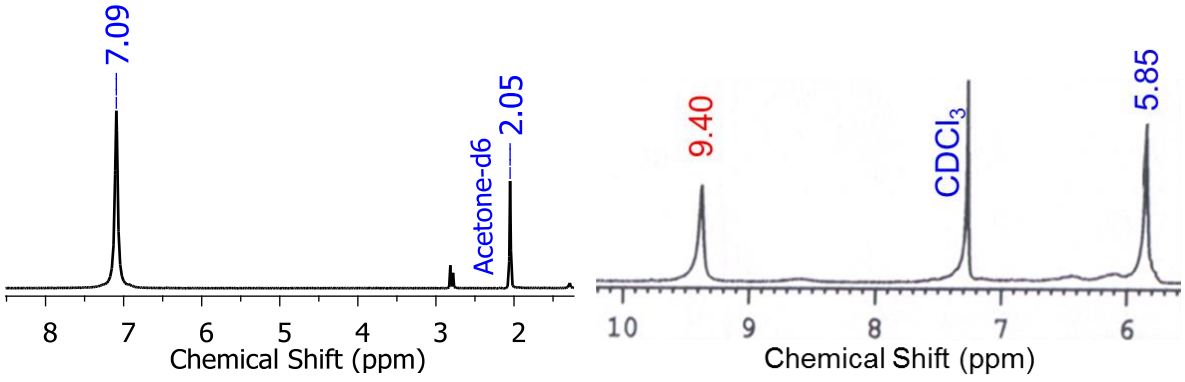

Figure-II.23: ^{1}H NMR spectra of **II.5** (left) and **II.8** (right) at room temperature.

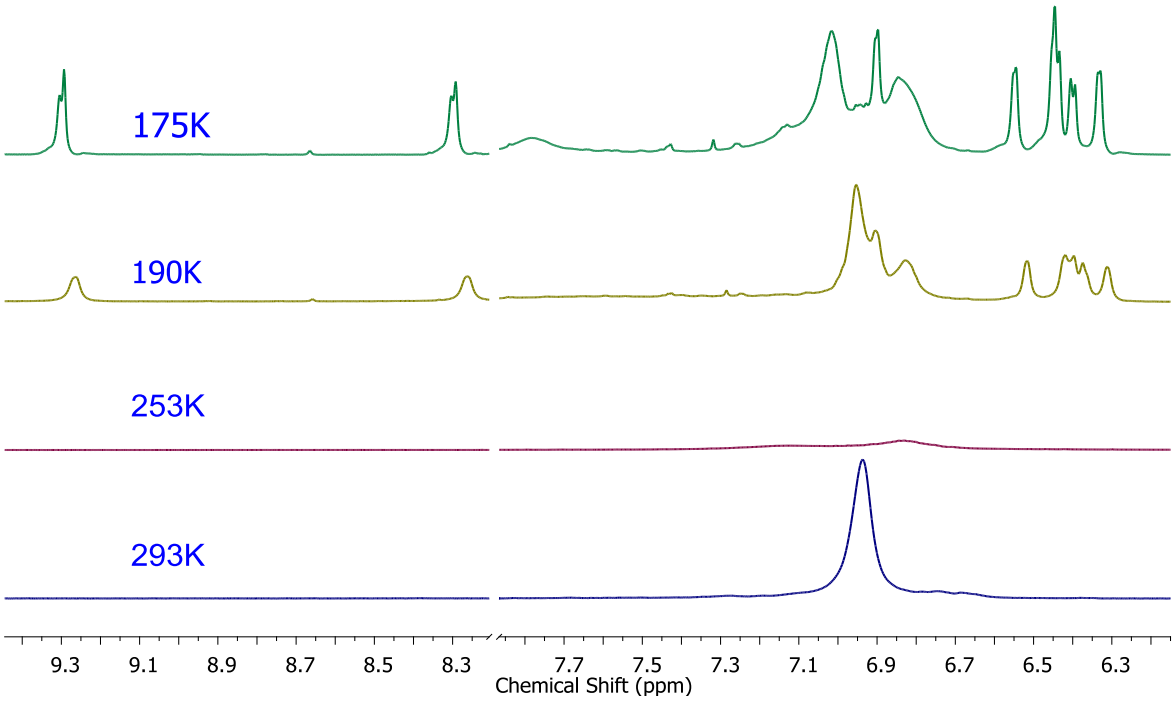

Figure-II.24: Variable temperature ^{1}H NMR spectra of **II.5**.

In the ^{1}H NMR spectrum a broad singlet at δ 7.09 corresponded to all the protons of **II.5** (**Figure-II.23)** whereas **II.8** displayed two singlets with equal intensity at δ 9.4 and 5.85 ppm for the inverted and non-inverted ring protons respectively. This suggested a planar structure of **II.8** with paratropic ring current effects. The observed broad singlet of **II.5** also suggested the possibility of fluxional behavior due to continuous flipping of thiophene rings. An attempt to arrest the fluxionality was made by recording its ^{1}H NMR spectrum at a lower temperature. As expected, the intensity of the signal at 7.09 ppm decreased with decrease in temperature and completely vanished at 253K. Two different singlets for the inner and outer protons were expected upon further decrease in temperature. However, instead of two signals, more number of signals were observed in the region between δ 9.5-6.0 ppm at 175K clearly suggesting the loss of symmetry upon reducing its temperature. Variable temperature ^{1}H NMR analysis (**Figure-II.24)** clearly suggested solution state conformational changes for **II.5** at lower temperatures.

Good quality single crystals were grown by slow diffusion of *n*-hexane into its DMSO solution. **II.5** crystallized in tetragonal symmetry with **I-4** space group and resembled the shape of a square. Four of the thiophene rings were inverted similar to that of **II.8 (Figure-II.25)**. This molecule was observed to be more planar in nature in comparison to **II.8.**

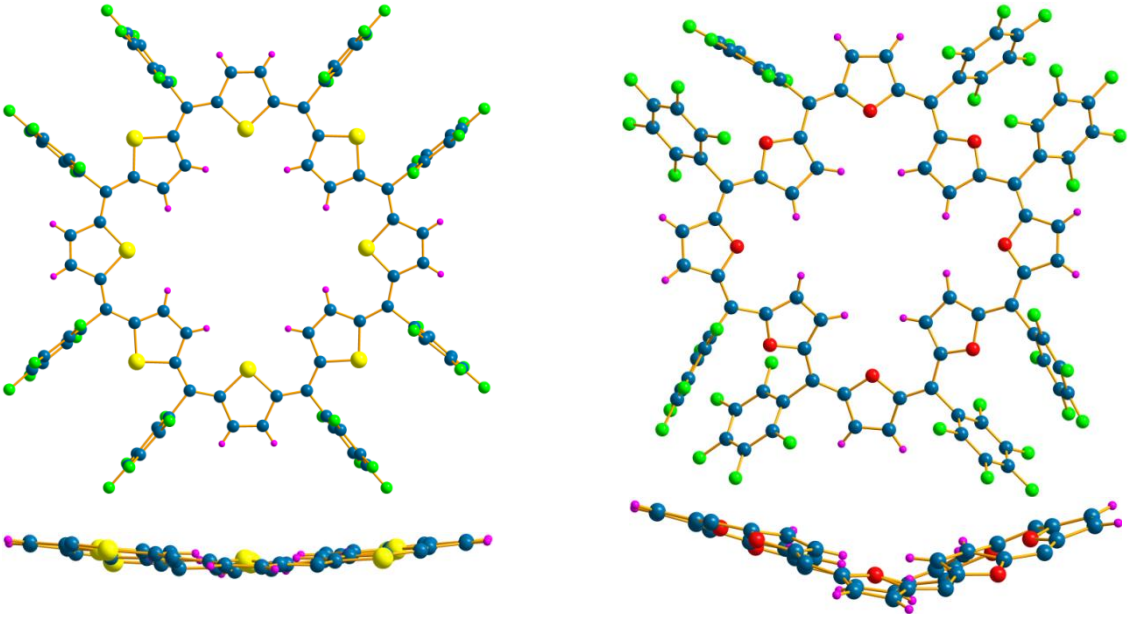

Figure-II.25: Molecular structures of **II.5** (left) and **II.8** (right)**.**

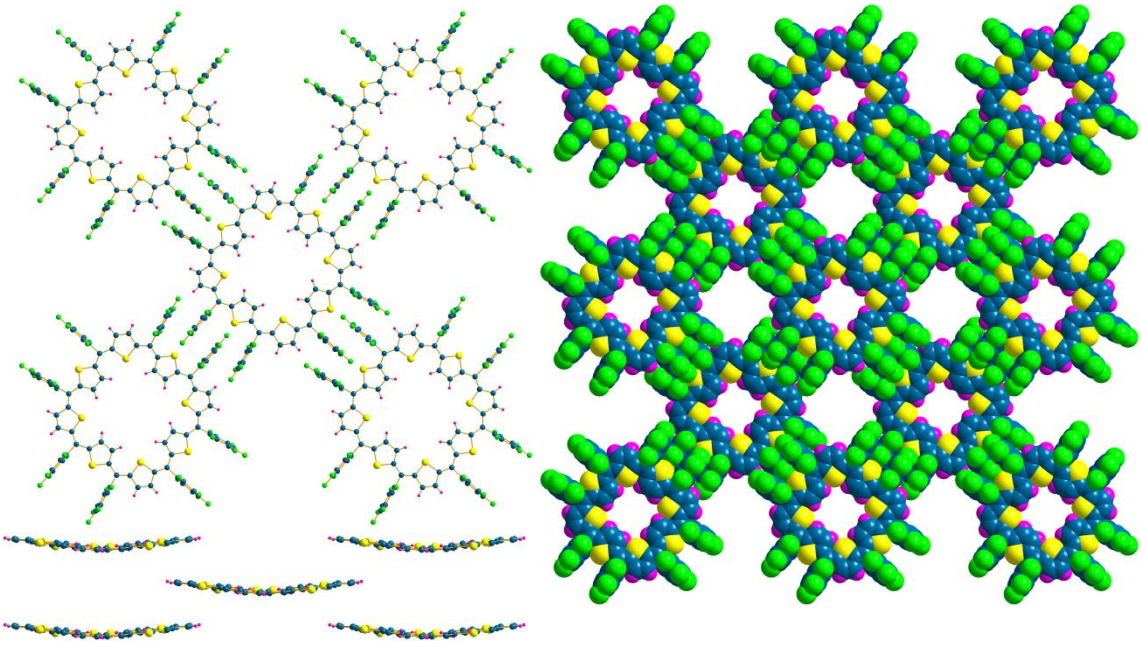

Figure-II.26: Inter molecular C-H…F interactions observed in the crystal packing of **II.5**.

Also this molecule displayed strong non covalent C-H…F interactions in its crystal packing diagram. Each macrocycle is surrounded by eight other molecules such that four are above and four below the molecular plane **(Figure-II.26)**. An inter-planar distance of 3.87 Å was observed between the central molecular plane and those surrounded above and below molecular planes. Attempts to elucidate the molecular structure of the compound at lower temperature ended up with limited success. The unstable nature of the crystals grown at lower temperatures under ambient conditions prevented further analysis.

II.15: Co-crystallization of II.5 with C_{60}:

However, an attempt was made to prevent the loss of symmetry through host-guest chemistry based on non-covalent interactions. It's a well-known fact that equimolar ratio of fullerene and porphyrin forms π complex where fullerene molecules bind exactly on the π- surface of a porphyrin **(Figure-II.27)**[52]. Expecting the formation of π -complex to arrest the fluxional behaviour of thiophene rings and conformational changes, fullerene and **II.5** was mixed in 1:1 ratio of acetone and toluene. This solution was undisturbed for few days to co-crystallize fullerene with the 40π octathiophene. After a few days, dark block shaped crystals were observed in the solution. Unexpected results were observed in single crystal X-ray diffraction analysis of these co-crystals. Instead of formation of π-dimer, the molecule was found to split into two symmetrical halves leading to the formation of two 20π tetrathiophene macrocycles. Similar thermal splitting reactions of Cu coordinated octaphyrin complexes are known for pyrrole based metal complexes of expanded porphyrins[53]. This symmetrical splitting can be envisaged only when a macrocycle undergoes a conformational change from planar to figure of eight conformation upon addition of C_{60} **(Figure-II.28)**. Perhaps, in this reaction, the fullerene induced a conformational change from a planar to a figure of eight conformation. Further studies on this mechanism are under progress.

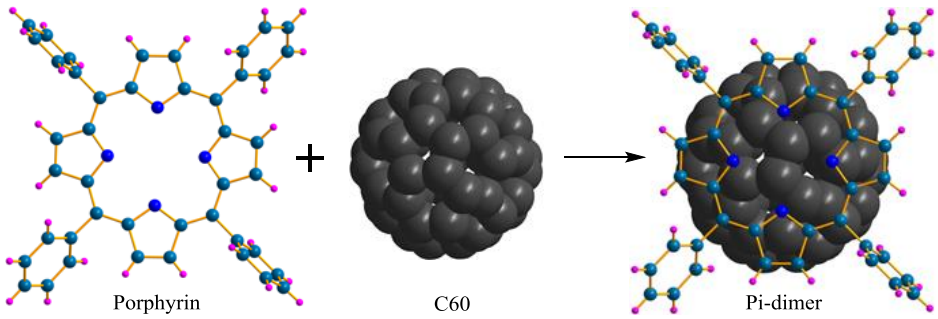

Figure-II.27: Non-covalent interactions of Porphyrin and C_{60}[52a].

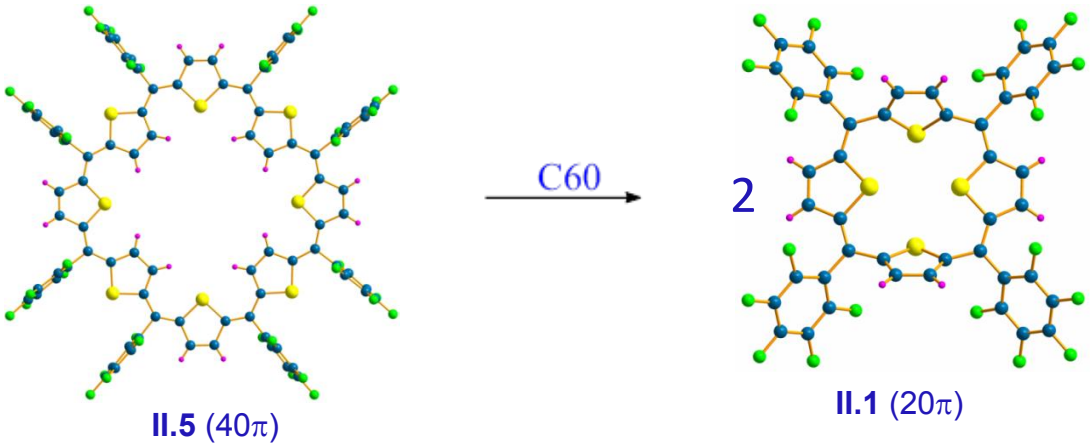

Figure-II.28: Symmetrical splitting of **II.5** in the reaction of C60 at room temperature.

II.16: Conclusions:

Thiophene reacts with pentafluoro benzaldehyde under oxidative conditions to yielded π-conjugated macrocycles bearing four, five, six, seven, eight, nine and ten thiophene units. Depending on the length of the conjugation the formal π electron count varies from 20π electrons in the tetra thiophene macrocycle to 50π electrons in the deca thiophene macrocycle. The nature of the products is dependent on the number of π electrons in the respective macrocycle. All possible forms of π-conjugated systems i.e. aromatic, antiaromatic, π-radicals and probably non-aromatic macrocycles could be identified in this reaction. In this regard, the nature of the products formed is different from that obtained by the reaction of pyrrole with pentafluoro benzaldehye. The macrocycles obtained in this reaction resemble the skeletal frame-work of isophlorins and hence they can be considered as expanded isophlorins. The pyrrole's ability to inter-convert the nitrogen between imine and amine forms makes the nitrogen to be a part of the π-conjugated network and hence such pyrrole based macrocycles resemble porphyrin. This aids the macrocycle to attain complete conjugation when odd number of carbon atoms connects the conjugated pathway. In contrast, the thiophene based macrocycles cannot utilize sulfur along the conjugated pathway and hence it is expected to be incompatible for macrocyclic systems with odd number of carbon bonds in the circular π framework. Interestingly, this turned out stabilize a neutral radical which can be accounted for 25π electrons in a pentathiophene macrocycle. The synthesis of such neutral and air-stable radicals are very scarce and hence this synthetic method is relatively simple with moderate yields of more than 35% for the 25π radical. Similar such macrocycles with 35 and 25 π-electrons were also formed in this reaction as analyzed by

mass spectrometry. More importantly, the radicals are stable enough to be isolated from column chromatography under ambient conditions. The stability of this radical was further confirmed by one-electron oxidation and reduction to the respective 24π antiaromatic and 26π aromatic macrocycles. These observations were also suitably supported by computational studies. In a rare observation for organic radicals, all the three states were characterized by a variety of spectroscopic techniques including single crystal X-ray crystallography. The 25π radical pentathiophene radical is the first example in the pentaphyrin class of macrocycles without ring inverted heterocyclic unit. The planar geometry can be considered crucial to the stabilization of the neutral 25π radical. The 40π octathiophene macrocycle was also characterized in solution and solid states. Variable temperature ^{1}H NMR studies strongly supported the fluxional behaviour of the macrocycle, even though it was found to be planar in the solid state. Four thiophene rings were found to be inverted in a structure similar to that of the 40π octafuran. However, its reactivity was found to be different in the presence of a guest molecule such as C_{60}. These studies suggested that the macrocycle can be split into to two equal halves that resemble the 20π tetra-thiophene. Breaking of such large macrocycles into smaller rings has been known in the presence of metal salts for the expanded porphyrins. However, 40π octathiophene represents the first example for such reactivity in expanded isophlorins. More studies are required to correlate the reactivity of such macrocycles to antiaromatic character of molecules in general. To conclude, thiophene appears to be suitable building block in the synthesis of variety of antiaromatic macrocycles. It can be observed that the properties and the reactivity of antiaromatic macrocycles vary significantly in contrast to aromatic molecules. However, more such macrocycles would be required to generalize the reactivity of antiaromatic system.

II.17: Experimental Section:

All reagents and solvents were of commercial reagent grade and were used without further purification except where noted. Dry CH_2Cl_2 was obtained by refluxing and distillation over CaH_2. Column chromatography was performed on basic alumina and silica gel (230-400 mesh) in glass columns. ^1H NMR and ^{19}F-NMR spectra were recorded either on a JEOL 400 MHz or Bruker 500 MHz spectrometer. Chemical shifts were reported as the delta scale in ppm relative to $(CH_3)_2CO$ ^1H (δ = 2.05 ppm), THF (δ = 1.73 ppm) or CH_3CN (δ = 1.94 ppm). Electron Paramagnetic Resonance (EPR) spectra were obtained using a Bruker ESP 300 EPR spectrometer. Thermogravimetric analysis was carried out on Perkin-Elmer STA 6000 TGA analyzer under N_2 atmosphere with a heating rate of 10°C min^{-1}. Electronic spectra were recorded on a Perkin-Elmer λ-950 ultraviolet−visible (UV−vis) spectro-photometer. High resolution mass spectra were obtained using WATERS G2 Synapt Mass Spectrometer. Single-crystal diffraction analysis data were collected at 100K with a BRUKER KAPPA APEX II CCD Duo diffractometer (operated at 1500 W power: 50 kV, 30 mA) using graphite-monochromated Mo Kα radiation (λ = 0.71073 Å). Cyclic voltammetry (CV) and Differential pulse voltammetry (DPV) measurements were carried out on a BAS electrochemical system using a conventional three-electrode cell in dry CH_2Cl_2 containing 0.1 M tetrabutylammonium perchlorate (TBAP) as the supporting electrolyte. Measurements were carried out under an Ar atmosphere. A glassy carbon (working electrode), a platinum wire (counter electrode), and saturated calomel (reference electrode) were used.

Quantum mechanical calculations were performed with the Gaussian09 rev D program suite using a High Performance Computing Cluster facility of IISER PUNE. All calculations were carried out by Density functional theory (DFT) with Becke's three-parameter hybrid exchange functional and the Lee-Yang-Parr correlation functional (B3LYP) and 6-31G(d,p) basis set for all the atoms were employed in the calculations. The molecular structures obtained from single crystal analysis were used to obtain the geometry optimized structures. To simulate the steady-state absorption spectra, the time-dependent TD-DFT calculations were employed on the optimized structures. Molecular orbital contributions were determined using GaussSum 2.2.Program package. The global ring centres for the NICS (0) values were designated at the non-weighted mean centres of the macrocycles. The NICS (0) value was obtained with gauge independent atomic orbital (GIAO) method based on the optimized geometries. We calculated the Anisotropy of the current-induced density (ACID) to visualize delocalized π electrons. The AICD plots can directly display the magnitude and direction of

the induced ring current when an external magnetic field is applied orthogonal to the macrocycle plane. Current density plots were obtained by employing the continuous set of gauge transformations (CSGT) method to calculate the current densities, and the results were plotted using POVRAY 3.7 for Windows. The molecular orbitals were visualized using Gauss View 4.1

Synthetic Procedure for II.1-II.6

A flame-dried 250-mL two neck round-bottomed flask was charged with thiophene (0.2 ml, 2.5 mmol) and pentafluorobenzaldehyde (0.3 ml, 2.5 mmol), in 100 ml of freshly distilled anhydrous dichloromethane under an argon atmosphere and degassed with argon for further ten minutes. $BF_3.OEt_2$ (0.16 ml, 1.25 mmol) was added under dark using a syringe, and the resulting solution was stirred for one hour under inert atmosphere. After adding anhydrous $FeCl_3$ (1.23 g, 7.5 mmol), the solution was opened to air and stirred for one more hour. A few drops of triethylamine were added and passed through a short basic alumina column. Solvent was evaporated from this mixture and was further separated by silica gel column chromatography by using CH_2Cl_2/hexane as the eluent.

HR-MS (ESI-TOF): m/z =1304.8992 (found, $[M]^+$), 1304.8987 (calcd. For $C_{55}H_{10}F_{25}S_5$). **UV-Vis** (CH_2Cl_2): λ_{max} (ε) L mol^{-1} cm^{-1} = 470 (195,000). **EPR:** g=2.0026. **Redox**: E^{1red} = -0.05mV, E^{1ox} = 0.68mV, E^{2ox} = 0.92mV, E^{3ox} = 1.27mV, and E^{4ox} = 1.36mV. **Crystal data**: $C_{55}H_{10}F_{25}S_5$ (*M*r = 1305.93), monoclinic, space group *P2 (1)/n (*no. 14), *a* = 12.847(11), *b* = 29.61(3), *c* = 17.770(15) Å, *β* = 98.264(16)° ,*V* = 6689(10)$Å^3$, *Z* = 4, *T* = 100(2) K , D_{calcd} = 1.297g cm^{-3}, R_1 = 0.0775 (I>2sigma(I)), R_w (all data) = 0.2058, GOF = 0.812.

Synthetic Procedure for $(II.2)^+$

A flame-dried 25-mL round-bottomed flask containing **II.2** (50 mg, 0.037 mmol) and triethyloxonium hexachloroantimonate (26 mg, 0.06 mmol) in anhydrous dichloromethane[46] (10 mL) was added under argon atmosphere at 0°C. The green coloured solution immediately turns to brown and this solution was stirred for another one hour and later poured to 20 mL of diethyl ether at -78 °C (dry ice-acetone bath). Dark colored crystals were formed after keeping this solution undisturbed for 15minutes. The crystals collected by vacuum filtration yielded mono cationic salt of hexachloroantimonate **$(II.2)^+$** in quantitative yield.

^{1}H NMR (400 MHz, Acetonitrile-d_3, 293K): δ = -6.77 (s =10H). **^{1}H NMR** (400 MHz, Acetonitrile-d_3, 230K): δ= -7.86 (s =10H).**^{19}F NMR** (376 MHz, Acetonitrile-d_3, 230K): δ= -145.95 (d, *J* = 19.8 Hz, 10F), -156.51 (t, *J* = 20.8 Hz, 5F), -159.33 (t, *J* = 19.6 Hz, 10F). **UV-Vis** (CH_2Cl_2): λ_{max} (ε) L mol^{-1} cm^{-1} = 513 (150,000).

Crystal data $C_{55}H_{10}Cl_6F_{25}S_5Sb$ (*M*r=1640.38), monoclinic, space group *c2/c* (no. 15), *a* = 47.660(14), *b* = 10.972(3), *c* = 33.722(10) Å, *β* = 126.706(4)°, *V* = 14137(7) $Å^3$, *Z* = 8, *T* = 100(2) K , D_{calcd} = 1.541g cm^{-3}, R_1 = 0.0699 (I>2sigma(I)), R_w (all data) = 0.1729, GOF = 1.075.

Synthetic Procedure for (II.2)$^-$

To a solution of **II.2** (50 mg, 0.037 mmol) in dry DMSO an excess amount of potassium superoxide (KO_2) dissolved in 18-crown-6 and anhydrous DMSO was added. Immediately the color of the solution changed from green to pink with simultaneous bubbling in the solution suggesting the liberation of O_2. The resulting pink colored solution was kept undisturbed for a day at room temperature to obtain greenish needle shaped crystals. The crystals collected by vacuum filtration gave (**II.2)$^-$** in quantitative yield.

^{1}H NMR (400 MHz, DMSO-d_6, 293K): δ= 11.15 (s =10H). **^{19}F NMR** (376 MHz, DMSO-d_6, 293K): δ= -140.04 (d, *J* = 23.9 Hz, 10F), -154.43 (t, *J* = 22.4 Hz, 5F), -162.46 (t, *J* = 22.5 Hz, 10F)**. UV-Vis** (DMSO): λ_{max} (ε) L mol^{-1} cm^{-1} = 542 (270,000) and 731 (24,000). **Crystal data:** $C_{67}H_{34}F_{25}KO_6S_5$ (*M*r=1609.34), orthorhombic, space group *P 2(1) 2(1) 2(1)* (no. 19), *a* = 7.987(9), *b* = 24.64(3), *c* = 45.16(5) Å, *V* = 8888(17) $Å^3$, *Z* = 4, *T* = 100(2) K , D_{calcd}=1.203g cm^{-3}, R_1 = 0.1444 (I>2sigma(I)), R_w (all data) = 0.3137, GOF = 0.921.

II.5 ^{1}H NMR (500 MHz, acetone-d_6, 293K): δ= 7.09 (s16H).**^{19}F NMR** (471 MHz, acetone-d_6) δ -141.20 (d, *J* = 13.8 Hz), -155.66 (t, *J* = 20.1 Hz), -163.23 (t, *J* = 18.7 Hz). **UV-Vis** (DCM): λ_{max} (ε) L mol^{-1} cm^{-1} = 546 (130,000).

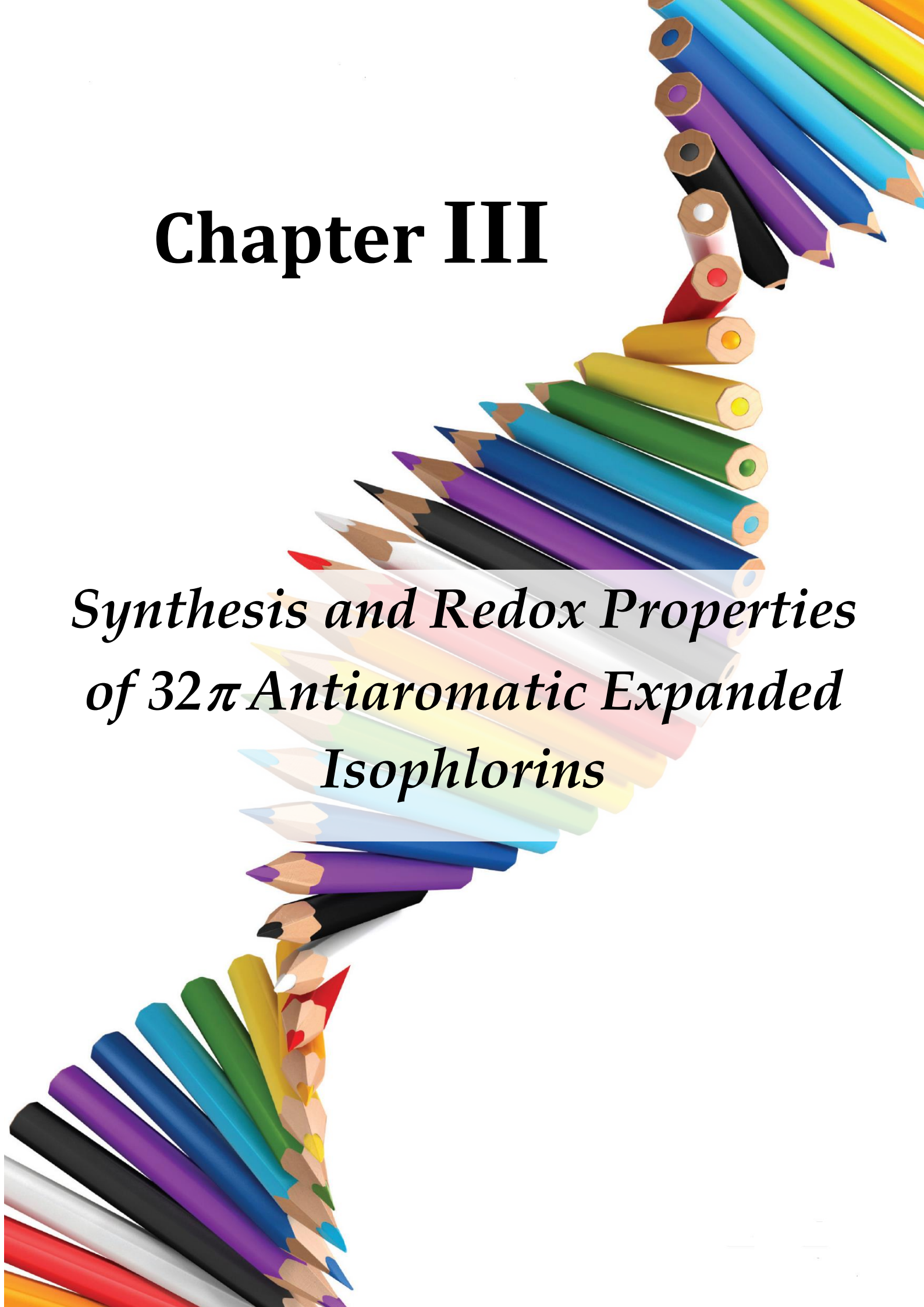

Chapter III

Synthesis and Redox Properties of 32π Antiaromatic Expanded Isophlorins

III.1. Introduction:

In the previous chapter, synthetic details of expanded isophlorins derived from thiophene sub-units were described along with their structural characterization. It can be envisaged that the length of the conjugated pathway in macrocyclic oligothiophenes can be extended by replacing few of the *meso* carbon atoms with ethylene (or) acetylene linkages. Replacing two *meso* carbon atoms of **II.3** [12] by ethylene bridges increases the π-count from 30 to 32 π-electrons (**Scheme-II.1**). This can induce altered ring current effects in the macrocycle due to the change from (4n+2) to 4n number of π electrons. Earlier attempts by Märkl and co-workers[23, 54] demonstrated the synthesis of such 32π tetraoxa annulenes by varying the number of ethylene linkages between two bi-furan units. However, it was discovered that such macrocycles adopt a flexible structure as analyzed from their ^{1}H NMR spectra. They could identify at least two or more structural isomers for a variety of 32π tetraoxa annulenes. As per IUPAC nomenclature[55], fluxional behavior is also considered as characteristic feature of antiaromatic molecule. In this context, synthesis of planar and rigid 32π annulenes by using simple cyclization methods remains a synthetic challenge.

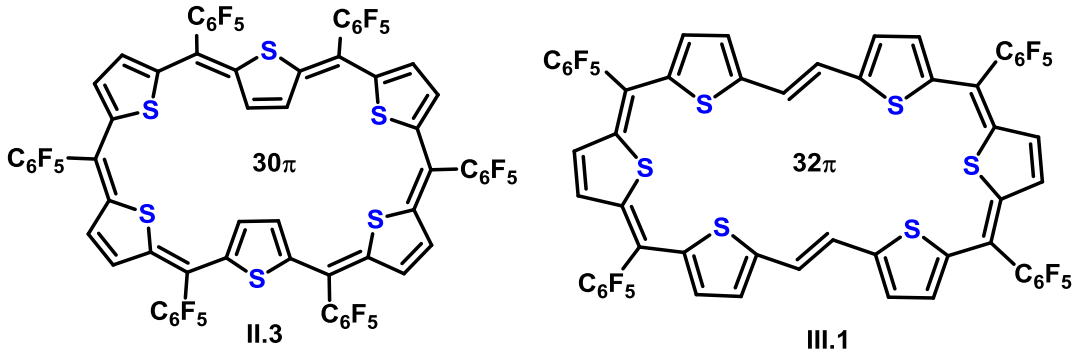

Scheme-III.1: 30π and 32π Expanded Isophlorins.

III.2. Syntheses:

In a process similar to modified Rothemund type synthesis[40], (**Scheme-III.2**), diols of five membered heterocycles were condensed with ethylene bridged bis-thiophene under dilute conditions. An equimolar concentration of (*E*)-1,2-di(thiophen-2-yl)ethene[56] and the corresponding diol were dissolved in 100 ml dry dichloromethane and degassed with Argon for ten minutes. Then, a catalytic amount of boron trifluoride diethyl etherate ($BF_3.OEt_2$) was added under dark using a syringe. After stirring for an hour, two equivalents of DDQ were added and stirring continued for an additional two hours. Apart from the expected product, low yields of larger macrocycles were also detected in the MALDI-TOF mass spectrum of the reaction mixture. Then, few drops of triethyl amine were added and the resultant solution

was passed through a short basic alumina column. This mixture was concentrated and further purified by silica gel column chromatography using CH_2Cl_2/hexane as eluent. By employing this procedure three different expanded isophlorins **III.1**, **III.2** and **III.3** (**Scheme-III.2**) could be synthesized with varying ratio of heterocyclic units. The reaction was also studied to explore the role of substituents on the thiophene rings in the formation of the macrocycles. β-methyl substituted derivatives **III.5** and **III.6** (**Scheme-III.3**) were synthesized by reacting (*E*)-1,2-bis(3-methylthiophen-2-yl)ethene, with thiophene (or) furan diols respectively. The other expanded isophlorins having more number of furan sub-units **III.6**, **III.7** and **III.8** (**Scheme-III.4**) were synthesized by condensing (E)-1,2-di(furan-2-yl)ethene either with thiophene or selenophene or furan diol under similar conditions.

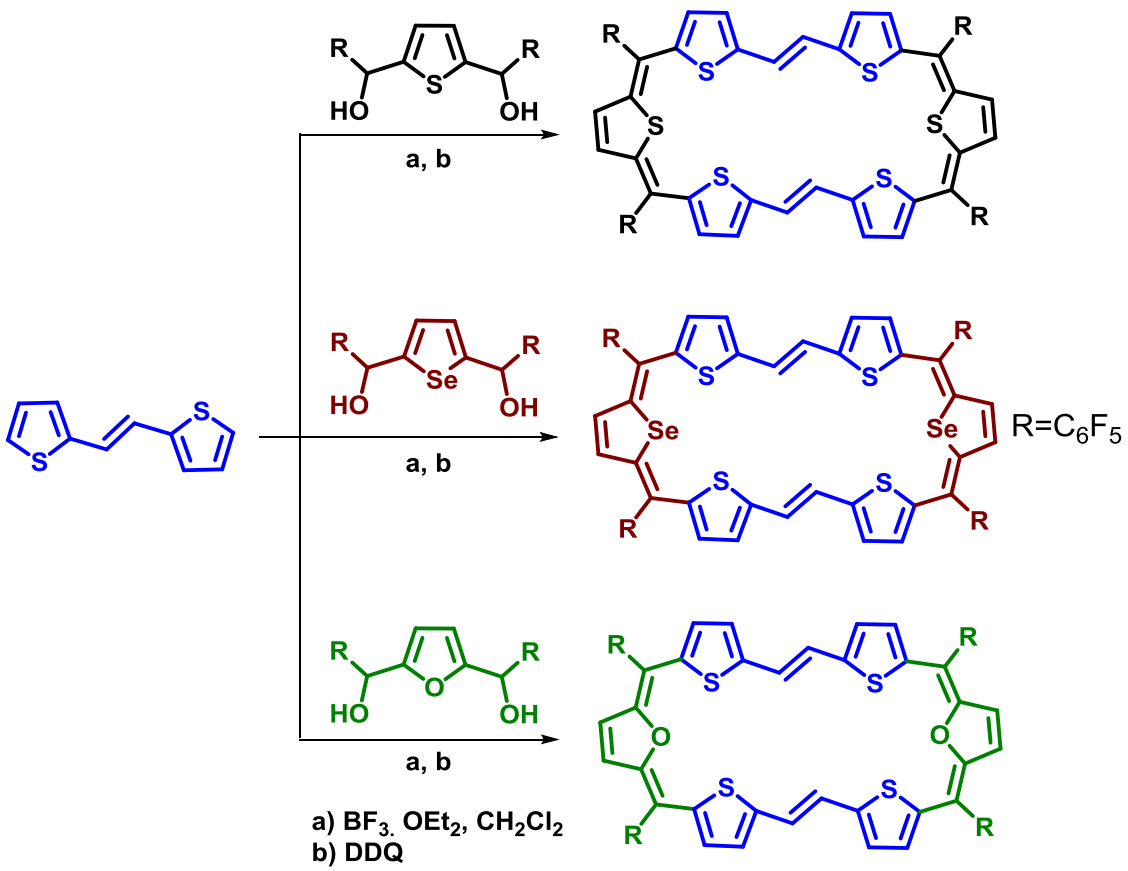

Scheme-III.2: Acid catalysed synthesis of 32π Expanded Isophlorins **III.1** - **III.3.**

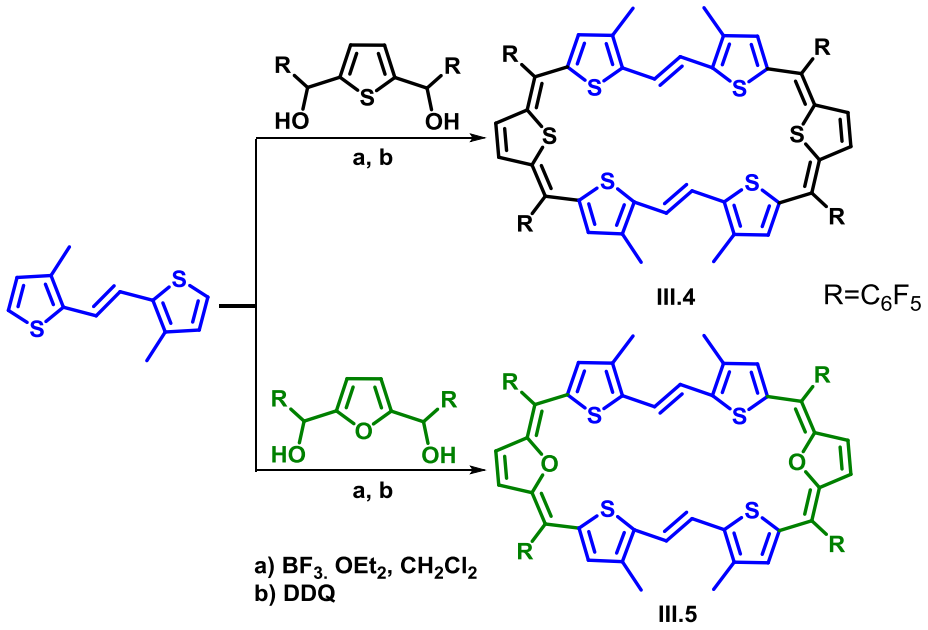

Scheme-III.3: Acid catalysed synthesis of 32π Expanded Isophlorins **III.4** - **III.5.**

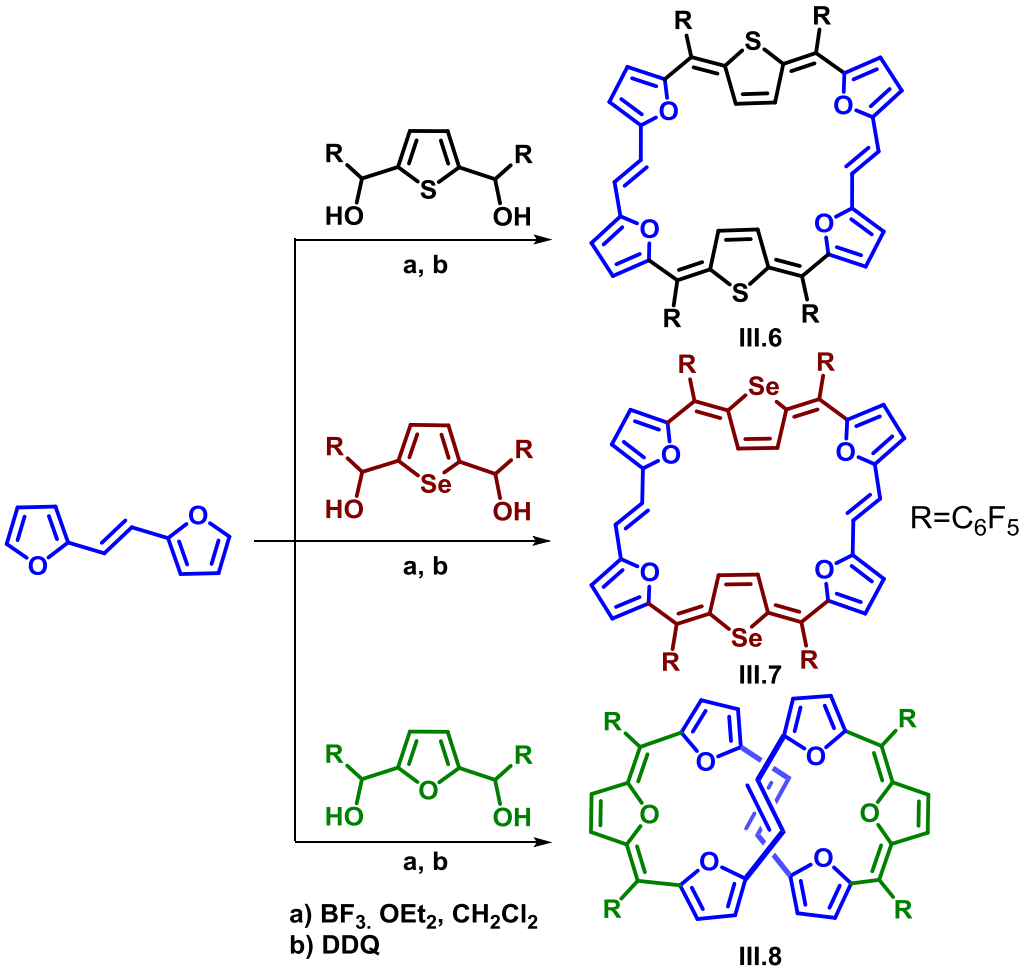

Scheme-III.4: Acid catalysed synthesis of 32π Expanded Isophlorins **III.6** - **III.8.**

Results and Discussions:

III.3. Spectral Characterization:

All the above molecules were analyzed by high resolution mass spectrometry, UV-Vis, NMR spectroscopy, cyclic voltammetric studies and single-crystal X-ray crystallography. High resolution mass spectrometry established the exact compositions of all these expanded isophlorins.

III.3.1 NMR Characterization

All the macrocycles, **III.1**- **III.8**, formally account for 32π electrons along the conjugated pathway and are hence considered to be antiaromatic systems. The hexa-thiophene expanded isophlorin **III.1** displayed only four signals in its ^{1}H NMR spectrum **(Figure-III.1)**, at 298K, indicating highly symmetrical structure in solution state. Two doublets at δ 5.97 and 5.62 ppm and two singlets at δ 5.59 and 8.76 ppm corresponding to four protons each were observed in the room temperature ^{1}H NMR spectrum. As expected of an antiaromatic macrocycle, the protons of the ethylene bridge must experience ring current effects and hence resonate at different chemical shift values. At the same time, the symmetry of this planar molecule suggested four doublets and a singlet corresponding to the protons on thiophene rings could be expected in is ^{1}H NMR spectrum. The observation of less than the expected number of signals led to the suspicion of fluxional behavior similar to that of tetraepoxy annulenes resulting in time averaged spectrum. ^{1}H NMR measurements at variable (low) temperature **(Figure-III.2)** confirmed the fluxional nature of the macrocycle. The intensity of the broad signal at δ 8.76 ppm decreased gradually and vanished at 253K. Upon further reduction in temperature to 175K, two new doublets were observed at δ 12.83 and 5.37 ppm, while the rest of the signals also doubled, indicating a rigid and stable conformation for the macrocycle. ^{1}H-^{1}H 2D COSY spectrum **(Figure-III.3)** at 175K displayed a strong correlation between the two doublets at δ 12.83 and 5.37 ppm. A difference of 7.5 ppm between the two peaks ascertained the paratropic ring current effect for the 32π system. Compared to the chemical shift values in the unsubstituted thiophene its protons in the macrocycle exhibited marked upfield shifts, which can be attributed to paratropic ring current effects as expected of 4nπ systems.

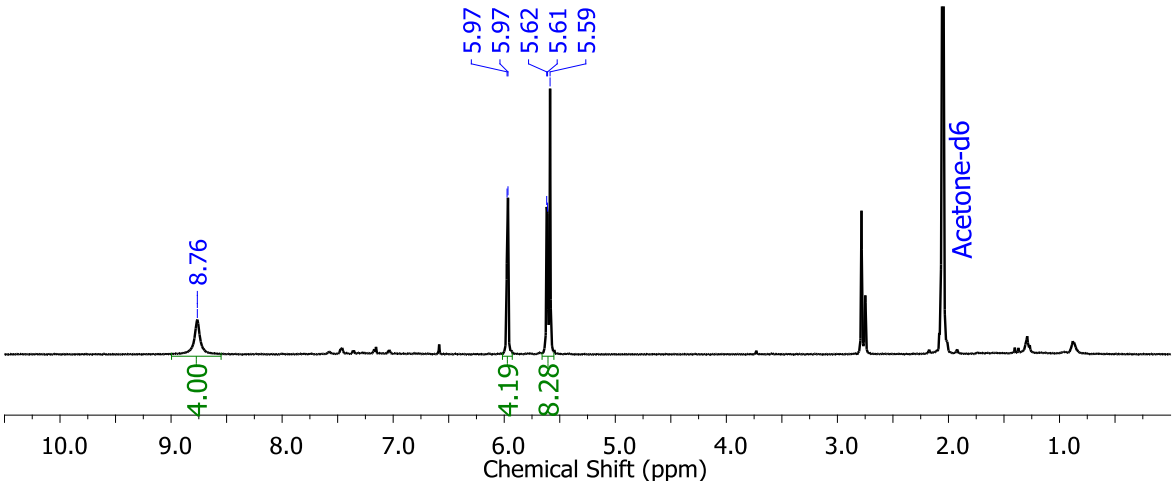

Figure-III.1: ^{1}H NMR spectrum of **III.1** in acetone-d_6 at 300K.

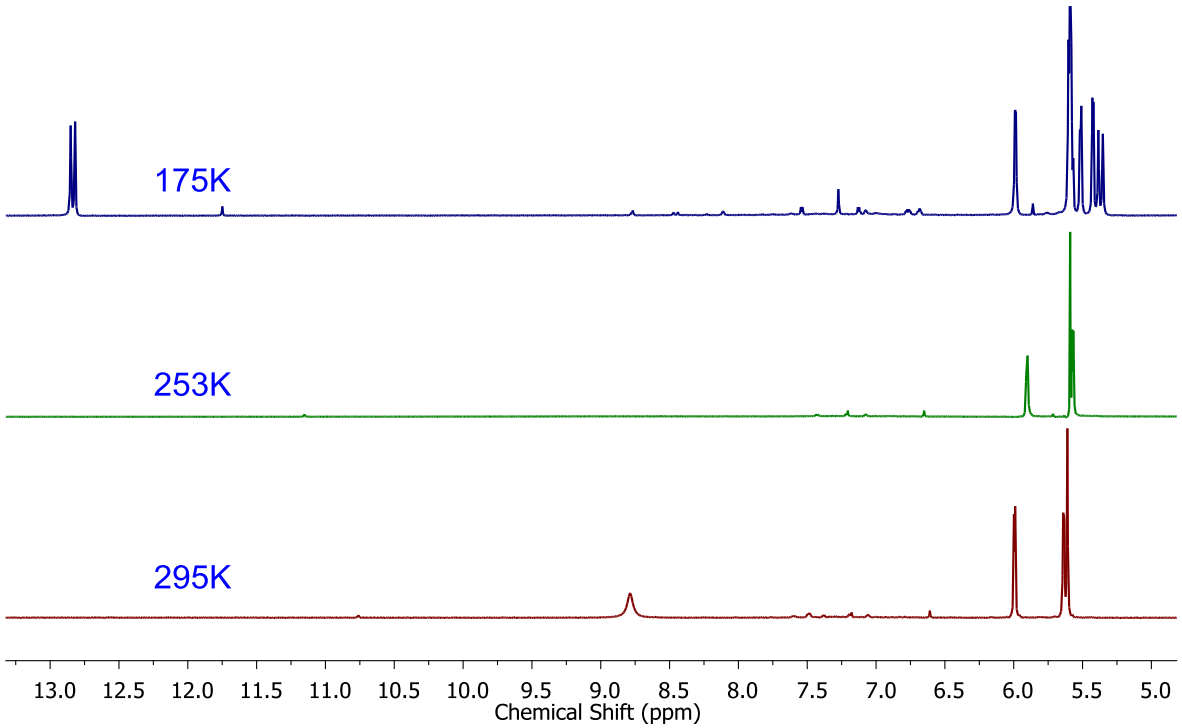

Figure-III.2: Variable temperature ^{1}H NMR spectra of **III.1** in acetone-d_6.

Further, the calculated coupling constant for the doublets at δ 12.83 and 5.37 ppm was found to be 16Hz[57]. Such a high value of the coupling constant and the large difference in their chemical shift values could be possible only for the ethylene bridged protons with an *E* conformation in the macrocycle. The large difference in the chemical shift values is attributed to the paratropic ring current effects expected of antiaromatic systems. ^{19}F NMR spectra displayed three different signals at -142.7 ppm, -156.42 ppm, and -163.31 ppm for corresponding ortho, meta and para substituted fluorines' of pentafluoro groups at both room temperature and lower temperatures.

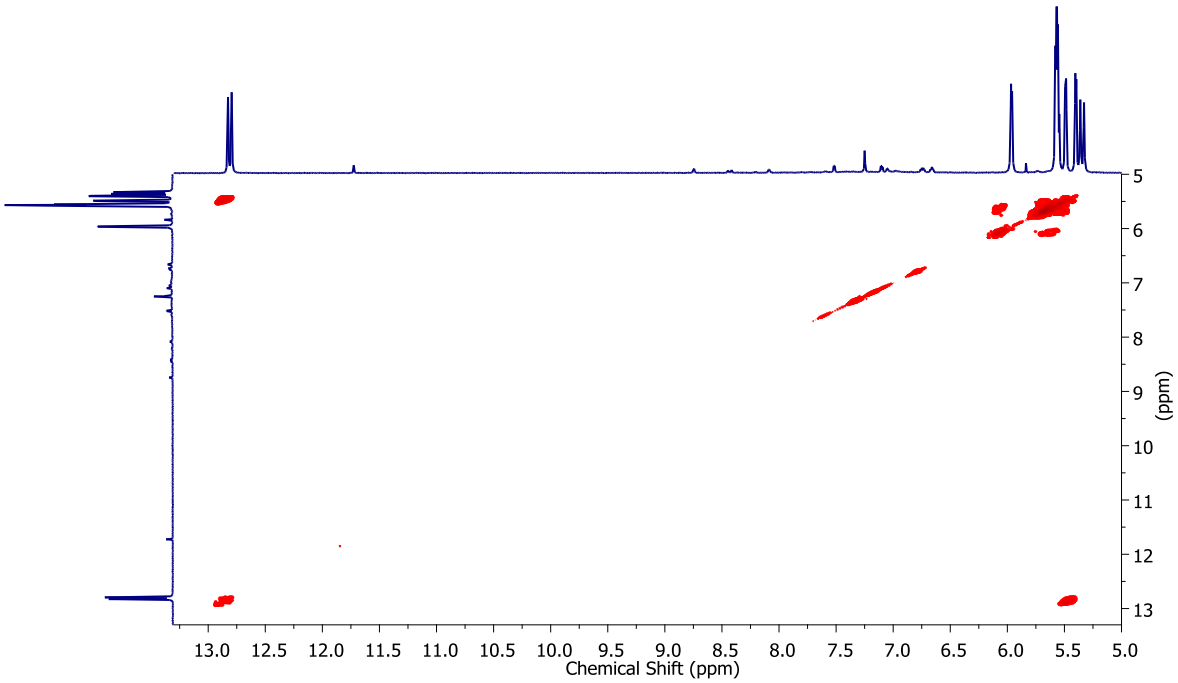

Figure-III.3: ^{1}H-^{1}H COSY spectrum of **III.1** in acetone-d_6 at 175K.

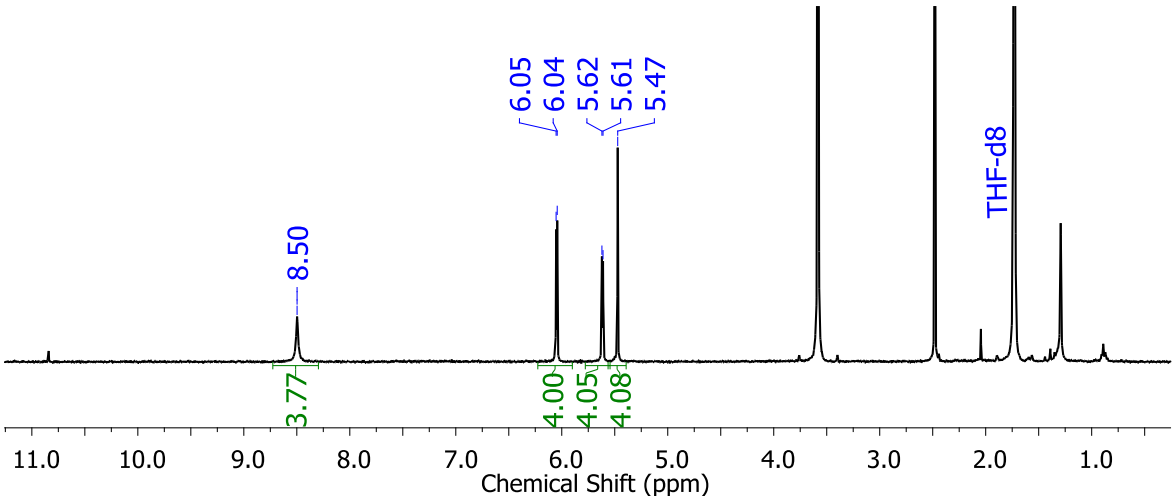

Figure-III.4: ^{1}H NMR spectrum of **III.2** in THF-d_8 at 300K.

III.2 also displayed ^{1}H NMR spectrum **(Figure-III.4)** similar to that of **III.1**. A broad singlet at δ 8.50 ppm corresponding to four protons of the ethylene bridge followed by two doublets at 6.05 and 5.62 ppm, each corresponding to two sets of four protons for the thiophene rings and a singlet at 5.47 ppm for the selenophene protons were observed. Variable temperature ^{1}H NMR studies also displayed similar results to that of **III.1.**

The ^{1}H NMR spectrum **(Figure-III.5)** of **III.3** displayed four different signals corresponding to equal number of protons in the region between δ 8-5 ppm. The protons of the thiophene rings, connected by ethylene carbons, resonated as two doublets at δ 6.75 and 6.40 ppm

suggesting weak paratropic ring current effects in the 32π macrocycle. A singlet for the protons of furan ring and the ethylene bridge was observed at δ 6.31and 8.01 ppm. In contrast to **III.1**, the signal at 8.01 ppm for **III.3** did not split into two signals even at 183K **(Figure-III.6)** suggesting rapid flipping of the ethylene bridge even at low temperatures.

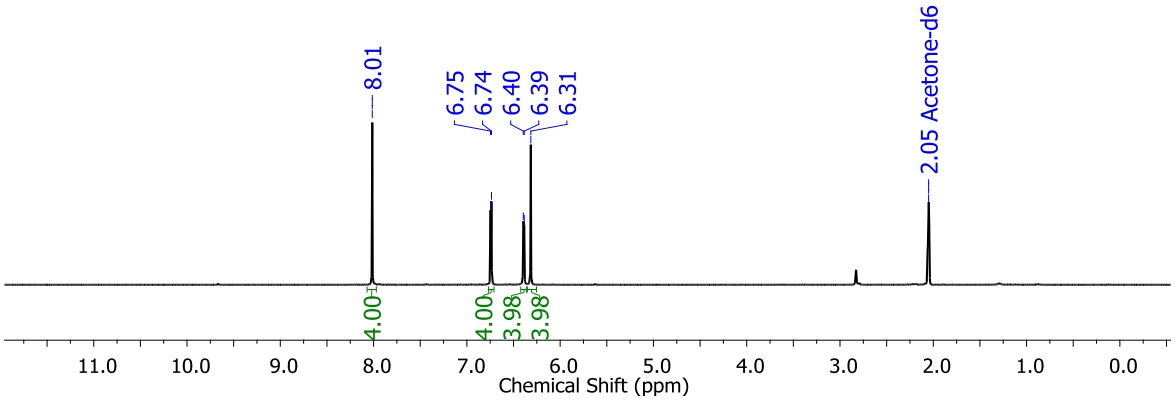

Figure-III.5: ^{1}H NMR spectrum of **III.3** in acetone-d_6 at 293K.

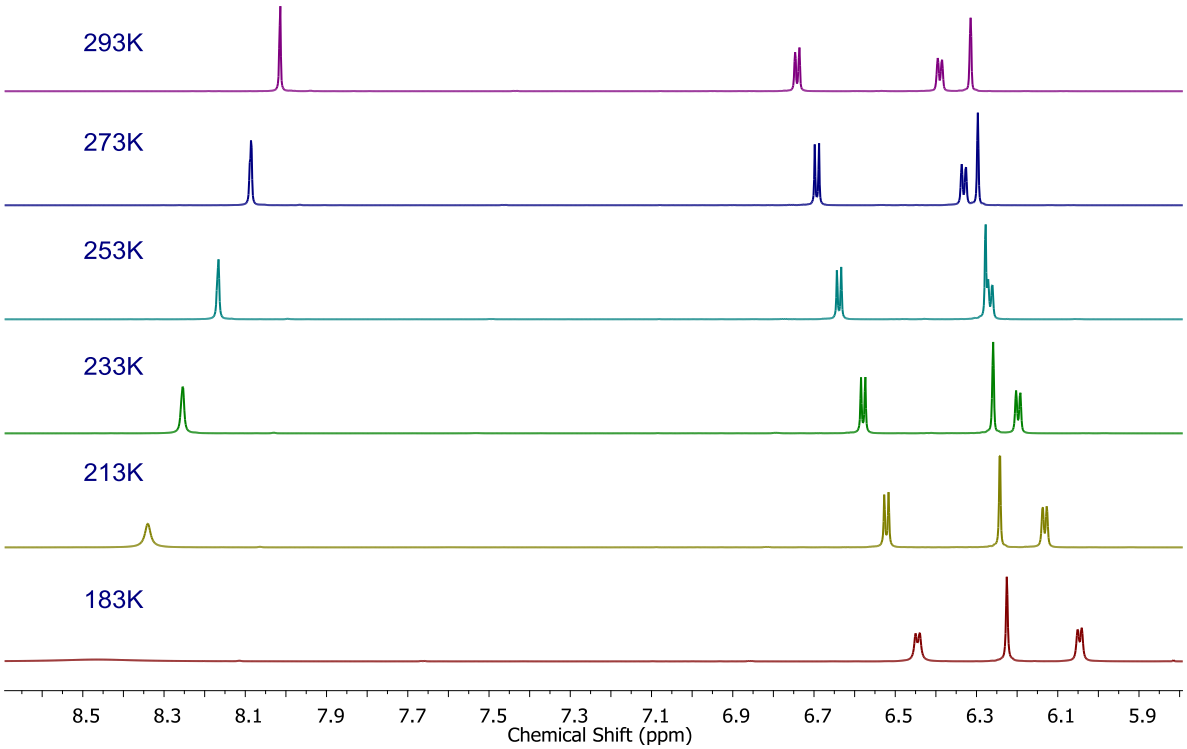

Figure-III.6: Variable temperature ^{1}H NMR spectra of **III.3** at acetone-d_6.

To understand the effect of substituents on the macrocyclic structure, methyl substituted thiophenes were employed to synthesize the 32π macrocycles. However, the ^{1}H NMR spectrum of **III.4 (Figure-III.7)** did not reveal any significant changes to its macrocyclic framework compared to **III.1**. A symmetrical spectrum with three singlets at δ

8.35 and 5.12 ppm corresponding to protons of the thiophene were observed. The β-methyl protons were found to resonate as a singlet at δ 1.55 ppm, while the ethylene bridged protons were found to resonate as a broad singlet at 8.35 ppm. This signal was resolved into two singlets upon lowering the temperature, suggesting the fluxional behavior of **III.4** akin to **III.1**.

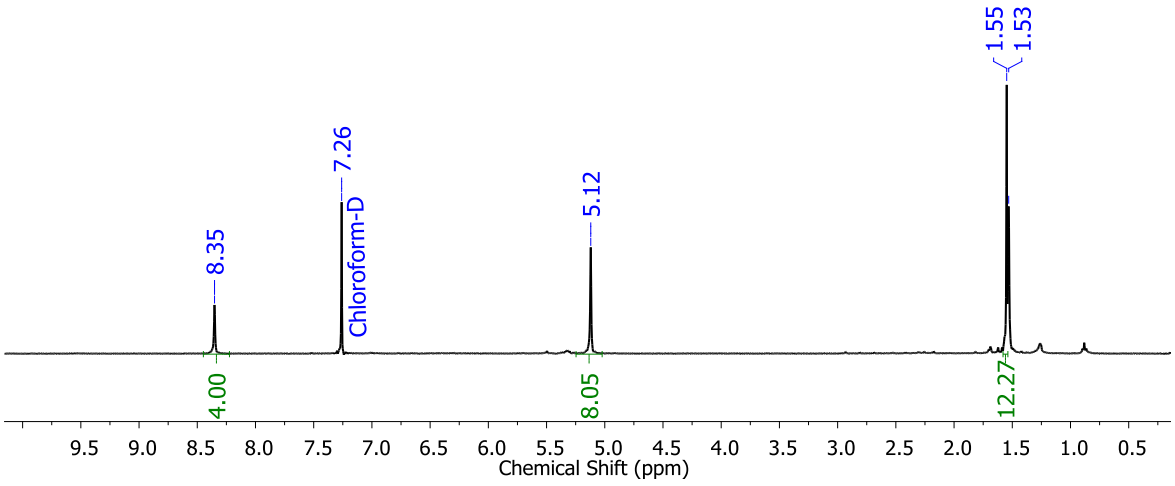

Figure-III.7: ^{1}H NMR spectra of **III.4** in $CDCl_3$ at 293K.

Replacement of bisthiophene unit in **III.1** by bisfuran yielded **III.6**. Its ^{1}H NMR at 293K displayed signals in the region between δ 13-5 ppm **(Figure-III.8)**. Unlike **III.1**, its ^{1}H NMR consisted of a sharp singlet at δ 12.61 ppm, a doublet at 4.92 ppm and broad signals at 11.80 and 5.43 ppm. This indicated solution state dynamics at room temperature. Upon reducing the temperature to 220K, eight doublets corresponding to two protons each were observed at δ 13.24, 13.14, 12.42, 5.52, 5.28, 5.00, 4.91 and 4.89 ppm **(Figure-III.8)**. The increase in the number of signals signified reduced symmetry and a modified conformation of the macrocycle when the ethylene bridged thiophene sub-units are replaced by furans in **III.1**. ^{1}H-^{1}H 2D COSY spectrum revealed four sets of correlations **(Figure-III.9)**. The calculated coupling constant for the cross-correlated signals at δ 12.42 and 5.00 ppm was found to be 16 Hz. Combined with a Δδ value of 7.42 ppm, it strongly supported the *E* conformation of the ethylene bridge and paratropic ring current effects expected of planar 4nπ systems. The low-field signals at δ 13.23 and 13.13 ppm coupled to each other implied the effect of paratropic ring current effect on the protons of heterocyclic rings with an inverted configuration.

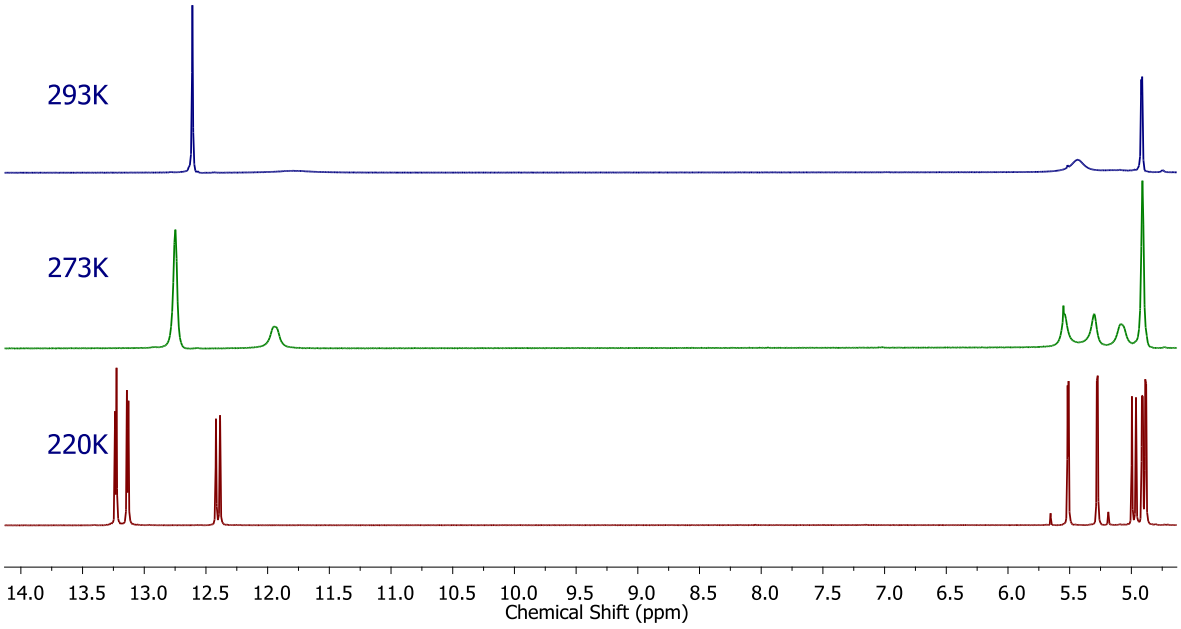

Figure-III.8: Variable temperature ^{1}H NMR spectra of **III.6** at THF-d_8.

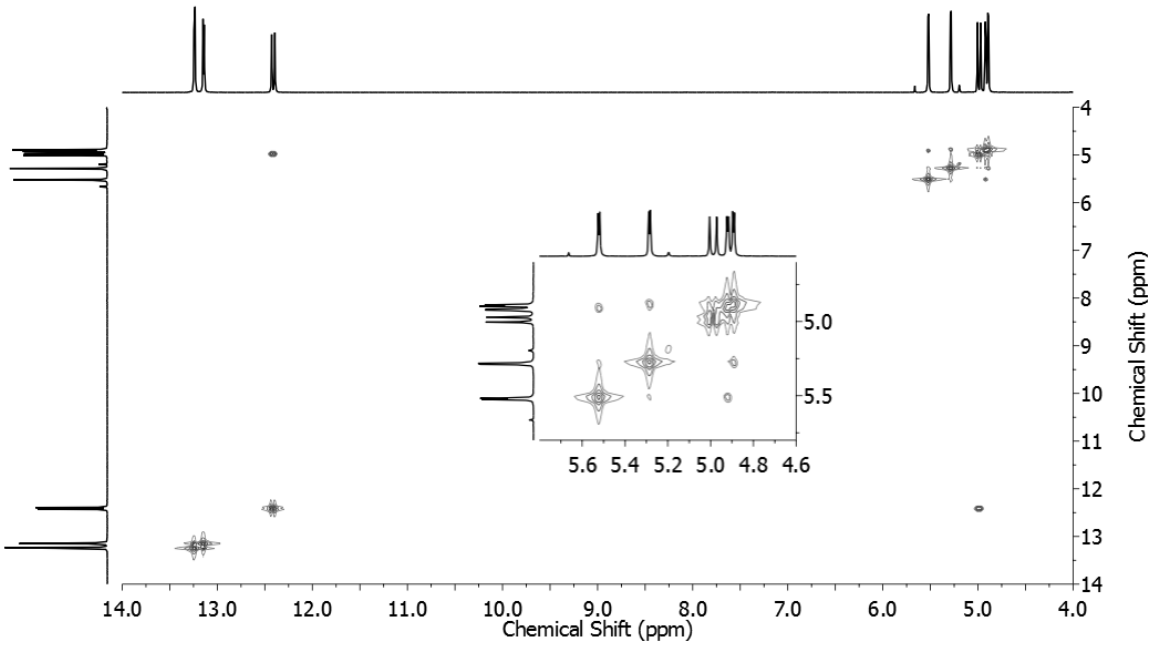

Figure-III.9: ^{1}H-^{1}H 2D COSY spectrum of **III.6** in THF-d_8 at 220K.

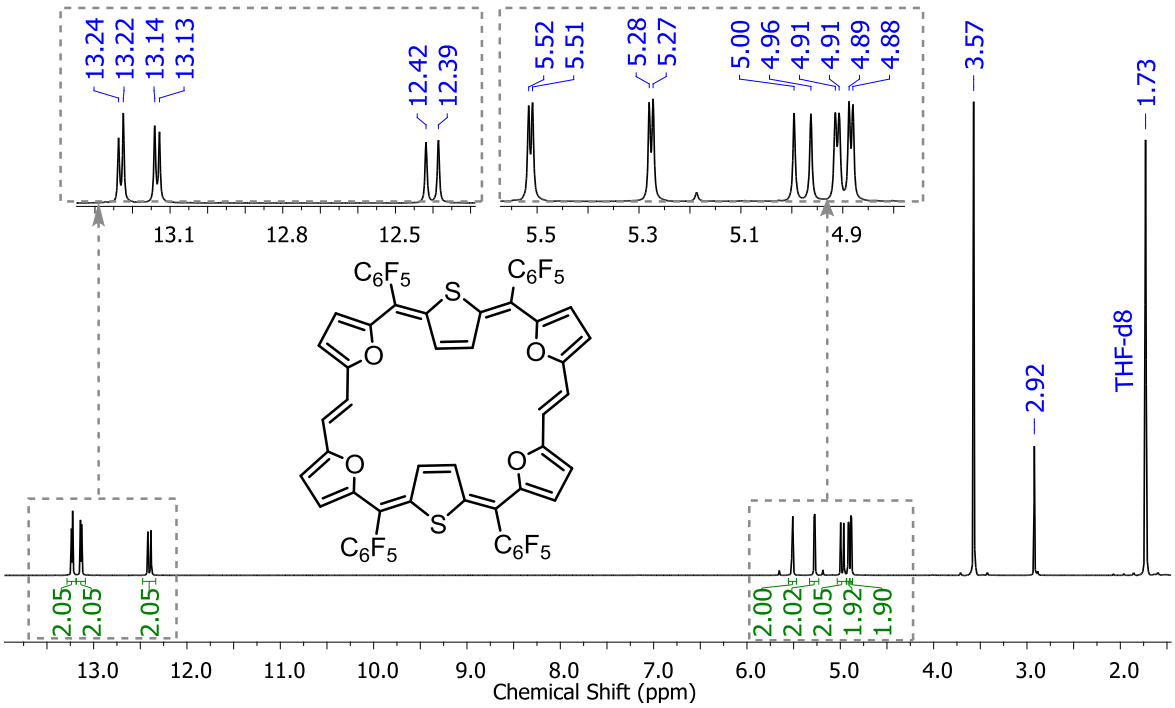

Figure-III.10: ^{1}H NMR spectrum of **III.6** in THF-d_8 at 220K.

The ^{19}F NMR spectra **(Figure-III.11)** of **III.6** exhibited three different signals at -141.1 ppm, -154.84 ppm, and -162.51 ppm for the ortho, meta and para substituted fluorines of pentafluoro groups.

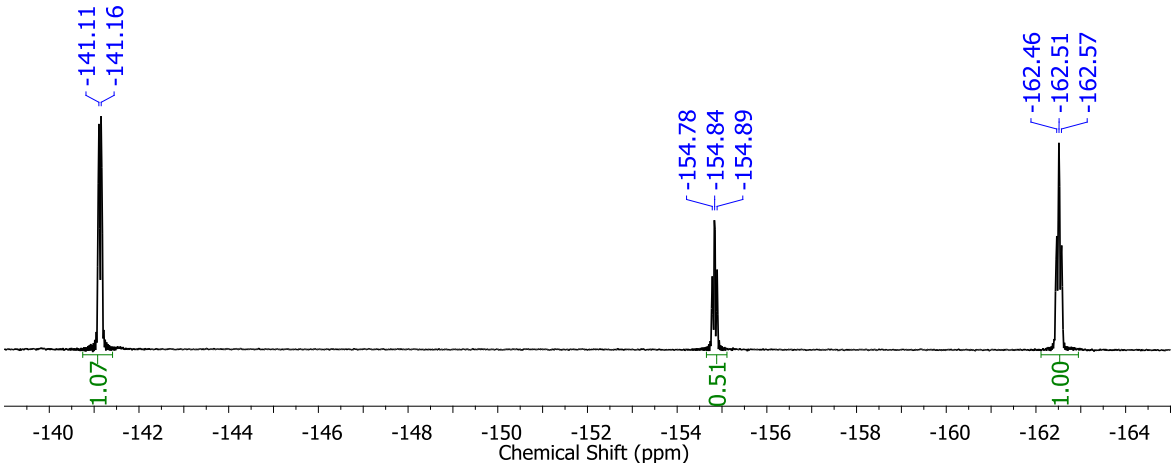

Figure-III.11:^{19}F NMR spectrum of **III.6** in THF-d_8 at 293K.

^{1}H NMR spectrum of **III.7** at 230K **(Figure-III.12)** also displayed eight doublets corresponding to two protons each. They were observed at δ 12.60, 12.52, 11.69, 5.71, 5.44, 5.28, 5.07 and 5.05 ppm similar to that of **III.6.**

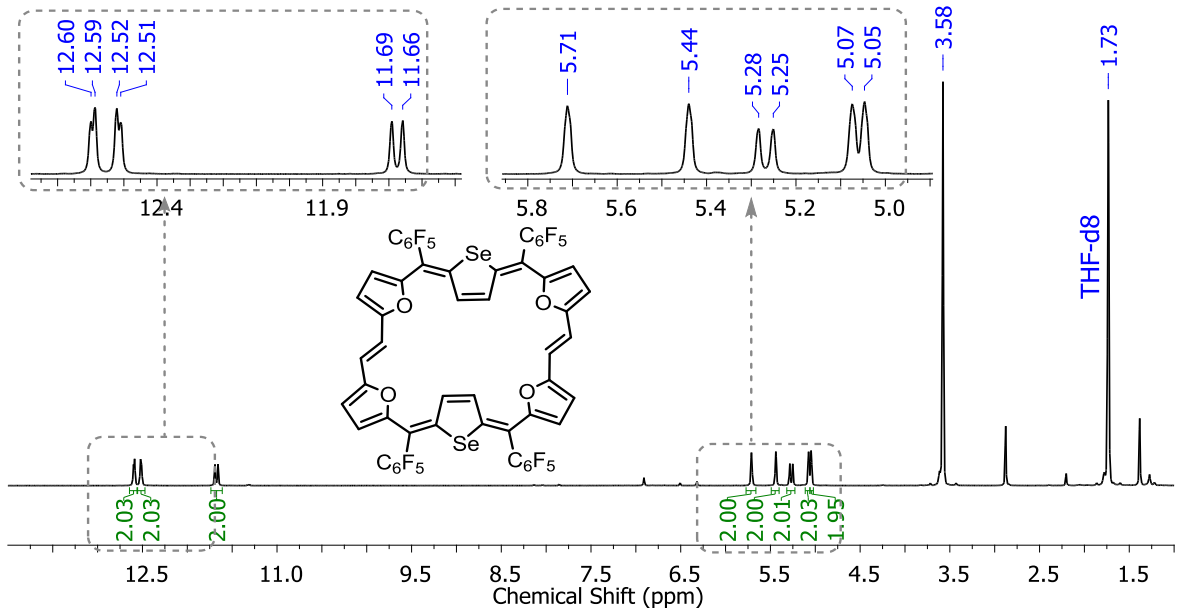

Figure-III.12: ^{1}H NMR spectrum of **III.7** in THF-d_8 at 230K.

In comparison to the macrocycles mentioned above, the hexafuran macrocycle **III.8** displayed a spectrum uncharacteristic of ring current effects. Its ^{1}H NMR spectrum at room temperature **(Figure-III.13)**, revealed two doublets and two singlets in the region between δ 7.5 and 3.5 ppm. Precisely, this observation suggested a highly symmetrical structure for **III.8** devoid of significant paratropic ring current effects. Poor solubility of the molecule in a variety of deuterated solvents prevented its variable (low) temperature NMR measurements.

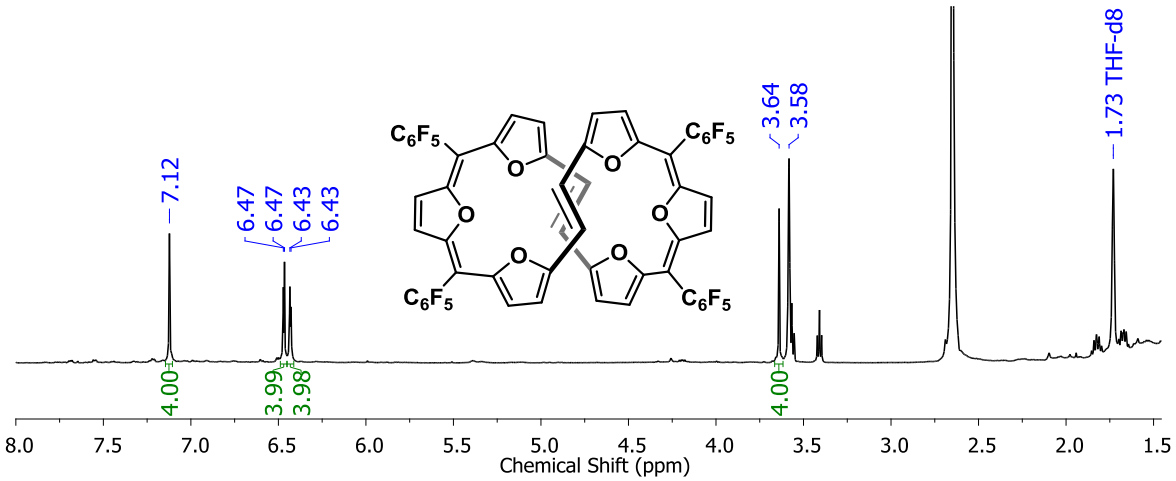

Figure-III.13: ^{1}H NMR spectrum of **III.8** in THF-d_8 at 300K.

Trifluoroacetic acid (TFA) was added to a solution of **III.8** to improve its solubility. Upon its addition, the color of the solution dramatically changed from the brownish-red to a deep-blue color. The mass spectrum of acidified **III.8** did not differ from its neutral form, suggesting no addition of protons to the free base. It displayed three signals in the upfield region at δ -9.93, -6.42, -6.02 ppm along with five other resonances in the down field region at δ 11.31, 11.42, 11.54, 12.40 and 14.04 ppm **(Figure-III.14)**. Since the number of signals was equal to that as observed for **III.6** at low temperature, a similar structural conformation can be envisaged for **III.8** upon addition of TFA. No additional signals for the hydrogens in the protonated form of the macrocycle were observed in ^{1}H NMR spectrum of **III.8** recorded with TFA at room temperature. Its ^{1}H-^{1}H 2D COSY spectrum confirmed the coupling between the doublets at δ -9.93 and 14.00 ppm. A large Δδ value of 24 ppm between these signals with a coupling constant of 16 Hz suggested *E* conformation of the ethylene bridge. However, the large difference in their chemical shift unambigously reflected a strong ring current effect in the macroccycle. Even though they are formally 32π antiromatic macrocycles, such a large difference in the chemical shift values were not not observed in the above mentioned macrocycles (**III.1**-**7**) in their respective neutral states. But a dramatic change in the color of the solution suggested a significant chemical change in the macrocycle.

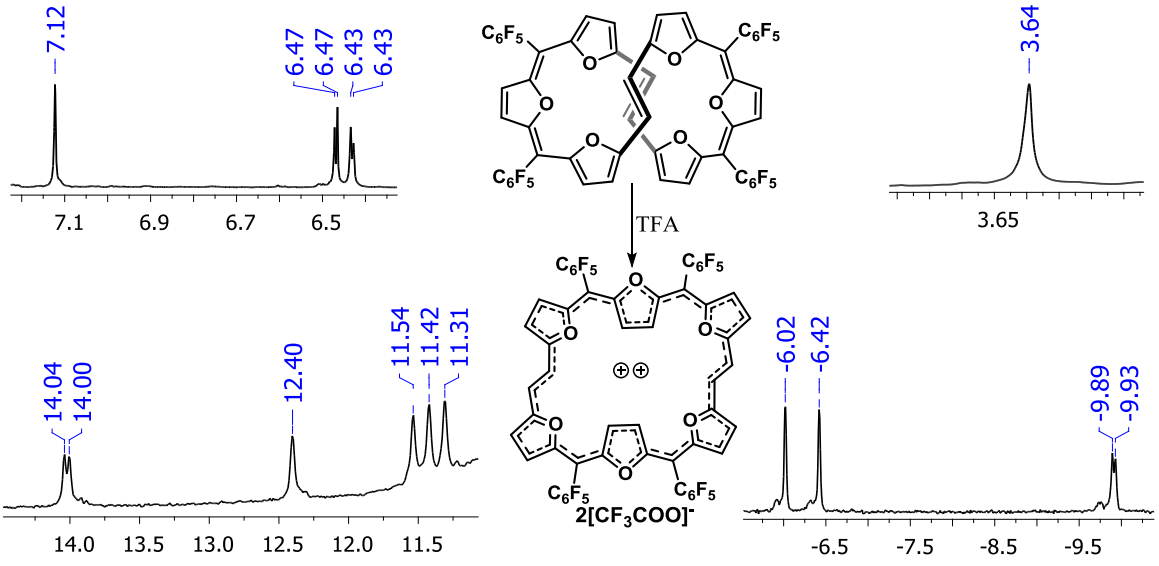

Figure-III.14: ^{1}H NMR spectral changes upon the addition of TFA to **III.8.**

Encouraged by this observation, we recorded the ^{1}H NMR for **III.6** in the presence of TFA **(Figure-III.15)**. Interestingly, this macrocycle also displayed a similar remarkable change in

its color and NMR spectrum, confirming an analogous renovated electronic structure of the macrocycle. However, the number of signals corresponding to the macrocycle remained the same as before the addition of the acid. The ^{1}H NMR spectrum of **[III.6]**$^{2+}$ recorded in *d*-TFA at 298K revealed a spectral pattern akin to **[III.8]**$^{2+}$. Eight doublets were observed, out of which five were in the low field region at δ 15.66, 13.75, 12.69, 12.34 and 12.18 ppm and three doublets in the upfield region δ at -6.41, -6.81 and -9.85 ppm **(Figure-III.15)**. From its ^{1}H-^{1}H 2D COSY spectrum it could be recognized that the drastically up-field shifted signals at δ -6.41 and -6.81 ppm were coupled to each other. The extreme two doublets at δ 9.85 and 15.66 ppm with a coupling constant of 16 Hz corresponded to the inner and outer protons of the ethylene bridge. A Δδ of 25.5 ppm was found to be more than three times the difference observed (Δδ = 7.4 ppm) for **III.6**. The apparent shielding and deshielding of the protons is ascribed to the significant change in ring current upon the addition of TFA.

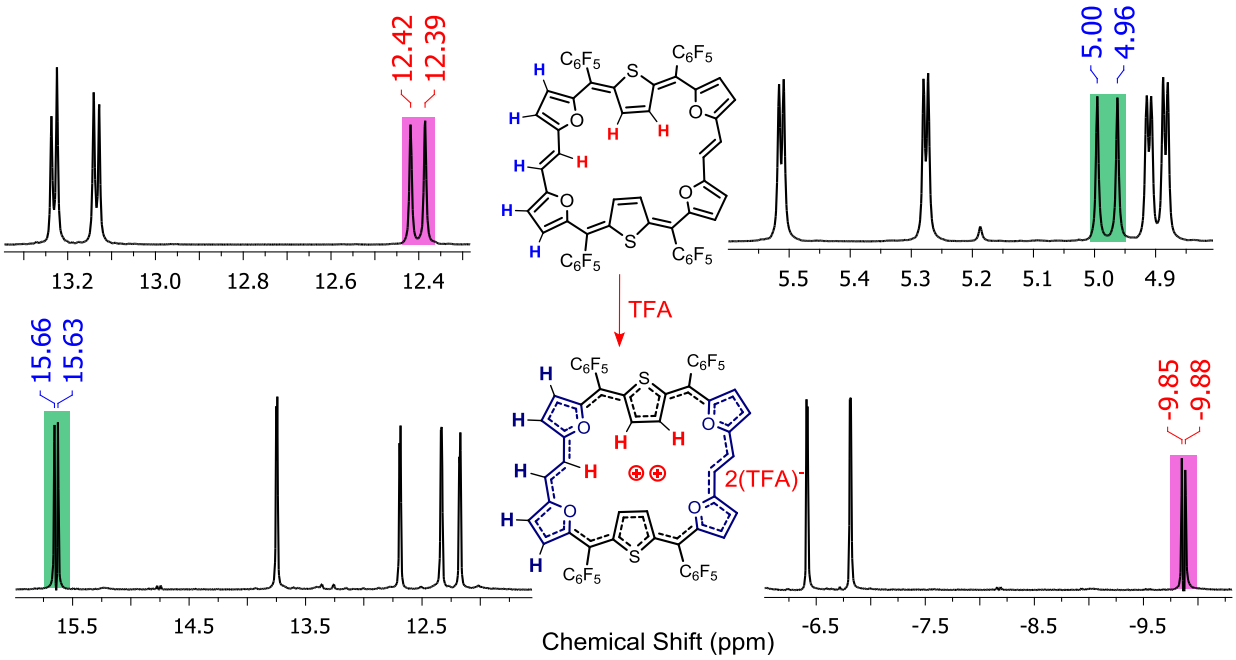

Figure-III.15: ^{1}H NMR spectral changes upon the addition of TFA to **III.6.**

The drastic change in the electronic properties suggested the reversed of ring current due to a two electron oxidation of the 4nπ system to a (4n+2)π dication. Such a prospect of oxidation can be feasible for two reasons: a) Isophlorins and tetra-epoxy annulenes were also known to undergo similar two electron oxidation in acidic medium. The 20π antiaromatic isophlorin was known to be oxidized by a mineral acid alone, hence Vogel coined the term "pseudo-metal" to form aromatic molecules from antiaromatic macrocycles[5a]. Even in such cases, a

drastic change in the chemical shift values were observed in their respective ^{1}H NMR spectrum. b) TFA's role as an oxidizing agent is rare, but possible[58]. It has been shown that oligo pyrroles undergo one-electron oxidation to form a radical cation. In this context, the macrocycles could undergo a similar oxidation to form a 30π aromatic dication. It could be observed that this reaction was feasible even under inert atmosphere suggesting the possibility of hydrogen evolution to complement ring oxidation through a radical mechanism. [$Et_3O^+SbCl_6^-$] is well known to oxidize aromatic hydrocarbons to their respective cation radicals[46]. Recent reports have revealed the oxidation of macrocyclic oligothiophenes to respective radical cation and bipolaron species[59]. Therefore the above macrocycles were subjected to oxidation in the absence of proton source. It was observed that the addition of TFA or [$Et_3O^+SbCl_6^-$] to **III.6** displayed similar color change and ^{1}H NMR spectrum at room temperature. The observation of a well resolved NMR spectrum clearly suggested the formation of diamagnetic species upon the oxidation of **III.6** by [$Et_3O^+SbCl_6^-$] to **[III.6]$^{2+}$.** The ^{1}H NMR spectrum of **[III.3]$^{2+}$** recorded with TFA at 298K displayed two signals at δ +15.46 and -9.58 ppm. A Δδ value of 25.0 ppm was observed between the chemical shifts of inner and outer ethylene protons **(Figure-III.16)**. Such a large difference in the chemical shift values could be possible only for the outer and inner ethylene protons respectively. The five other signals corresponding to β-hydrogens of furans and thiophenes were observed at δ 12.96, 11.80, 11.12, 11.02 and 10.43 ppm.

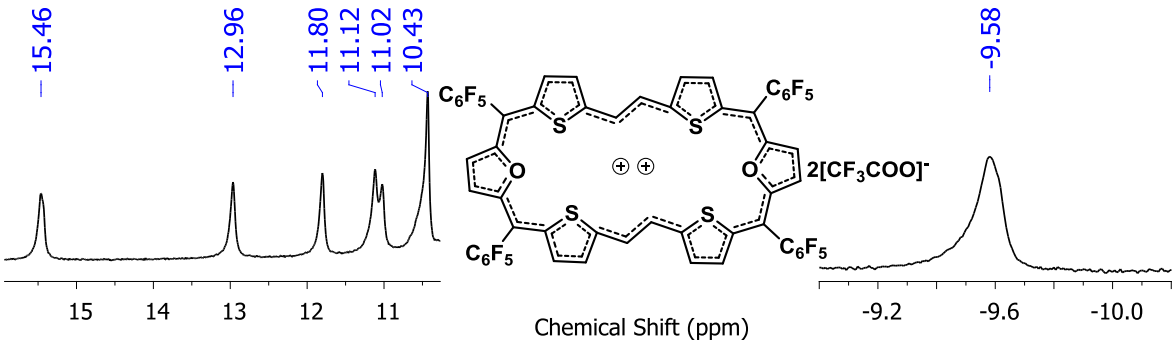

Figure-III.16: ^{1}H NMR spectrum of **[III.3]$^{2+}$** in THF-d_8 at 300K.

III.3.2. Single Crystal X-ray Diffraction Studies:

The molecular structure of all these macrocycles **III.1-III.8** and their trifluoroacetate salts were unambiguously determined from single crystal X-ray diffraction studies. Good quality single crystals were grown from suitable solvent combinations. **III.1** exhibited a planar structure with the sulfur atoms of all the thiophene pointing towards the center **(Figure-III.17)**. The macrocycle adopted a rectangular shape due to the lengthy bis-thiophene units. Both the ethylene bridges in this macrocycle sustained *E* conformation similar to that of the precursor **(E)-1,2-di(thiophen-2-yl)ethene**. A comparison of the carbon-carbon (C-C) bond length in the precursor, and their corresponding macrocycles substantiated the delocalization of π electrons in the cyclic systems. The C_β-C_β bond length of 1.46Å in **(E)-1,2-di(thiophen-2-yl)ethene** was reduced to 1.39Å in hexa thiophene **III.1**. It was observed that the distance between the two thiophene units decreased upon cyclization. Similar changes in bond lengths were observed for **III.2** and **III.4** too. The two pairs of diagonally opposite pentafluorophenyl rings form a dihedral angle of 78º and 67º with the plane of the macrocycle defined by the eight carbon atoms that connect the six thiophene rings.

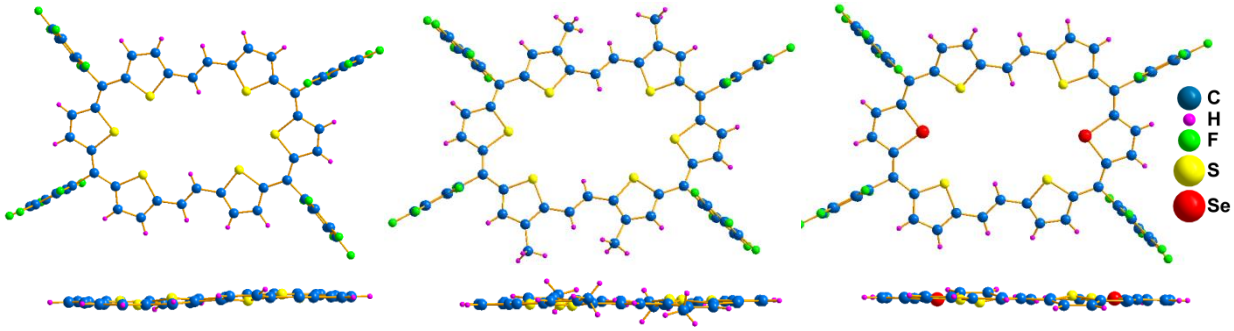

Figure-III.17: Molecular structure of **III.1** (left), **III.2** (right), and **III.5** (center). Solvents were omitted for clarity. Phenyl groups are omitted in the side view.

In the crystal packing, the cavity of each macrocycle is sandwiched by the near perpendicular orientation of pentafluorophenyl rings from two other macrocycles **(Figure-III.18)**, facilitating their *ortho* and *meta* fluorine atoms to be in close proximity to the cavity of the macrocycle. These four fluorines are found involved in weak non-covalent interactions (two bifurcated hydrogen bonds per hydrogen; 138º and 2.53Å; 2.6Å and 147º) with the hydrogens, on the ethylene bridge, pointing towards the center of the macrocycle. At the same time a distance of 3.11Å and 3.24Å was observed for F…S contacts between the *ortho* or *meta* fluorine atoms and the sulfur of the thiophene ring.

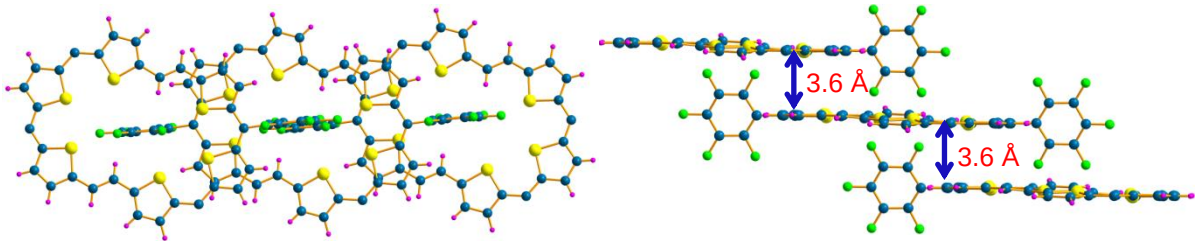

Figure-III.18: Non-covalent interactions in **III.1** top view (left) and side view **III.2** (right). Solvents are omitted for clarity.

These observations lead to four interesting scenarios: *a)* for the first time in isophlorinoids, intermolecular non-covalent interactions between two macrocycles are observed without hydrogens; *b)* the heteroatoms from the core of the macrocycle are directly involved in the intermolecular contacts[60]; *c*) the four fluorines are found within a distance of just 1.5Å (above and below) from the mean macrocyclic plane, suggesting F…π interactions[61]; *d)* offset type π stacking between two macrocycles, that share the F…S contacts, was observed in the crystal packing of **III.1**. The plane formed by the two thiophene rings adjacent to pentafluorophenyl ring (involved in F…S interactions) was found to overlap with a similar plane from another macrocycle with an inter-planar distance of 3.6Å **(Figure-III.18)**. This distance is very similar to the value expected for offset type π stacking in aromatic molecules.

The macrocycle **III.3** also displayed a planar structure with arrangement of heterocycles **(Figure-III.19)** such that all the heteroatoms were facing the center of the macrocycle similar to that of **III.1**. It crystallized in triclinic system with a centro symmetric P-1 space group and adopted a rectangular shape. However, **III.3** is more elongated than **III.1**, due to the increased length between the diagonally opposite furans and a contraction between the opposite bis-thiophene units. It was observed that the distance between the sulphur atoms of the ethylene bridged thiophenes increased from 5.62Å in **III.1** to 5.96Å in **III.3**. Contrary to **III.1, III.2,** and **III.4** no π-stacked intermolecular interactions were observed in **III.3**. Instead, strong C-H...F (2.40 Å, 154^{o}) intermolecular interactions were observed which can be due to the contraction in the distance between the two opposite thiophenes from 4.82Å (**III.1**) to 3.55Å **(Table-III.1)**. The consequent stretching of the ethylene bridge encouraged its fluxional character and hence the NMR resonance of the ethylene protons could not be resolved even at 183K.

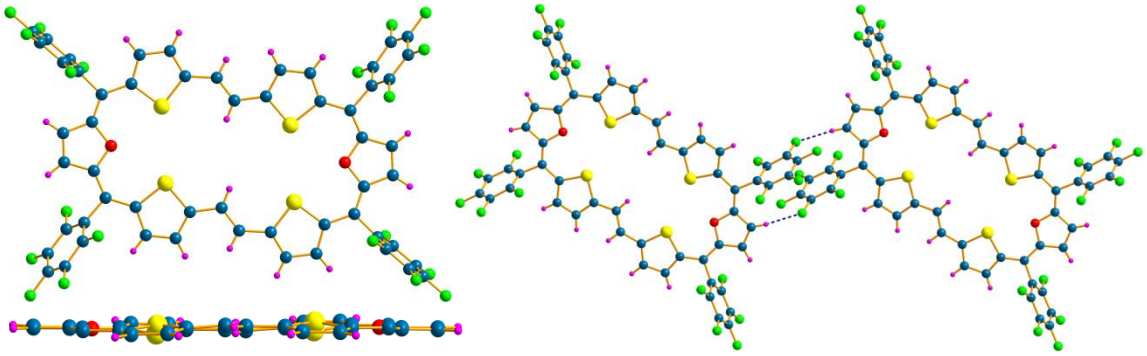

Figure-III.19: Molecular structure of **III.3** (left) and **C-H...F** interactions in **III.3** (right). Solvents are omitted for clarity.

The replacement of bisthiophene unit of **III.4** with **(**E)-1,2-bis(3-methylthiophen-2-yl)–ethene yielded **III.5.** This compound lost its planarity to adopt a bowl-like conformation. Two of the four thiophene units in bisthiophene unit were found to be inverted, which favored steric crowding in the molecule due to small cavity of the macrocyclic core leading to a non-planar conformation of the compound **(Figure-III.20)**.

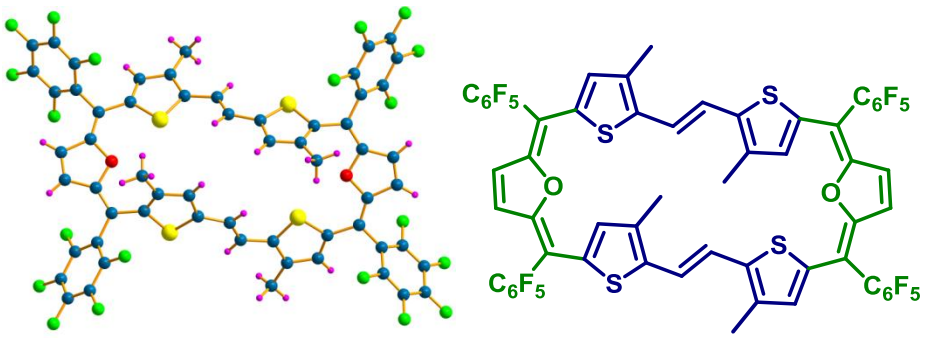

Figure-III.20: Molecular structure of **III.5**. Solvents are omitted for clarity.

The macrocycles **III.6** and **III.7** also formed planar structures with a square shape contrary to **III.1**. Supporting the ^{1}H NMR characterization, single crystal X-ray diffraction confirmed the ring inverted structures. The oxygen atoms of all the four furans point towards the centre and two thiophene rings are inverted such that their β-carbons are exposed to the centre of the macrocycle **(Figure-III.20)**. Both the ethylene bridges were found to sustain *E* conformation similar to that of the precursor bisfuran. In the crystal packing, it was observed that the large π-surface of bisfuran groups are involved in offset type π stacking with an inter-planar distance of 3.48Å and 3.42Å (**Table-III.1**) for **III.6** and **III.7** respectively **(Figure-III.21)**.

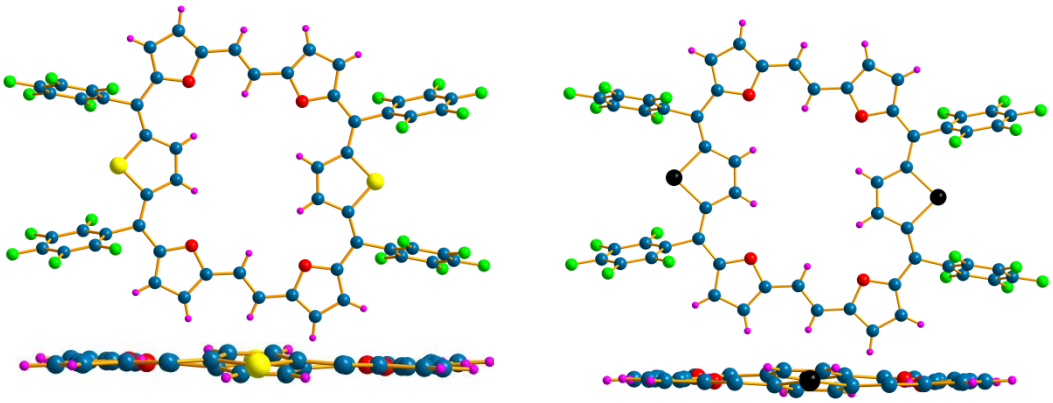

Figure-III.20: Molecular structuresof **III.6** (left) and **III.7** (right). Solvents are omitted for clarity.

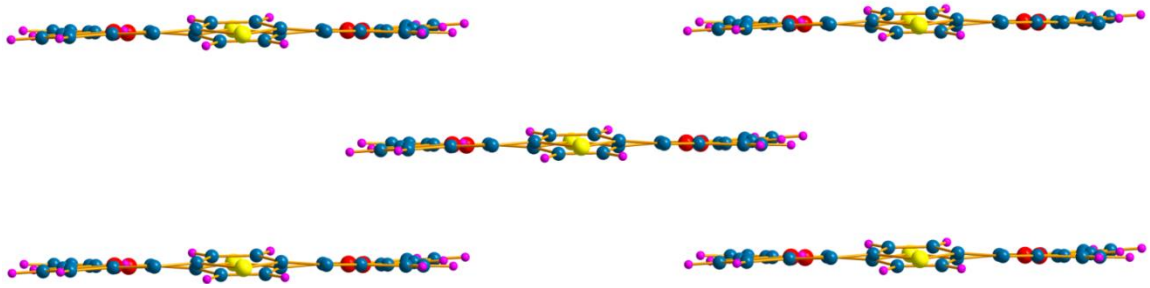

Figure-III.21: π-stacking of **III.6.** Phenyl groups and solvents are omitted for clarity.

III.8 adopted a twisted conformation, which could explain its ^{1}H NMR spectral pattern. The single crystal X-ray diffraction analysis of **III.8** revealed a figure of eight configuration **(Figure-III.22)**, with overlapping ethylene bridges and oxygen atoms of all the furans pointing towards the core of the macrocycle. Due to its non-planar geometry, π-stacking interactions could be observed in the packing diagram of its single crystal. However, it displayed intermolecular C-H…F interactions (2.47Å, 133^{0}) **(Figure-III.23)**. Even though such macrocyclic structures are observed in expanded porphyrins, it represents a two sided twisted Hückel conformation in a 4nπ isophlorinoid leading to structure induced loss of paratropicity. Hence it can be distinguished as *non-antiaromatic* in nature.

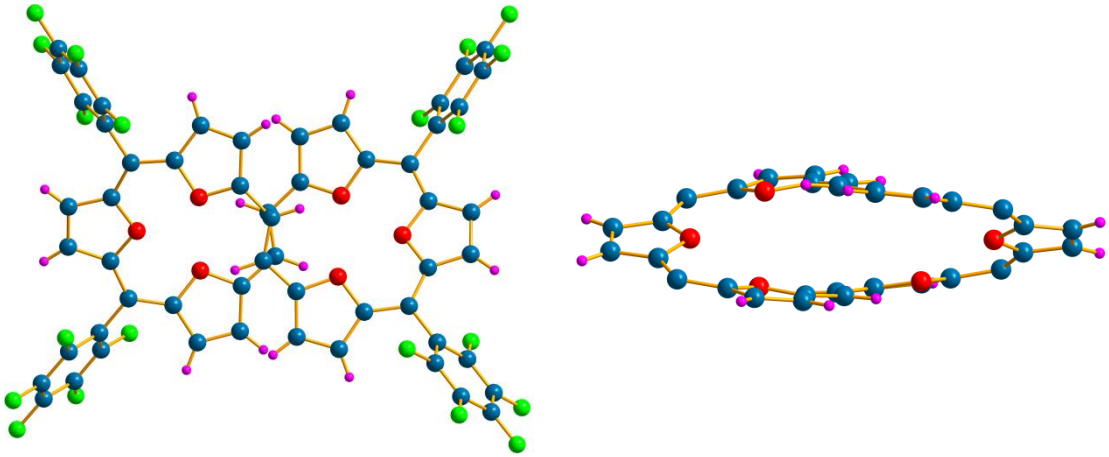

Figure-III.22: Molecular structure of **III.8**. Top view (left) and side view (right). Solvents are omitted for clarity. Phenyl groups and solvents are omitted for clarity in side view.

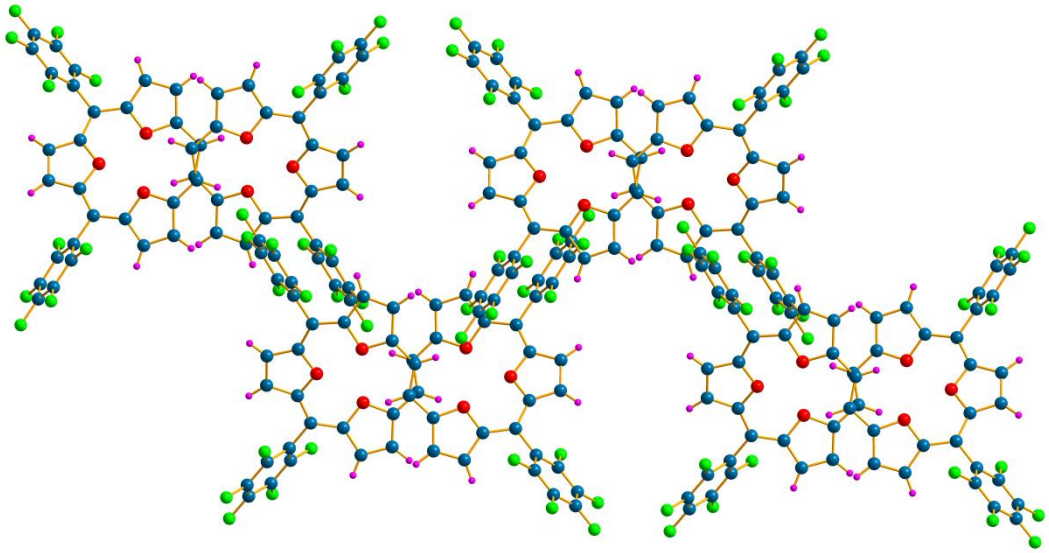

Figure-III.23: Intermolecular **C-H...F** interactions in **III.8.**

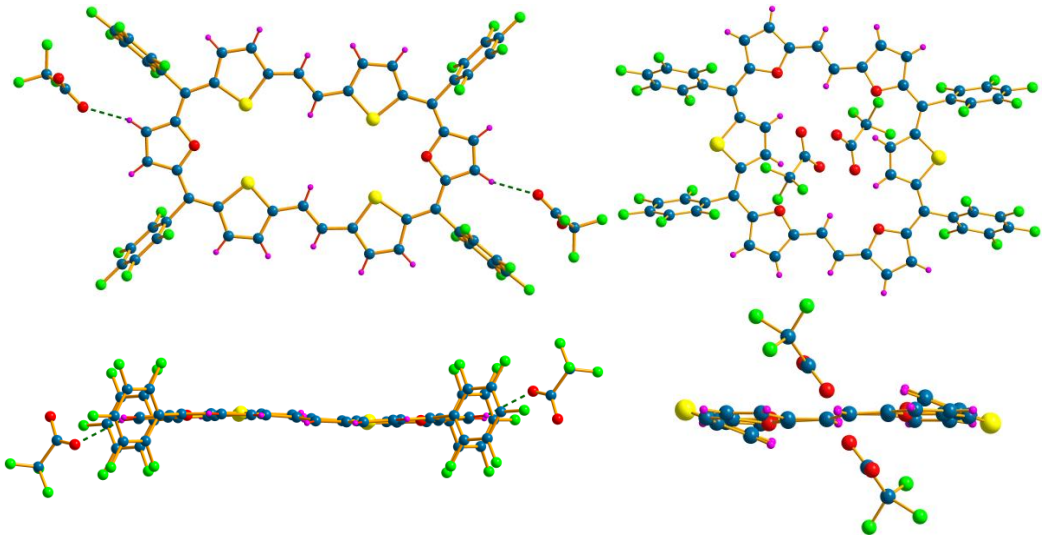

Figure-III.24: Molecular structure of **[III.3]**$^{2+}$(left) and **[III.8]**$^{2+}$ (right)**.**

Macrocycle	F...X (Å)	F...π (Å)	π-π(Å)	C-H...F (Å) , Angle(^{0})
III.1	X = S (3.11, 3.24)	1.5	3.6	-
III.2	X = S (2.99) X = Se (3.3)	1.35	3.6	-
III.3	-	-	-	2.40 , 154
III.4	X = S (2.98)	1.5	3.6	
III.5	-	-	-	2.54, 160
III.6	-	-	3.48	-
III.7	-	-	3.42	-
III.8	-	-	-	2.47, 133

Table-III.1: Non-covalent interactions in 32π Expanded Isophlorins**.**

The dicationic salt of these macrocycles was also characterized by single crystal X-ray analysis. Good quality single crystals were grown by slow evaporation of their solutions in trifluoroacetic acid. The molecular structures of **[III.3]$^{2+}$** and **[III.6]$^{2+}$** displayed planar structures with arrangement of heterocyclic units similar to that of neutral **c**ongeners **III.3** and **III.6 (Figure-III.24)**. Both the macrocycles are associated with two trifluoroacetate ions in their respective molecular structures. The β-carbons of thiophenes of **[III.6]$^{2+}$** were found to slightly deviate from the mean macrocyclic plane. It was also found to be associated with two trifluoroacetate ions situated at a distance of 0.89Å above and below the ring framework favouring the formation of 30π aromatic dication.

In stark contrast, the twisted conformation of **III.8** transformed into a planar configuration upon the addition of TFA. The molecular structure of **[III.8]$^{2+}$** is similar to that of **[III.6]$^{2+}$** where two of the furan rings are inverted **(Figure-III.25)**. This structure also supported the drastic change in its ^{1}H NMR spectrum upon addition of TFA. In its neutral form, the non-planar structure did not signify ring current effect as observed from the chemical shift values, in support of weak delocalization of π electrons. However, the planar structure of the dicationic species favoured the delocalization of π electrons as revealed by its ^{1}H NMR spectrum. The molecular structure of **[III.5]$^{2+}$** was found to be similar to that of the **III.5 (Figure-III.26)**.

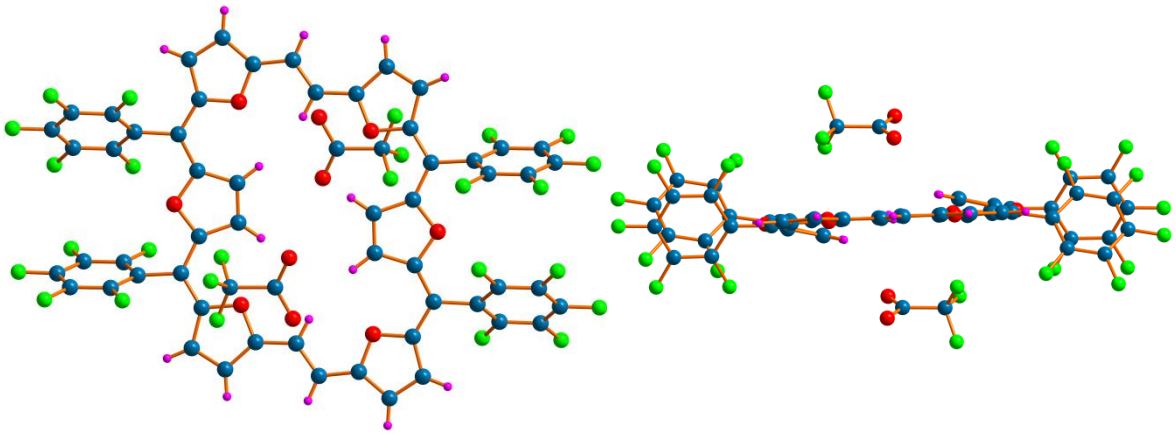

Figure-III.25: Molecular structures of **[III.8]**$^{2+}$ side view (left) and top view (right)**.**

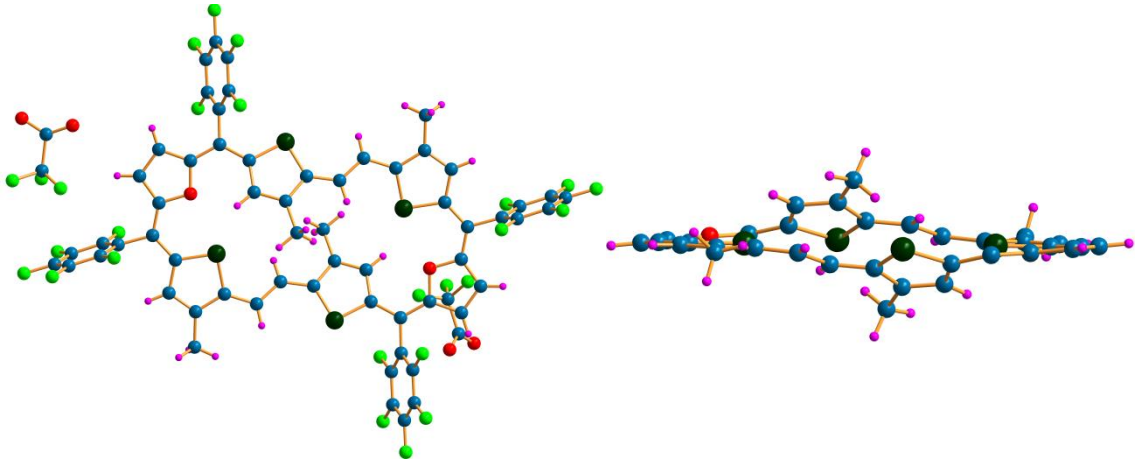

Figure-III.26: Molecular structures of **[III.5]**$^{2+}$ side view (left) and top view (right)**.**

III.3.3. Electronic Absorption Studies:

The structural diversity in 32π expanded isophlorinoids was confirmed from ^{1}H NMR spectroscopy and single crystal X-ray diffraction analysis. In support of these analyses, the expansion of the delocalized π electrons network was also well demonstrated by the large red shifted absorptions in comparison to the 20π isophlorin derivatives. All the macrocycles (**III.1-III.8**) displayed intense brown color in common organic solvents. The hexathia expanded isophlorin **III.1** exhibited intense absorptions at 495 nm (ε = 1.1 x 10^5) (**Table-III.2)** and 446 nm (1.0 x 10^5), (**Figure-III.26)** while the methyl derivative **III.4** displayed less intense absorptions at 494 nm (6.7 x 10^4) and 447 nm (5.9 x 10^4). Interestingly, these relatively small macrocycles have much more intense and red shifted absorptions compared to giant cyclo[n]thiophenes. Intense absorptions at 485 nm (1.3 x 10^5) and 445 nm (1.2 x 10^5) were observed for the selenium derivative, **III.2** and the other two macrocycles **III.6** and **III.7**. In contrast, **III.3** and **III.8** were found to display different absorption features. The macrocycle **III.3** absorbed at 482 nm (1.3 x 10^5) and 430 nm (1.6 x 10^5) (**Figure-III.26**),

whereas the twisted conformation of **III.8** had two close intense absorptions at 467nm (1.65 x 10^5) (**Table-III.2)** and 499 nm (1.62 x 10^5) along with a high energy shoulder at 450 nm (1.3 x 10^5) (**Figure-III.26)**.

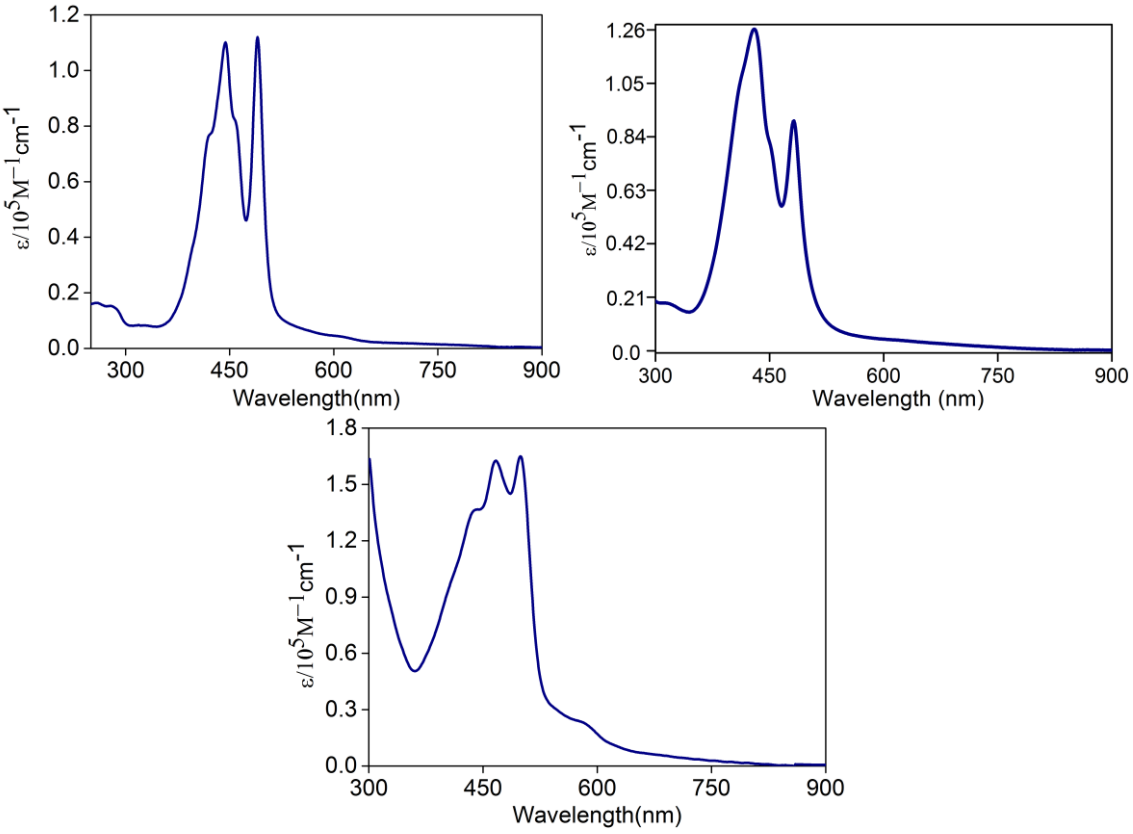

Figure-III.26: Electronic absorption spectra of 10^{-6}M solutions of **III.1** (top left), **III.3** (top right) and **III.8** (bottom) recorded in CH_2Cl_2.

These macrocycles displayed characteristic UV-Visible absorption changes upon addition of oxidising agents such as such as trifluoroacetic acid (TFA) **(Scheme-III.5)**, Meerwein's salt $[Et_3O]^+[SbCl_6]^-$] and $NOBF_4$. Addition of TFA to **III.1** changed its color to deep blue and this drastic change in color induced large red shifted absorptions at 617 nm with two other weak transitions in the region between 800-1000 nm **(Figure-III.27)**. A bathochromic shift by more than 100 nm and with a threefold increase in the absorption coefficient of its intense absorption band indicated a phenomenal change in the electronic character of the macrocycle. Similar color changes were observed for all other macrocycles. Controlled addition of TFA to a solution of **III.6** in dichloromethane indicated a one-to-one conversion of the macrocycle to its corresponding dication through a 31π monocationic radical cation intermediate. The radical nature of intermediate was characterized by EPR spectroscopy **(Figure-III.28)**. Similar to planar macrocycles, the twisted conformation **III.8** also underwent a 150 nm red

shift to show an intense absorption at 610 nm followed by weak transitions in the region between 800-1000 nm.

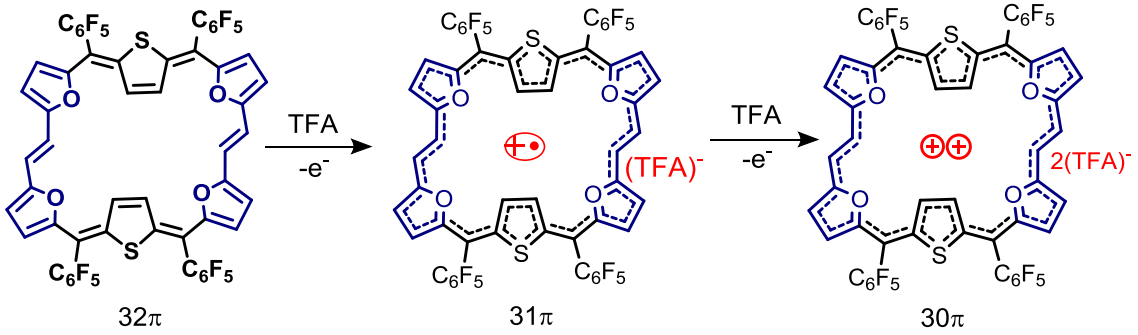

Scheme-III.5: Oxidation of 32π **III.6** to 30π dication upon addition of trifluoroacetic acid.

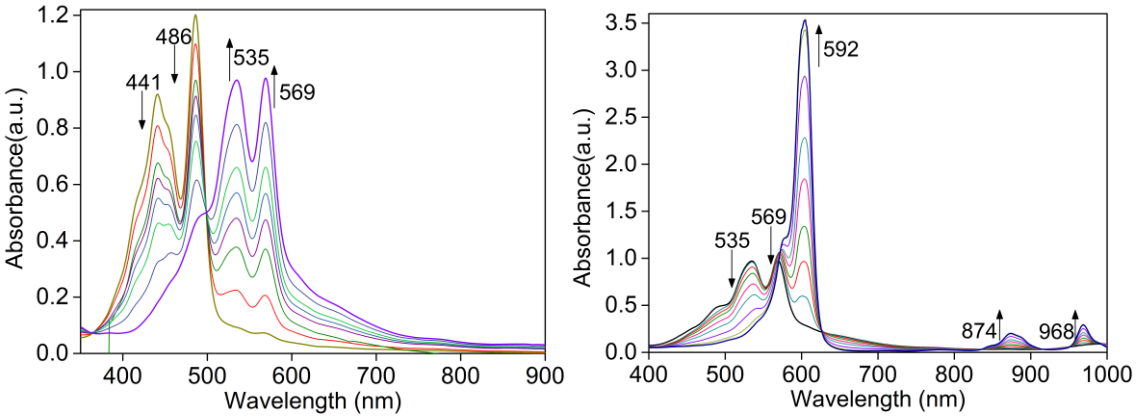

Figure-III.27: Spectral changes in the electronic absorption upon the slow addition of TFA to **III.6** in CH_2Cl_2.

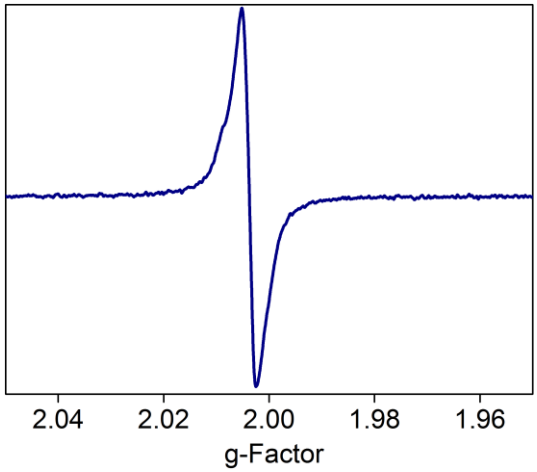

Figure-III.28: EPR spectrum of 31π monocation radical cation of **III.6.**

The 30π dicationic systems were found to be stable under ambient conditions and quite inert to moisture. Addition of triethylamine to [**III.8**]$^{2+}$ changed the deep blue solutions to the

original reddish-brown color with the same absorption features as of **III.8**, confirming the twisting of a planar molecule to a figure of eight conformation. Similar inter-conversion was observed even for other macrocycles (**III.n**) exemplifying acid-base induced conformational exchange in an antiaromatic expanded isophlorinoid. Very interestingly, it was observed that acid and base could act as two-electron redox reagents with the antiaromatic macrocycles. It has been observed that triethyl amine can act as electron donor to reduce the cationic species through the formation of its own radical cation and hence completes the cycle of inter-conversion between antiaromatic and aromatic states through a redox process **(Scheme-III.6)**. Apart from triethyl amine, metal based reducing agents such as $FeCl_2$ and Zinc could also reduce 30π dicationic species to the respective neutral 32π antiaromatic systems **(Figure-III.29)**.

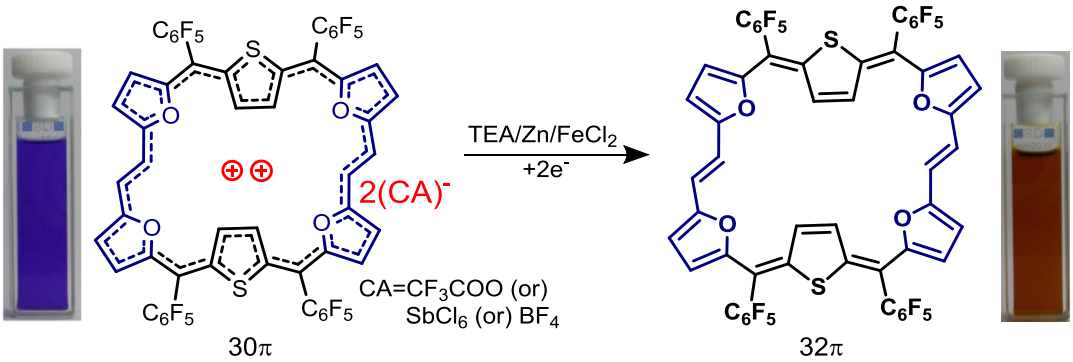

Scheme-III.6: Reduction of [**III.6**]$^{2+}$ to **III.6**.

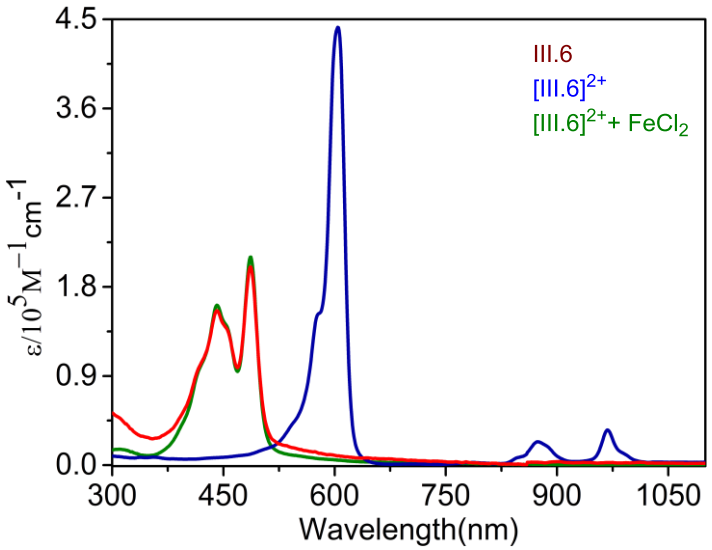

Figure-III.29: Reversible reduction of **III.6.** Electronic absorption spectra indicating the reversible oxidation of **III.6** in CH_2Cl_2.

Macrocycle	Absorption	$\epsilon*10^{-5}$	Macrocycle	Absorption	$\epsilon*10^{-5}$
III.1	495 446	1.12 1.09	**(III.1)$^{2+}$**	617 899 1017	
III.2	485 445	1.31 1.21	**(III.2)$^{2+}$**	627 911 1028	-
III.3	482 432	1.37 1.62	**(III.3)$^{2+}$**	592 874 968	2.40 , 1.54
III.4	494 447	0.67 0.59	**(III.4)$^{2+}$**	622 904 1024	
III.5	-	-	**(III.5)$^{2+}$**		2.54, 1.60
III.6	487 442	2.1 1.6	**(III.6)$^{2+}$**	592 874 968	-
III.7	486 443	1.85 1.52	**(III.7)$^{2+}$**	599 882 978	-
III.8	499 467	1.65 1.62	**(III.8)$^{2+}$**	610 875 966	2.47, 133

Table-III.2: Electronic absorption data for 32π expanded isophlorins & their respective dications.

III.3.4. Cyclic voltammetric Studies:

Cyclic voltammetric studies of **III.6** exhibited reversible oxidation and reduction at +0.5 V and -1.0 V respectively. **III.3** also displayed similar signals in its cyclic voltammogram supporting reversible redox nature of these 32π isophlorins **(Figure-III.30)**.

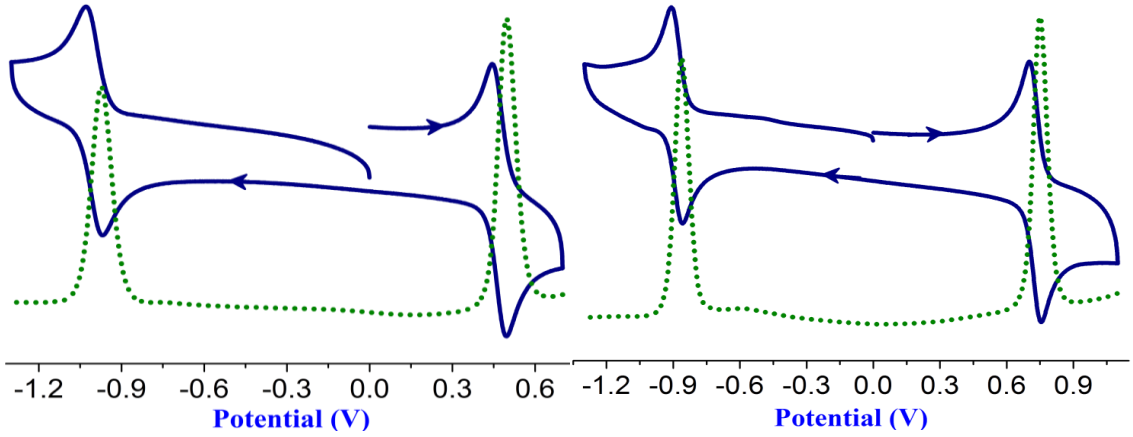

Figure-III.30: Cyclic voltammograms of **III.3** (left) and **III.6** (right) in dichloromethane containing 0.1 M tetrabutylammonium perchlorate as the Supporting electrolyte recorded at a 50 mV s^{-1} scan rate.

III.4. Quantum mechanical calculations:

The antiaromatic character of 32π expanded isophlorins was further confirmed by Nucleus Independent Chemical Shift (NICS) calculations at global ring centers[49]. All the macrocycles **(III.1-III.7)** displayed positive NICS values ranging between +10 to +12 ppm. The computed NICS value of +2.83 ppm for **III.5** could be attributed to its non-planar structure. Similarly the low NICS value of +1.16 ppm for **III.8** confirmed its non-antiaromatic character. The aromatic character for all the dications was supported by the negative NICS values ranging between 14-16 ppm. The corresponding change in the NICS values clearly confirmed the two electron oxidation of the neutral antiaromatic macrocycles to dication diradicals. Computed molecular orbital energy levels indicated relative stabilization of HOMO and LUMO in the dications compared to their corresponding neutral macrocycles[51] **(Table-III.3)**.

Macrocycle	NICS(0) ppm	HOMO-LUMO (eV)	Hückel Aromaticity
III.1	11.8	1.41	
III.2	11.99	1.44	
III.3	10.02	1.48	
III.4	11.99	1.38	Antiaromatic
III.5	2.83	1.68	
III.6	11.24	1.41	
III.7	10.75	1.45	
III.8	1.16	1.49	*Non-antiaromatic*
[**III.1**]$^{2+}$	-14.77	1.53	
[**III.2**]$^{2+}$	-14.70	1.50	
[**III.3**]$^{2+}$	-15.31	1.60	
[**III.4**]$^{2+}$	-14.25	1.57	
[**III.5**]$^{2+}$	-15.92	1.53	Aromatic
[**III.6**]$^{2+}$	-14.01	1.57	
[**III.7**]$^{2+}$	-13.97	1.56	
[**III.8**]$^{2+}$	-13.9	1.56	

Table-III.3: NICS and HOMO-LUMO band gap calculated from DFT calculations for 32π expanded isophlorin & their respective dications..

Anisotropy of the induced current density (AICD) plots of **(III.1 - III.7)** further confirmed the anticlockwise ring currents **(Figure-III.31)** in support of its antiaromatic behaviour[50]. An obscured AICD plot of **III.8 (Figure-III.32)** could not confirm specific ring current effects as expected in the absence of delocalization of π electrons. But all the dicationc species displayed a clear clockwise ring currents in support of their aromatic character.

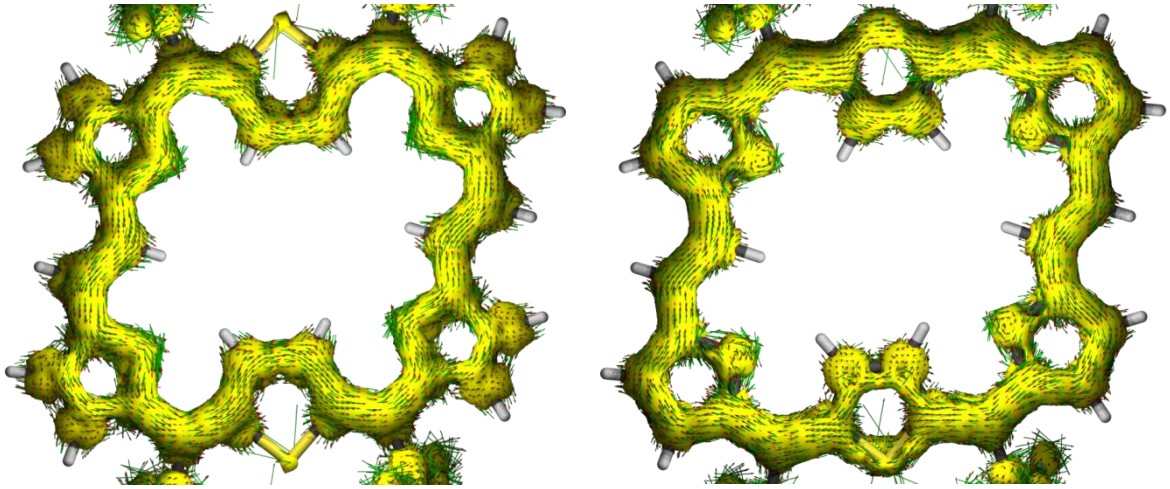

Figure-III.31: AICD plot of **III.6** (left) and **[III.6]**$^{2+}$ (right)**.** The external magnetic field is applied orthogonal to the macrocycle plane.

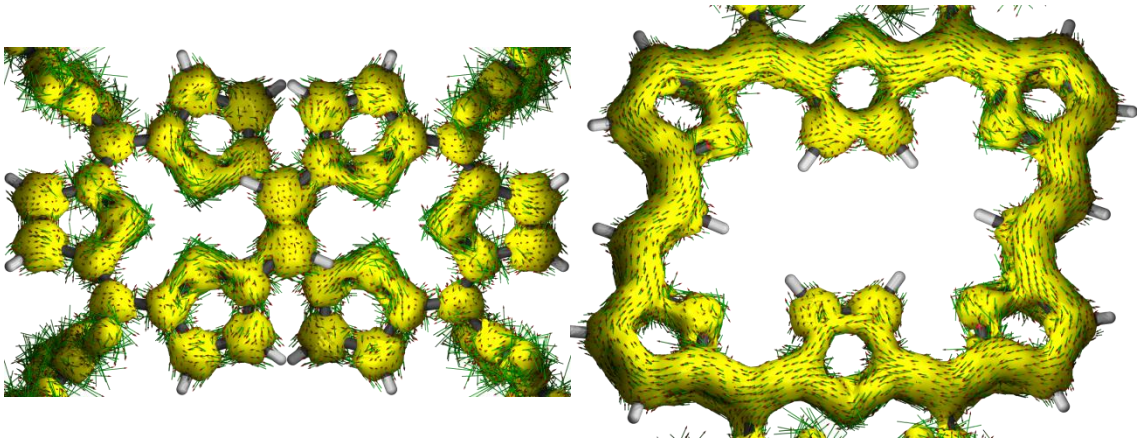

Figure-III.32: AICD plot of **III.8** (left) and **[III.8]**$^{2+}$ (right)**.** The external magnetic field is applied orthogonal to the macrocycle plane.

III.5 Conclusions:

In a simple synthetic procedure, 32π expanded isophlorins with different composition of heterocyclic rings were synthesized and characterized structurally. These macrocycles exhibit diverse structural characteristics depending on the nature and number of the heteroatoms present in the core of the macrocycles. They can adopt either planar or figure of eight conformation, which was reflected in their photo-physical properties. A significant feature common to all these macrocycles was in their ability to effectively delocalize the π electrons to stabilize antiaromaticity. The introduction of an ethylene bridge was accompanied by fluxional behaviour of the macrocycle as evidenced from the variable temperature ^{1}H NMR spectroscopy. Only planar systems could adopt the properties expected of π-delocalized systems. Loss of planarity also induced loss of ring current effect, which was explicitly observed in the hexa-furan (**III.8**) 32π macrocycle. In contrast to the diverse structural features, these systems exhibited similar redox properties with respect to each other. All the 32π macrocycles were found to undergo a reversible two-electron oxidation to form the corresponding 30π aromatic dication. The change in the electronic properties was confirmed by electronic absorption and ^{1}H NMR spectroscopy. These molecules displayed remarkable change in the color of their solutions with a variety of oxidizing agents such as TFA, Meerwein's salt $[Et_3O]^+[SbCl_6]^-$ and $NOBF_4$. They yield the same oxidized product as identified by the similar electronic absorption spectrum even when oxidized by any of the three oxidizing agents. Such an oxidation is attributed to the ring oxidation of the macrocycles, wherein the two π-electrons of the 4nπ system are lost by the macrocycles to form a 30π aromatic dication. This dication was stabilized by suitable counter anions such as $(CF_3COO)^-$, $[SbCl_6]^-$ or $[BF_4]^-$. The adduct nature of the oxidized species was confirmed by single crystal-X-ray diffraction analysis. The ^{1}H NMR spectra also supported the structural features of these macrocycle in the form of diatropic ring current effects. Hexa-furan system (**III.8**), displayed a significant change in its structure by uncurling into a planar macrocycle upon oxidation. However, all the 30π dications could be reduced to the corresponding 32π antiaromatic neutral macrocycle by employing either triethyl amine or metal based reducing agents such as Zn powder and $FeCl_2$. Further support for the change in the ring current came by estimating the NICS values for the 32π neutral macrocycles and their corresponding 30π dications. The estimated NICS values for the 32π systems were found to have positive values in the range between +10 to +12 ppm. All the dications had negative NICS values in the range between -13 to -16 ppm. This change in the values unequivocally confirmed the two-electron oxidation of the 32π expanded isophlorins to 30π dications. The non-planar

macrocycles **III.5** and **III.8** were found to have very low positive NICS values suggesting weak delocalization of the π electrons and hence considered as non-antiaromatic in nature.

Overall, the expansion of the π circuit in isophlorins exhibited a remarkable change in their redox properties. The 20π isophlorin with *meso* pentafluorophenyl substituents are hard to be oxidized and the formed dicationic species were found to be unstable under ambient conditions. On the other hand expanded isophlorins with 32π electrons undergo easier and reversible two-electron oxidation to form stable 30π dications with a variety of oxidizing agents. This observation suggests the relative ease for the oxidation of large antiaromatic by two electrons in comparison to the one-electron oxidation of aromatic molecules to form radical species. It would be of interest to synthesize and explore the relative ease of redox reactions in much larger antiaromatic systems.

III.6. Experimental section:

An equimolar concentration of ethylene bridged bis-thiophene/furan and the corresponding diol were dissolved in 100 ml dry dichloromethane and degassed with Argon for ten minutes. Then, a catalytic amount of boron trifluoride diethyl etherate ($BF_3.OEt_2$) was added under dark using a syringe. After stirring for an hour, two equivalents of DDQ were added and stirring continued for an additional 2 h. Then few drops of triethyl amine were added and the resultant solution was passed through a short basic Alumina column. This mixture was concentrated and further purified by silica gel column chromatography using CH_2Cl_2/hexane as eluent. The dications were generated by the addition of TFA to a solution of the macrocycle in dichloromethane. Evaporation of the solvent gave the dication as a metallic blue solid. Dicationic salt of hexachloroantimonate was prepared as per earlier report[46].

III.1: Bisthiophene (192 mg, 1 mmol) and thiophene diol (476 mg, 1 mmol) were reacted in presence of $BF_3.OEt_2$, (0.13 ml, 1 mmol), as described above to yield **III.1** in 4% yields. **^{1}H NMR** (400 MHz, $CDCl_3$, 298K) δ = 8.4 (s, 4H), 5.78 (d, J = 5.0 Hz, 4H), 5.29 (d, J = 5.0 Hz, 4H), 5.15 (s, 4H). **^{1}H NMR** (500 MHz, $CDCl_3$, 175K) δ = 12.83 (d, 2H, 16 Hz), 5.98 (d, 4H, 4 Hz), 5.60-5.56 (m, 12H), 5.51 (d, 4H, 4 Hz), 5.42 (d, 4H, 4 Hz), 5.37 (d, 2H, 16 Hz) **UV-Vis** (CH_2Cl_2): $\lambda_{max}(\varepsilon)$ L mol^{-1} cm^{-1} = 495(1,12,000) and 446 (1,09,000). **HRMS** *m*/*z*: calcd. For $C_{56}H_{16}F_{20}S_6$: 1259.9258; Observed: 1259.9291 (100.0%) M^+

III.2: Bisthiophene (192 mg, 1 mmol) and selenophene diol (523 mg, 1 mmol) were reacted, in presence of $BF_3.OEt_2$, (0.13 ml, 1 mmol), as described above to yield **III.2** in 2.5% yields. **^{1}H NMR (**400 MHz, d_8-THF, 298K) δ = 8.50 (s, 4H), 6.05 (d, J = 4.0 Hz, 4H), 5. 62 (d, J = 4.0 Hz, 4H), 5.47 (s, 4H). **UV-Vis** (CH_2Cl_2): λ_{max}(ε)L mol^{-1} cm^{-1} = 485 (1,31,000) and 445 (1,21,000): **HRMS** *m*/*z* calcd. for $C_{56}H_{16}F_{20}S_4Se_2$ = 1355.8146: Observed = 1355.8141 (100%)

III.3: Bisthiophene (192 mg, 1 mmol) and furan diol (460 mg, 1 mmol) were reacted in presence of $BF_3.OEt_2$, (0.065 ml, 0.5 mmol), as described above to yield **III.3** in 8% yields. **^{1}H NMR** (400 MHz, acetone-d_6, 295K): δ= 8.01 (s, 4H), 6.75 (d, *J* = 4.1 Hz, 4H), 6.40 (d, *J* = 4.1 Hz, 4H), 6.31 (s, 4H). **^{19}F NMR** (376 MHz, acetone-d_6, 295K): δ= -141.83 (d, *J* = 20.9 Hz), -156.33 (t, *J* = 20.9 Hz), -163.33 (d, *J* = 21.0 Hz). **^{1}H NMR** (400 MHz, acetone-d_6, 183K): δ= 6.44 (d, *J* = 4.0 Hz, 4H), 6.23 (s, 4H), 6.05 (d, *J* = 3.9 Hz, 4H). **UV-Vis** (CH_2Cl_2): λ_{max} (ε) L mol^{-1} cm^{-1} = 482 (137,000) and 430 (160,000). **HR-MS** (ESI-TOF): *m*/*z* = 1227.9747; (found, $[M]^+$): 1227.9714 (calcd. For $C_{56}H_{16}F_{20}O_2S_4$).**Crystal data** $C_{56}H_{16}F_{20}O_2S_4$ (M_r=1228.97), triclinic, space group *P*-1 (no. 2), *a* = 8.691(3), *b* = 18.185(6), *c* = 18.675(6)Å, *a* = 112.283(5)° *β* = 97.143(6)° γ = 101.375(5)°, *V* = 2612.1(15)Å^3, *Z* = 2, *T* = 100(2) K , D_{calcd} = 1.563g cm^{-3}, R_1 = 0.0746 (I>2s(I)), R_w (all data) = 0.1709, GOF = 0.827; [**III.3**]$^{2+}$: **^{1}H NMR** (400 MHz, acetonitrile-d_3, 298K): δ= 15.46 (s, 2H), 12.96 (s, 2H), 11.80 (s, 2H), 11.12 (4H), 10.43 (s, 4H), -9.58 (s, 2H). **UV-Vis** (CH_2Cl_2/ TFA): λ_{max} (ε) L mol^{-1} cm^{-1}= 580 (388,000), 611 (176,000), 867 (16,000) and 974 (29,000). **Crystal data** $C_{56}H_{16}F_{20}O_2S_4.4(C_2F_3O_2).4(C_2HF_3O_2).2(CHCl_3)$' ($M_r$=2375.90), triclinic, space group *P*-1 (no. 2), *a* = 11.686(2), *b* = 13.031(2), *c* = 15.575(3)Å, *a* = 92.223(5)° *β* = 97.143(6)° γ = 101.375(5)°, *V* = 2163.6(7)Å^3, *Z* = 1, *T* = 100(2) K , D_{calcd} = 1.824g cm^{-3}, R_1 = 0.0688 (I>2s(I)), R_w (all data) = 0.1488, GOF = 0.896.

III.4: β-methyl bisthiophene (220 mg, 1 mmol) and thiophene diol (476 mg, 1 mmol) were reacted, in presence of $BF_3.OEt_2$, (0.13 ml, 1 mmol), as described above to yield **III.4** in 6% yields. **^{1}HNMR** (400MHz, $CDCl_3$, 298K) δ = 8.34 (s, 4H), 5.11 (s, 8H),1.53 (s, 12H). **UV-Vis** (CH_2Cl_2): λ_{max}(ε)L mol^{-1} cm^{-1} = 494 (67,000) and 447 (59,100). **HRMS** *m*/*z* calcd. for $C_{60}H_{24}F_{20}S_6$:1315.9883; Observed 1315.9863(100.0%).

III.6: Bisfuran (160 mg, 1 mmol) and thiophene diol (476 mg, 1 mmol) were reacted in presence of $BF_3.OEt_2$, (0.065 ml, 0.5 mmol), as described above to yield **III.6** in 8.5% yields. **^{1}H NMR** (500 MHz, THF-d_8, 293K): δ= 12.61 (s, 4H), 5.43 (br s), 4.91 (s, 2H), 4.92 (s, 2H).**^{19}F NMR** (376 MHz, THF-d_8, 295K): δ= -141.11 (d, *J* = 19.7 Hz), -154.84 (t, *J* = 20.3 Hz), -162.51 (t, *J* = 19.9 Hz). **^{1}H NMR** (500 MHz, THF-d_8, 220K): δ= 13.24 (d, *J* = 6.3 Hz, 2H), 13.14 (d, *J* = 6.3 Hz, 2H), 12.42 (d, *J* = 16.5 Hz, 2H), 5.52 (d, *J* = 3.7 Hz, 2H), 5.28 (d, *J* = 3.8 Hz, 2H), 5.00 (d, *J* = 16.5 Hz, 2H), 4.91 (d, *J* = 3.7 Hz, 2H), 4.89 (d, *J* = 3.7 Hz, 2H). **UV-Vis** (CH_2Cl_2): λ_{max} (ε) L mol^{-1} cm^{-1} = 487 (210,000) and 442 (160,000).
HR-MS (ESI-TOF): m/z =1196.0219 (found, $[M]^+$), 1196.0171 (calcd. For $C_{56}H_{16}F_{20}O_4S_2$). **Crystal data** $C_{56}H_{16}F_{20}O_4S_2.2CHCl_3$ (*M*r=1435.56), triclinic, space group *P*-1 (no. 2), *a* = 7.2697(8), *b* = 10.7459(12), *c* = 20.929(2) Å, *a* = 91.624(2)° *β* = 90.414(2)° *γ* = 108.644(2)°, *V* = 1548.3(3) Å^3, *Z* = 1, *T* = 100(2) K , D_{calcd} = 1.540g cm^{-3}, R_1 = 0.0567 (I>2s(I)), R_w (all data) = 0.1454, GOF = 0.90.

[**III.6**]$^{2+}$: **^{1}H NMR** (400 MHz, CF_3COOD, 298K): δ= 15.66 (d, *J* = 15.1 Hz, 2H), 13.75 (d, *J* = 4.6 Hz, 2H), 12.69 (d, *J* = 4.4 Hz, 2H), 12.34 (d, *J* = 4.1 Hz, 2H), 12.17 (d, *J* = 3.9 Hz, 2H), -6.41 (d, *J* = 4.9 Hz, 2H), -6.81 (d, *J* = 4.9 Hz, 2H), -9.85 (d, *J* = 16.0 Hz, 2H). **UV-Vis** (CH_2Cl_2/ TFA): λ_{max}(ε) L mol^{-1} cm^{-1}= 592 (442,000), 874 (19,000) and 968 (30,000).
Crystal data $C_{56}H_{16}F_{20}O_4S_2.4(C_2F_3O_2).2(C_2HF_3O_2)$. (*M*r=1876.96), triclinic, space group *P*-1 (no. 2), *a* = 12.6533(12), *b* = 13.0303(13), *c* = 13.0593(13)Å, *a* = 113.933(2)° *β* = 97.581(2)° *γ* = 112.749(2)°, *V* = 1705.1(3)Å^3, *Z* = 1, *T* = 100(2) K , D_{calcd} = 1.828g cm^{-3}, R_1 = 0.0531 (I>2s(I)), R_w (all data) = 0.1566, GOF = 1.129.

III.7: Bisfuran (160 mg, 1 mmol) and selenophene diol (523 mg,1 mmol) were reacted in presence of $BF_3.OEt_2$, (0.065 ml, 0.5 mmol), as described above to yield **III.7** in 6.5% yields. **^{1}H NMR** (500 MHz, THF-d_8, 323K): δ= 11.88 (s, 1H), 5.62 (s, 1H), 5.07 (d, *J* = 3.6 Hz, 1H). **^{19}F NMR** (376 MHz, THF-d_8, 298K): δ= -141.63 (d, *J* = 21.8 Hz), -154.88 (d, *J* = 21.4 Hz), -162.27 (br, s). **^{1}H NMR** (500 MHz, THF-d_8, 230K): δ= 12.60 (d, *J* = 6.0 Hz, 2H), 12.52 (d, *J* = 5.8 Hz, 2H), 11.69 (d, *J* = 16.4 Hz, 2H), 5.71 (s, 2H), 5.44 (s, 2H), 5.28 (d, *J* = 16.4 Hz, 2H), 5.07 (s, 2H), 5.05 (s, 2H). **UV-Vis** (CH_2Cl_2): λ_{max} (ε) L mol^{-1} cm^{-1} = 486 (185,000) and 443 (152,000). **HR-MS** (ESI-TOF): m/z = 1291.9125 (found, $[M]^+$);1291.9075 (calcd. For $C_{56}H_{16}F_{20}O_4Se_2$). **Crystal data** $C_{56}H_{16}F_{20}O_4Se_2.2CHCl_3$ (*M*r=1529.34), triclinic, space group *P*-1 (no. 2), *a* = 7.2187(15)Å, *b* = 10.775(2), *c* = 20.913(4) Å, *a* = 91.108(5)° *β* = 90.893(5)° *γ*

= 108.324(5)°, V = 1543.6(6) Å^3, Z = 1, T = 100(2) K , D_{calcd} = 1.645g cm^{-3}, R_1 = 0.0436 (I>2s(I)), R_w (all data) = 0.1194, GOF = 0.843;

III.8: Bisfuran (160 mg, 1 mmol) and furan diol (460 mg, 1 mmol) were reacted in presence of $BF_3.OEt_2$, (0.065 ml, 0.5 mmol), as described above to yield **III.8** in 6% yields.
^{1}H NMR (500 MHz, THF-d_8, 298K): δ= 7.12 (s, 4H), 6.47 (d, J = 3.4 Hz, 4H), 6.43 (d, J = 3.3 Hz, 4H), 3.64 (s, 4H). **^{19}F NMR** (376 MHz, THF-d_8, 298K) δ= -139.82 (d, J = 21.2 Hz), -156.39 (t), -163.67 (t, J = 20.1 Hz). **UV-Vis** (CH_2Cl_2): λ_{max} (ε) L mol^{-1} cm^{-1} = 499 (165,000) and 467 (162,000). **HR-MS** (ESI-TOF): m/z =1164.0656 (found, [M]$^+$);1164.0627 (calcd. For $C_{56}H_{16}F_{20}O_6$). **Crystal data** $C_{56}H_{16}F_{20}O_6$ (Mr=1164.69), monoclinic, space group *c2/c* (no. 15), a = 15.2699(17), b = 25.017(3), c = 19.300(3) Å, β = 111.411(2)°, V = 6864.2(15) Å^3, Z = 4, T = 100(2) K , D_{calcd} = 1.127g cm^{-3}, R_1 = 0.0629 (I>2s(I)), R_w (all data) = 0.1765, GOF = 1.067.

[**III.8**]$^{2+}$: **^{1}H NMR** (500 MHz, Acetonitrile-d_3, 298K): δ= 14.04 (d, J = 13.8 Hz, 2H), 12.40 (s, 2H), 11.54 (s, 2H), 11.42 (s, 2H), 11.31 (s, 2H), -6.02 (s, 2H), -6.42 (s, 2H), -9.89 (d, J = 13.9 Hz, 2H). **UV-Vis** (CH_2Cl_2 / TFA): λ_{max}(ε) L mol^{-1} cm^{-1}= 610 (442,000), 875 (29,000) and 966 (36,000). **Crystal data**$C_{56}H_{16}F_{20}O_6.4(C_2F_3O_2).4(C_2HF_3O_2)$. ($M_r$=2072.88), monoclinic, space group *P*21/*n*, (no. 14), a = 15.393(3), b = 13.327(3), c = 19.506(4) Å, β = 108.702(4)°, V = 3790.1(14) Å^3, Z = 2, T = 100(2)K, D_{calcd} = 1.816 g cm^{-3}, R_1 = 0.0836 (I>2s(I)), R_w (all data) = 0.2089,0.2120, GOF=1.280.

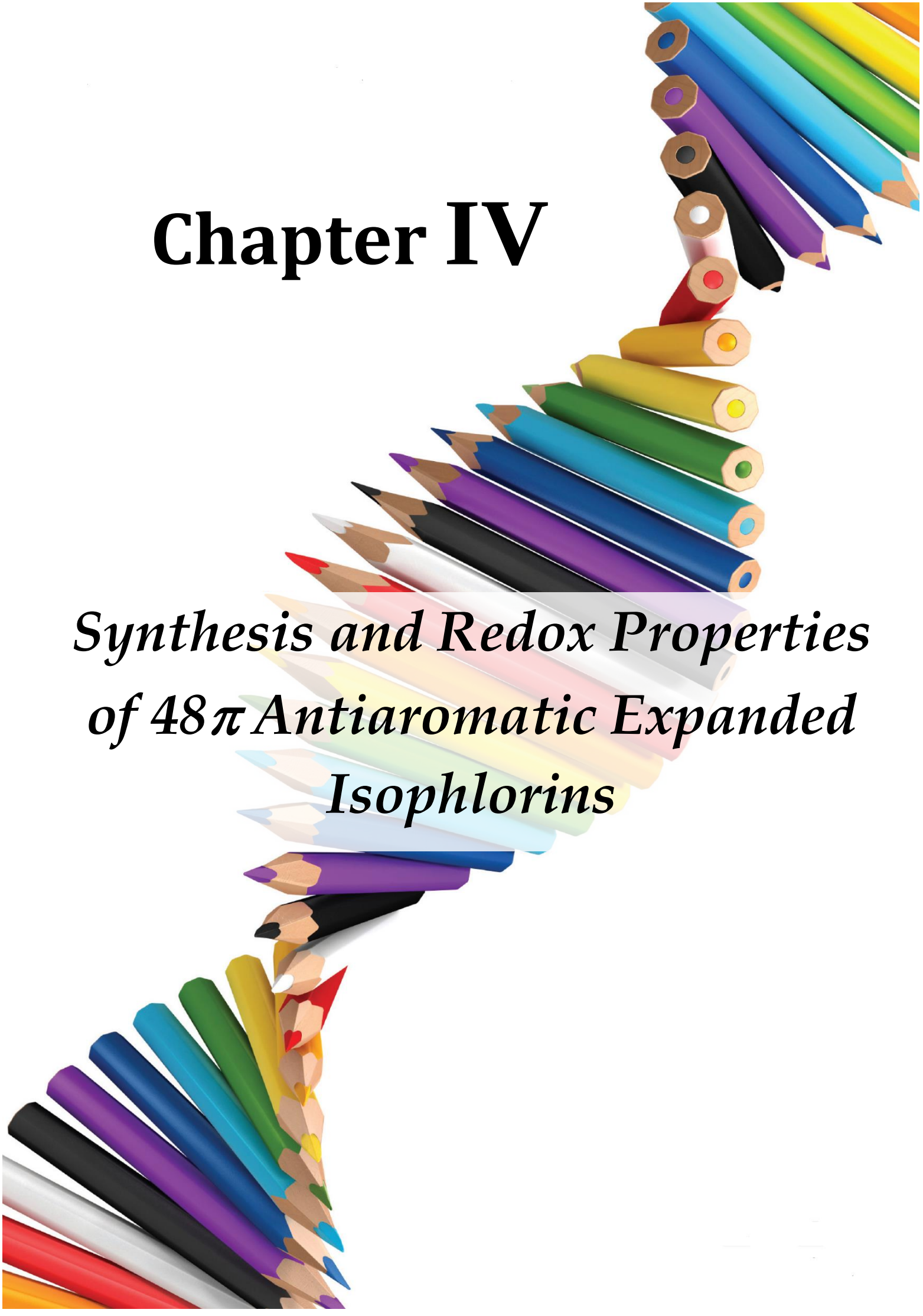

Chapter IV

Synthesis and Redox Properties of 48π Antiaromatic Expanded Isophlorins

IV.1. Introduction:

Synthesis of large macrocycles with effective delocalization of π electrons is a difficult task due to their flexible geometry. This is evident from the reports on giant porphyrinoids that are well known for structure-induced loss of aromaticity[62]. In one of the earliest reports, the decapyrrolic macrocycle turcasarin synthesized by Sessler and co-workers was shown to adopt a "figure eight" conformation both in solution and in the solid state[63]. A variety of octapyrrolic macrocycles were reported by Vogel and co-workers[64], which were characterized in soild state to confirm their twisted conformation. The 32π octapyrrolic macrocycle octaphyrin-(1.0.1.0.1.0.1.0) with *meso* carbon bridges between bipyrrolic units was unable to sustain a planar structure. Other cyclooctapyrroles with 34π and 36π electrons were also found to adopt non-planar structures[65]. Even larger macrocycles were also found to deviate from planar structure. Giant porphyrinoids with twelve and sixteen pyrrole units, such as [48]dodecaphyrin-(1.0.1.0.1.0.1.0.1.0.1.0) and [64]hexadecaphyrin-(1.0.1.0.1.0.1.0.1.0.1.0.1.0.1.0), were synthesized by Setsune and co-workers[66]. The single crystal X-ray diffraction analysis of these molecules clearly indicated multiple twists, resembling a helical architecture in these macrocyles. Further, Osuka and co-workers were successful in the one-pot synthesis of a series of expanded porphyrins from pyrrole and pentaflourobenzaldehyde[42]. The octapyrrolic macrocycle with equal number of pyrrole and *meso* carbons adopted a "figure eight" conformation. Similarly, the nine pyrrolic nonaphyrin and the ten pyrrolic decaphyrin were also characterized as twisted macrocycles[67]. On the contrary, some planar tetra-epoxy annulenes have been synthesized and were to known to adopt multiple conformations due to *E* and *Z* configurations for the ethylene like bridges that connected the bifuran units[24]. All these reports unequivocally supported the absence of planar & rigid structural features in giant π-conjugated macrocycles. However, attempts to prevent the curling of giant macrocycles have surfaced through innovative synthetic design of these macrocycles. Sessler and co-workers reported an octa pyrrolic macrocycle without *meso* carbon bridges[68]. The eight pyrroles were interlinked through C_α-C_α bonds between the adjacent pyrrole rings to form an aromatic 30π macrocycle. Later Osuka and co-workers achieved the synthesis of planar octaphyrin and decaphyrin with an internal *p*-quinodimethane bridge[69]. The presence of such covalently linked groups in the centre of the macrocycle induced steric hindrance for the twisting of the macrocycle. Similarly, Chandrashekar and co-workers have explored the synthesis of core-modified expanded porphyrins with a thiophene unit at the centre of a 26π hexaphyrins[70]. However, non-pyrrolic macrocycles were found to adopt a different structure in comparison to the pyrrole

counter-part. Anand and co-workers reported the successful synthesis of a planar 40π antiaromatic cyclo-octa furan [1.1.1.1.1.1.1.1] from commercially available precursors[33]. It was found to sustain a planar conformation both in solution and solid states without any internal bridges. Cyclo(n)thiophenes reported individually by Bauerle and Iyoda were found to be non-anti aromatic in nature[29, 31a]. Till date, there are no reports of rigid and planar macrocycles bearing more than eight heterocyclic rings with significant delocalization of π electrons. In this context the synthesis of planar macrocyclic systems with nine (or) more heterocyclic units appears to be a synthetic challenge and of wide interest.

IV.2. Syntheses:

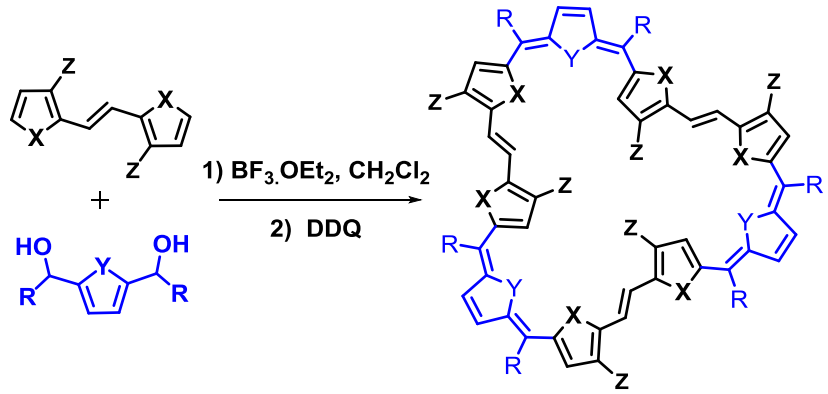

	X	Y	Z	R
IV.1	S	S	H	C_6F_5
IV.2	S	S	H	Ph
IV.3	S	S	Me	C_6F_5
IV.4	S	Se	H	C_6F_5
IV.5	O	S	H	C_6F_5
IV.6	O	O	H	C_6F_5

Scheme-IV.1: Acid catalysed synthesis of 48π Expanded Isophlorins.

Expanded isophlorins with 48π electrons were synthesized by employing a synthetic procedure similar to that of 32π macrocycles (Schemes-**III.2, III.3** and **III.4**). Both, 32π and 48π macrocycles could be isolated from the acid catalyzed condensation of either (*E*)-1,2-dithienylethylene or (*E*)-1,2-furylethylene with furan/thiophene/selenophene diols (**SchemeIV.1**) in different yields. Upon varying the concentration of the reactants, moderate yields of the 48π (**IV.1- IV.6**) macrocycles were obtained in the same reaction **(Scheme-IV.1)**. The proportion of heterocyclic rings in the macrocycles was varied by appropriate changes in the precursors. These macrocycles could be easily identified in silica gel column chromatography due to their intense color in common organic solvents. The isolated 4nπ compounds were found to be stable as they did not show any sign of degradation under ambient conditions. Even larger macrocycles were also identified in this reaction, but were in too low yields to be isolated for further characterization.

Results and Discussions:

IV.3. Spectral Characterization:

The composition of these macrocycles was confirmed by mass spectrometry and further characterized by NMR spectroscopy, electronic absorption and single crystal X-ray crystallography. High resolution mass spectrometry established the exact composition of all these expanded isophlorins.

IV.3.1. NMR Characterization

The ^{1}H NMR spectrum of **IV.1** displayed only three signals in the region between δ 8.00 - 6.5 ppm. The number of signals was much less than expected of a planar **IV.1** and hence indicated the fluxional behavior anticipated in large sized macrocycles. Therefore, variable temperature ^{1}H NMR was employed to arrest the probable dynamic behavior of the macrocycle in the solution. This was confirmed upon lowering the temperature to 206K to observe a well resolved spectrum **(Figure-IV.1)**.

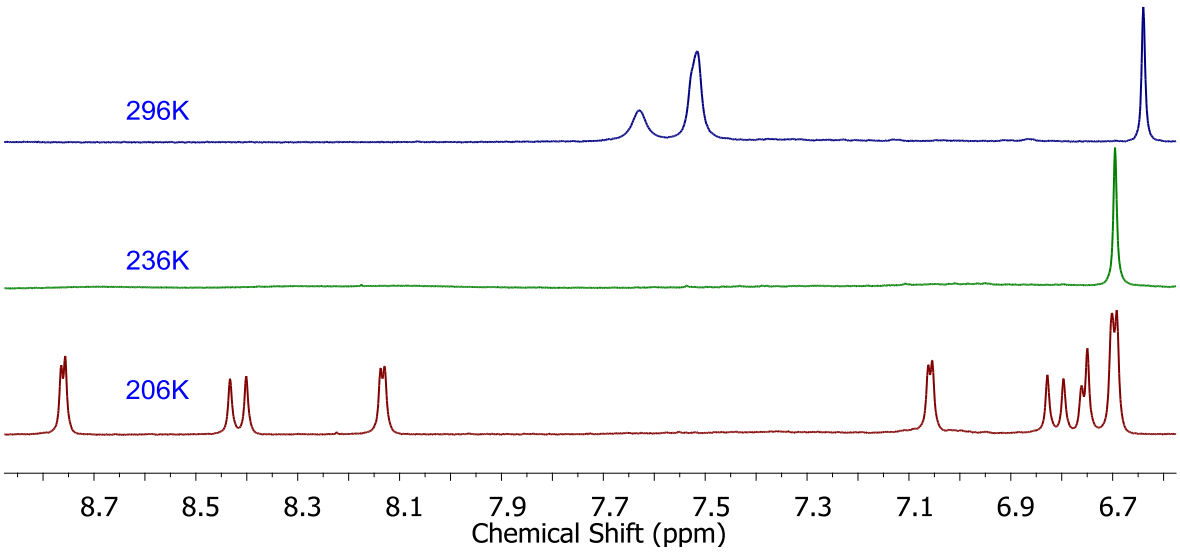

Figure-IV.1: Variable temperature ^{1}H NMR spectra of **IV.1** in acetone-d_6.

The broad signals observed at room temperature resolved into seven different signals at 206K in the region between δ 9.00 – 6.5 ppm **(Figure-IV.2)**. Overall, six doublets were observed at δ 8.73, 8.39, 8.09, 7.02, 6.75 and 6.72 ppm corresponding to same number of protons. The signal at 6.66 ppm corresponded to twice the number of protons compared to other signals.

^{1}H-^{1}H 2D COSY spectrum **(Figure-IV.3)** recorded at 206K displayed four different cross peaks to confirm the highly symmetrical nature of this macrocycle. The signal at δ 6.66 ppm was found to have two different correlations with the signals at 7.02 and 6.72 ppm, suggesting the overlapping of two doublets at the same resonant position. The calculated coupling constant for the cross-correlated signals at δ 6.75 and 8.39 ppm was found to be 16 Hz, suggestive of *E* conformation for the ethylene bridge and weak paratropic ring current effects for the 4nπ system. A meager Δδ value of 1.7 ppm between these two signals implied very weak antiaromatic character in this 48π macrocycle. The cross-correlated low-field signals at δ 8.73 and 8.09 ppm coupled to each other further emphasized the weak paratropic ring current effect on the protons of heterocyclic rings with an inverted configuration.

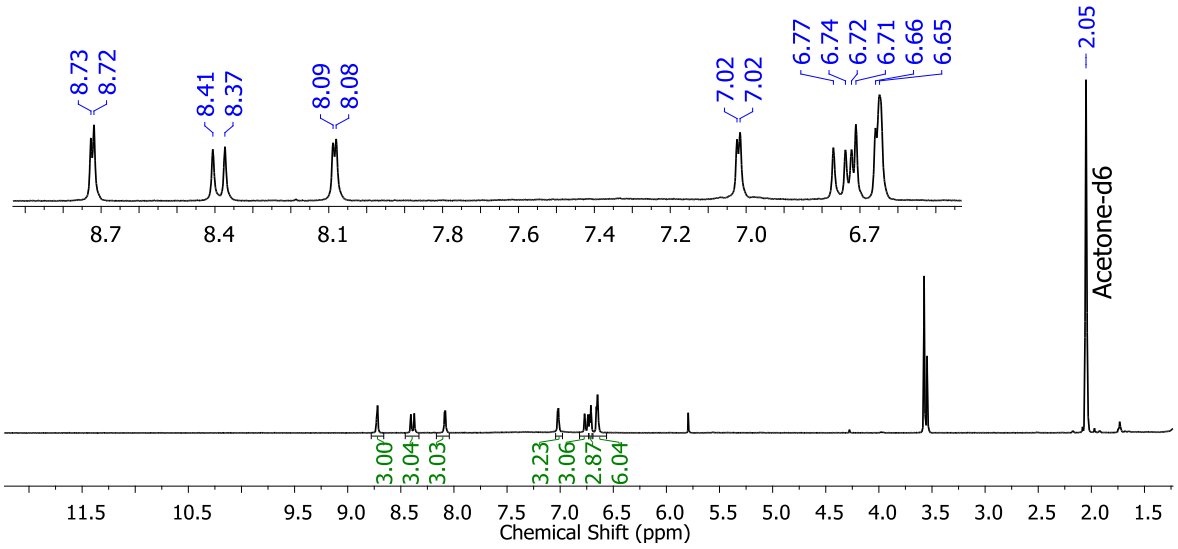

Figure-IV.2: ^{1}H NMR spectrum of **IV.1** in acetone-d_6 at 206K.

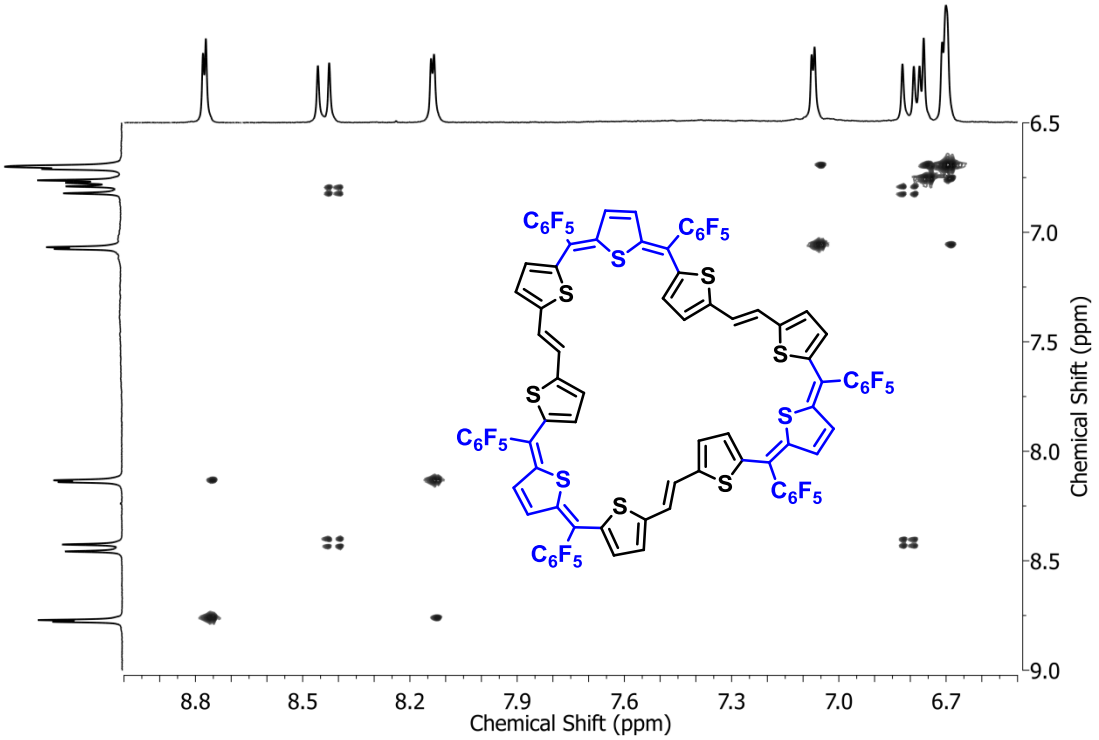

Figure-IV.3: ^{1}H-^{1}H 2D COSY spectrum of **IV.1** in acetone-d_6 at 206K.

Room temperature ^{19}F NMR of **IV.1** displayed three sets of signals at -141.77, -155.55 and -163.10 corresponding to ortho, para and meta fluorines of pentafluoro substituents. Upon reducing the temperature, it was observed that each signal splits into two signals to further confirm the fluxional behaviour of this macrocycle **(Figure-IV.4)** at room temperature.

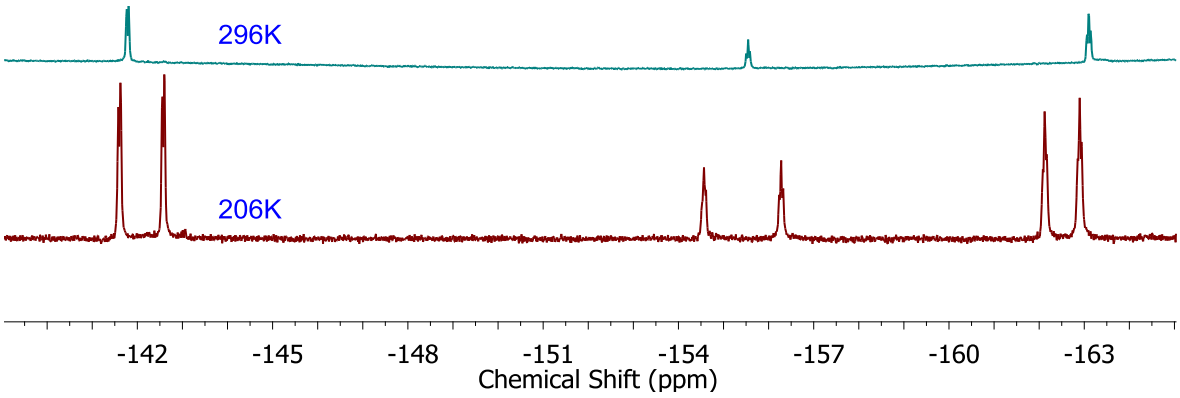

Figure-IV.4: Variable temperature ^{19}F NMR spectra of **IV.1** in acetone-d_6.

Two other macrocycles, **IV.2** and **IV.3**, having the same composition of thiophene rings, but with different substituents were synthesized through a similar synthetic procedure. Temperature dependence on their ^{1}H NMR spectrum was comparable to **IV.1** suggesting

analogous fluxional behavior irrespective of the substituents on the macrocycle **(Figure-IV.5)**. The effect of paratropic ring current effect was evident by the observation of two different signals at 3.57 and 1.80 ppm for the methyl protons of **IV.3** corresponding to inverted and non-inverted thiophenes **(Figure-IV.6)**.

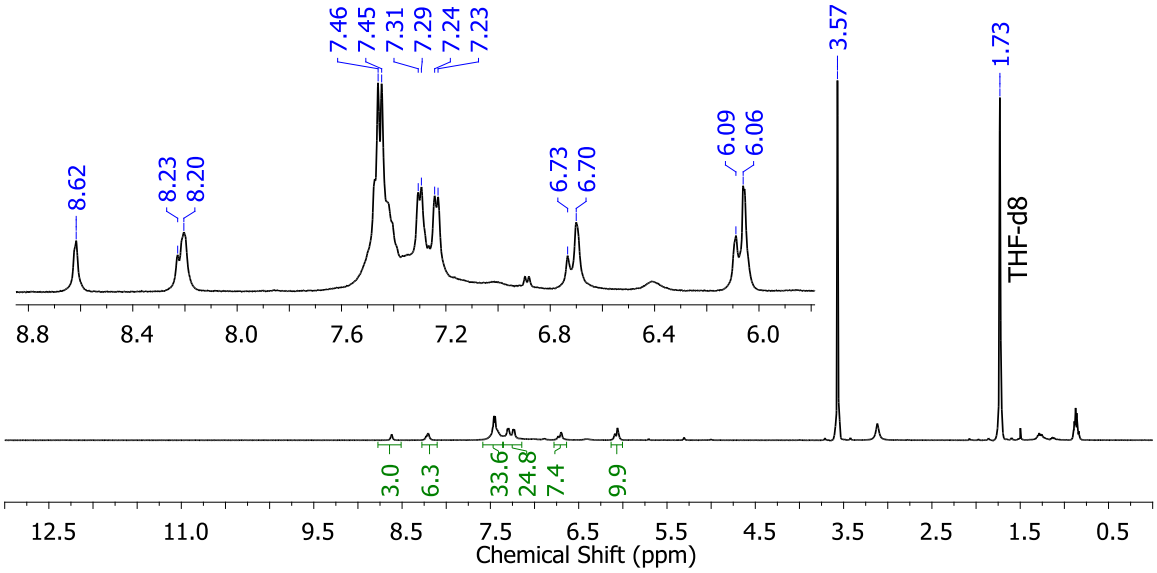

Figure-IV.5: ^{1}H NMR spectrum of **IV.2** in THF-d_8 at 195K.

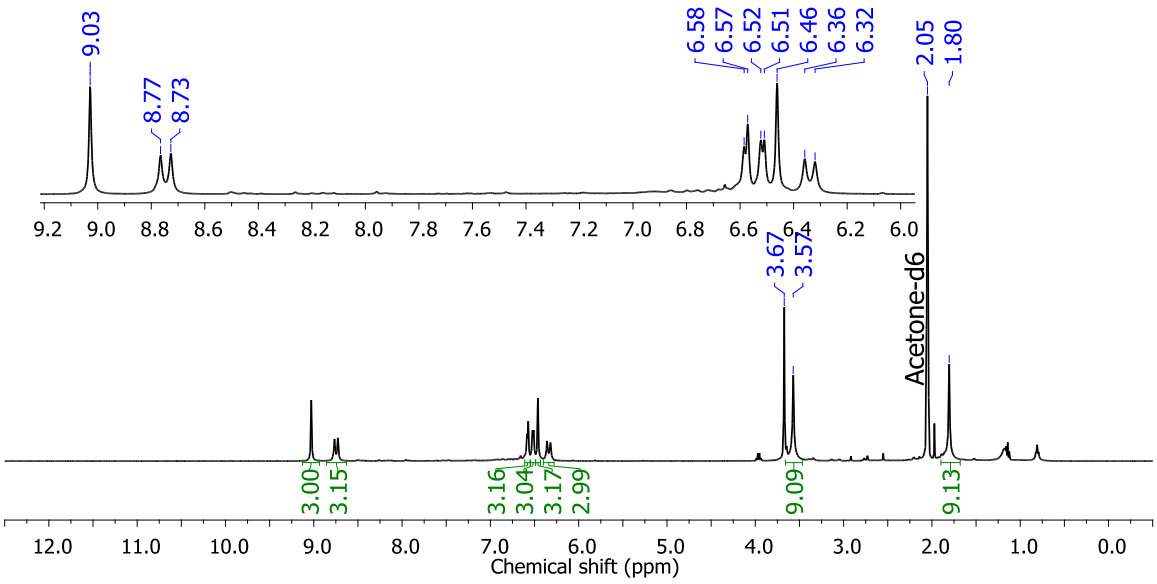

Figure-IV.6: ^{1}H NMR spectrum of **IV.3** in acetone-d_6 at 185K.

The 48π macrocycles **IV.4** and **IV.5** was synthesized by replacing three thiophene units with selenophene or furan, respectively, in **IV.1**, through a similar synthetic methodology. It was observed that their ^{1}H NMR spectrum was also dependent on temperature similar to that of **IV.1** to reveal the characteristic fluxional behavior at room temperature.

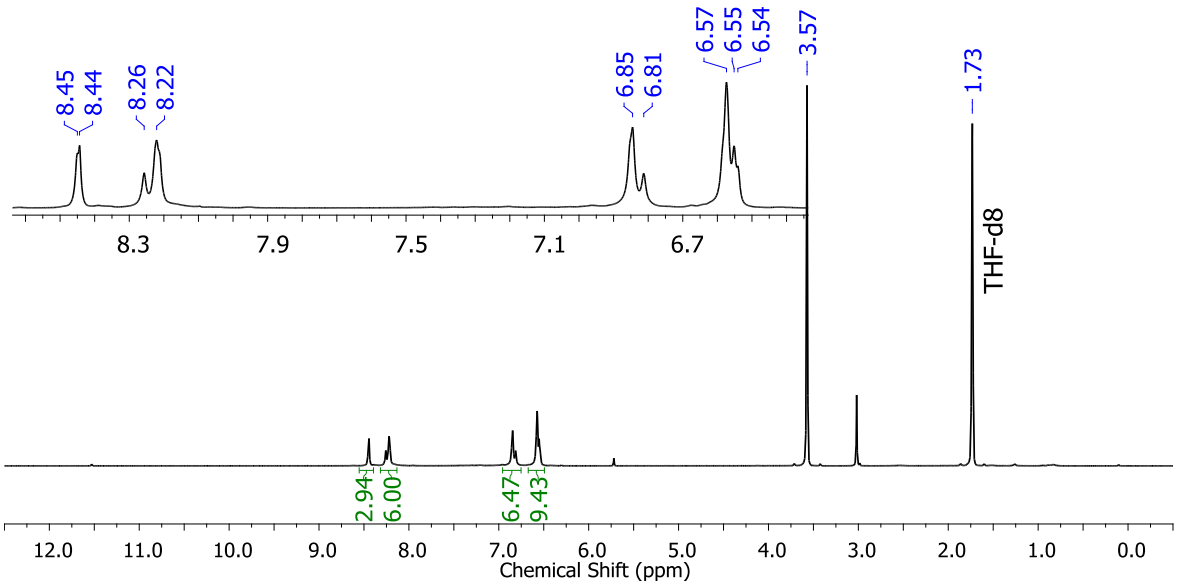

Figure-IV.7: ^{1}H NMR spectrum of **IV.4** in THF-d_8 at 190K.

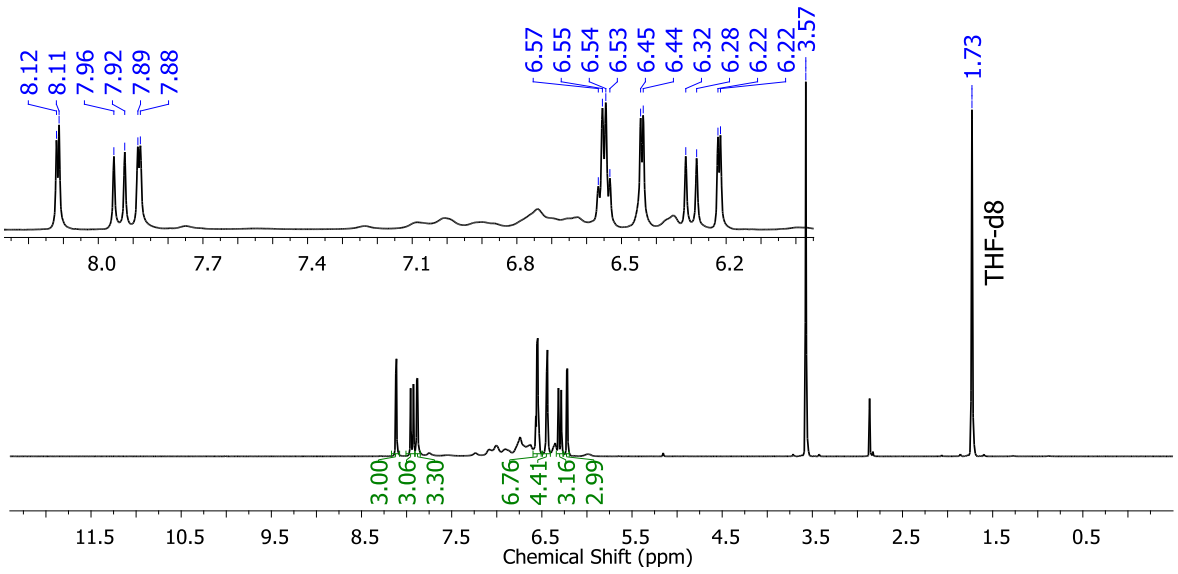

Figure-IV.8: ^{1}H NMR spectrum of **IV.5** in THF-d_8 at 228K.

All the thiophene units in **IV.1** were replaced by furan to obtain the nonafuran macrocycle **IV.6**. It displayed a well-resolved ^{1}H-NMR spectrum at room temperature **(Figure-IV.9)**. However the observed number of signals was sufficiently larger than expected in the region between 10.00–6.00 ppm. This suggested a characteristic unsymmetrical feature of this macrocycle. Its ^{1}H-^{1}H 2D COSY spectrum at room temperature revealed multiple cross-correlated signals suggestive of an irregular macrocyclic structure. Lowering the temperature did not affect the number of signals observed in the spectrum, indicating the absence of fluxional behaviour.

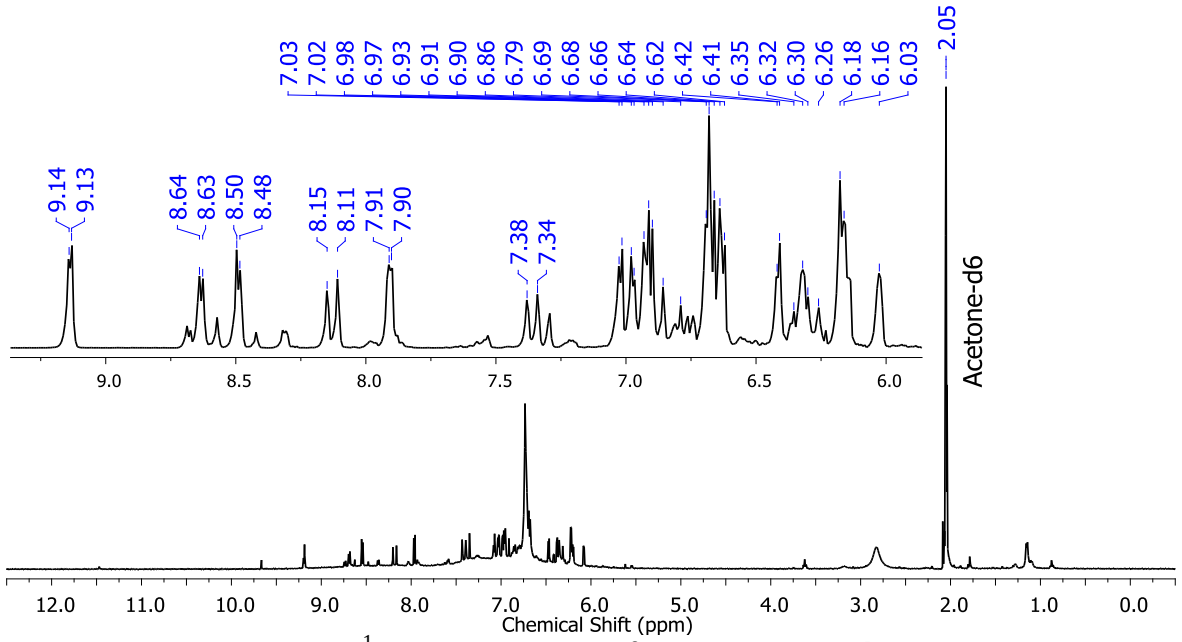

Figure-IV.9: ^{1}H NMR spectrum of **IV.6** in acetone-d_6 at 295K.

IV.3.2. Electronic Absorption Studies:

All the macrocycles (**IV.1-IV.6**) displayed intense pink colored solution in common organic solvents. Specifically, the pink colored **IV.1** exhibited a single and a relatively broad absorption at 565 nm (ε = 335,000). This relative red shift in the absorption with respect to the 32π anti-aromatic expanded isophlorins can be attributed to the increased length of the extended π conjugation in 48π macrocycles. It was curious to explore the reversible oxidation process as observed for the 32π expanded isophlorins. The 32π antiaromatic macrocycles underwent reversible ring oxidation in presence of trifluoroacetic acid or other oxidizing agents such as Meerwein's salt or $[NO]^{+}[BF_4]^{-}$ to yield 30π aromatic dications. These dications displayed a change in the chemical shift values of proton signals due to the remarkable inversion in the ring current effect of the macrocycle. Envisaging a similar reaction, 48π antiaromatic macrocycles were subjected to a similar oxidation process.

Addition of TFA to a pink colored solution of **IV.1** in dichloromethane induced a dramatic change to a dark green solution. A similar change in the color of solution was observed even upon the addition of Meerwein's salt or $[NO]^+[BF4]^-$, suggesting the oxidation of the 48π macrocycle to 46π aromatic dication. The green colored dicationic species displayed a much more intense absorption at 906 nm (419,000) with a bathochromic shift of 340 nm followed by significant absorptions in the near-IR region at 1328 nm (37,000) and 1560 nm (81,000) (**Figure-IV.9)**.

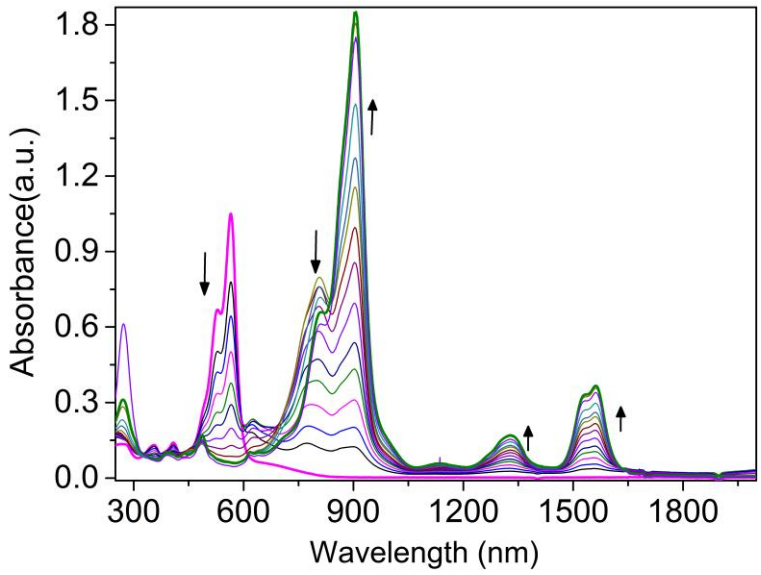

Figure-IV.10: Changes in the absorption spectrum upon the addition of dichloromethane solution of $[Et_3O]^+$ $[SbCl_6^-]$ to **IV.1**.

The other macrocycles **IV.2**, **IV.3, IV.4**, **IV.5** and **IV.6** also underwent the identical oxidation process upon the addition of TFA or other oxidizing agents mentioned above (**Figure-IV.11**). Even though **IV.5** was found to show distinct color change upon oxidation, its absorption spectrum was dissimilar compared to that observed for macrocycles mentioned above (**Figure-IV.11**). **IV.5** has a relatively broad absorption 567 nm (261,000), while **$[IV.5]^{2(.+)}$** exhibited split absorption bands with a hypsochromic and bathochromic shift relative to 567 nm. A blue shifted band at 458 nm (274,000) along with a red shifted band at 885 nm (287,000) with comparable intensity was followed by broad and weak absorptions in the near IR region between 1100 -1600 nm.

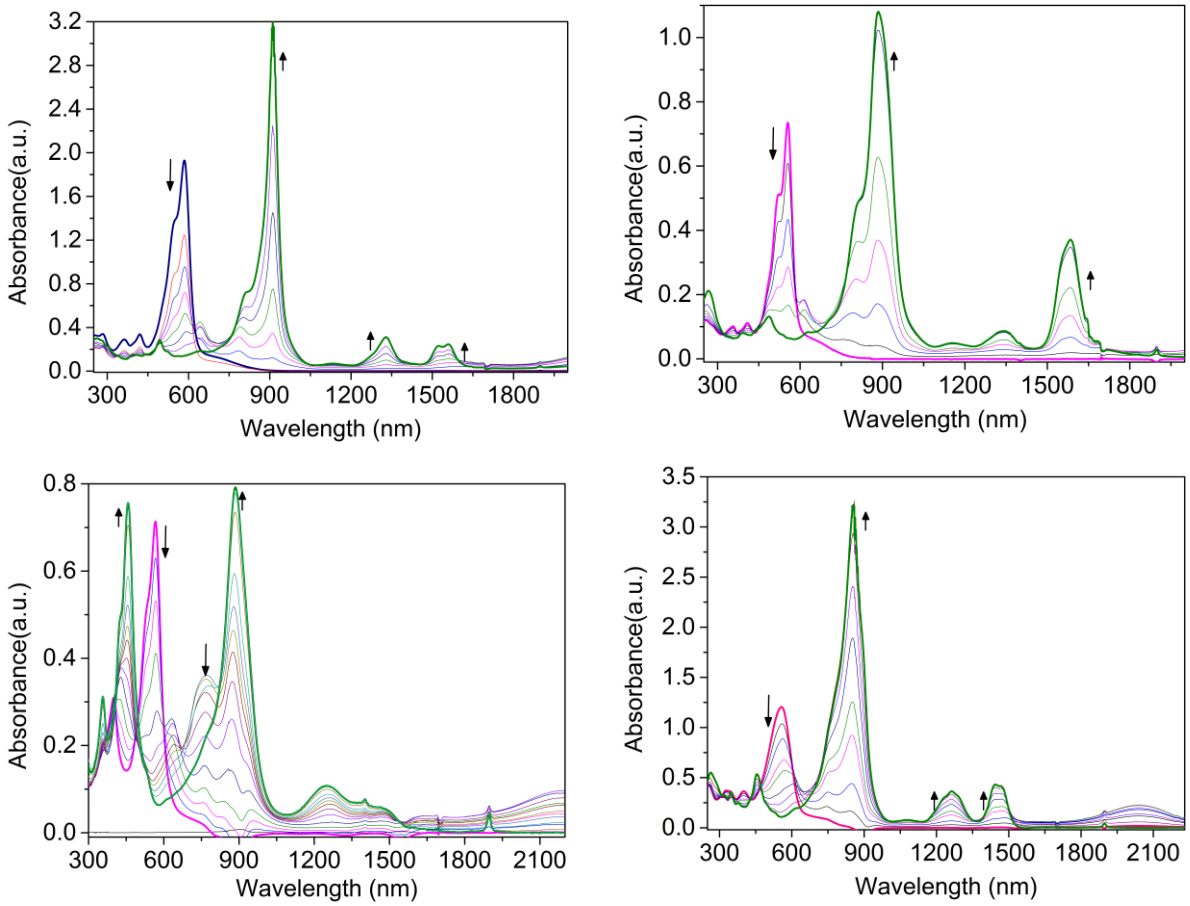

Figure-IV.11: Observed changes in absorption spectrum upon the addition of dichloromethane solution of $[Et_3O]^+ [SbCl_6^-]$ to **IV.3** (top left), **IV.4** (top right), **IV.5** (bottom left) and **IV.6** (bottom right)

More importantly these 46π dicationic radicals could be reduced by two electrons with appropriate reducing agents. Addition of triethyl amine to the TFA salt regenerated the absorption spectrum of the neutral molecule. Addition of metal based reducing agents $FeCl_2$ or Zn also reduced the dication generated from Meerwein's salt[46] or $[NO]^+[BF4]^-$. An interesting aspect of this redox process is the significant change in the absorption characteristics of these macrocycles. Almost all the macrocycles displayed 300nm red-shifted absorption with enhanced molar extinction co-efficient upon oxidation. Moreover, all these macrocycles were also found to absorb in the near IR region of the electromagnetic spectrum (**Table-IV.1**). It can be implied that all the 48π systems with similar structural feature adhere to comparable redox properties.

Macrocycle	Absorption	$\epsilon*10^{-5}$	Macrocycle	Absorption	$\epsilon*10^{-5}$
				905	4.19
IV.1	565	3.35	**(IV.1)$^{2(.+)}$**	1328	0.31
				1560	0.81
				920	3.56
IV.2	569	3.36	**(IV.2)$^{2(.+)}$**	1340	0.20
				1616	0.50
				911	5.48
IV.3	586	4.19	**(IV.3)$^{2(.+)}$**	1330	0.40
				1584	0.31
				886	4.20
IV.4	556	3.45	**(IV.4)$^{2(.+)}$**	1339	0.33
				1585	1.44
				458	2.74
IV.5	567	2.61	**(IV.5)$^{2(.+)}$**	885	2.87
				1252	0.39
				853	4.00
III.6	558	2.34	**(IV.6)$^{2(.+)}$**	1263	0.45
				1413	0.54

Table-IV.1: UV-Vis spectral data of 48π Expanded Isophlorins **IV.1 – IV.6** and their dication.

IV.3.3. ESR and HRMS characterization of dication:

The oxidized product was isolated and subjected to ^{1}H NMR analysis. Surprisingly, no signals were observed in its ^{1}H NMR spectrum as expected of an aromatic dication species. It was suspected as incomplete oxidation of the macrocycle, which could have perhaps generated a 47π radical cation intermediate in the process of two-electron oxidation. ESR spectrum of this product displayed a signal with a *g* value of 2.002 akin to an organic free radical (**Figure-IV.12**).

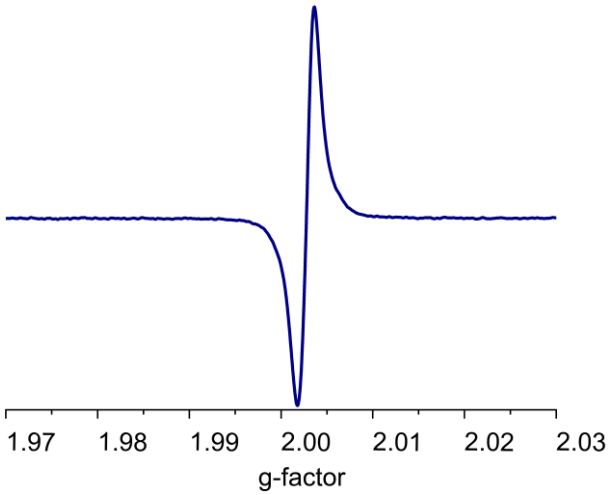

Figure-IV.12: ESR spectrum of the oxidized **IV.1** in CH_2Cl_2 at room temperature.

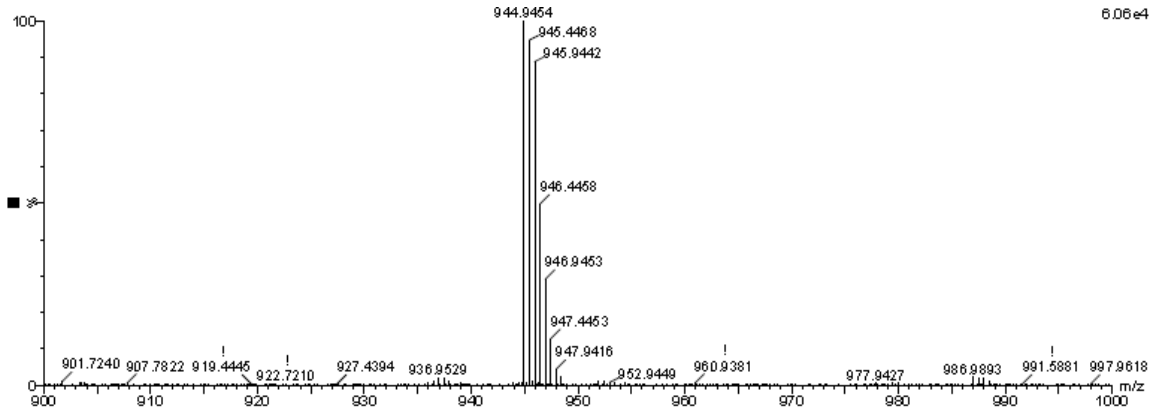

Figure-IV.12: HR-ESI-TOF mass spectrum of $[\mathbf{IV.1}]^{2\,(.+)}$.

Assuming that the signal corresponded to a cation radical, additional equivalents of the oxidizing agent were added to this sample. Nevertheless, annihilation of this signal could not be observed as expected for a 46π aromatic dication. Rather, the intensity of the ESR signal increased upon addition of excess equivalents of oxidizing agents. Even upon varying the temperature from 296K to 360K no significant change was observed in the ESR signal. The high-resolution mass spectrum of this species displayed at *m*/*z* value of 944.9454 (with separation of 0.5 amu) corresponding to half the molecular mass of the neutral macrocycle (1890.8456), confirming the two-electron oxidation of **IV.1**. ESR spectroscopy, electronic absorption and mass spectrometry revealed the oxidation of **IV.1** to a 46π dication diradical, $\mathbf{[IV.1]^{2(.+)}}$.

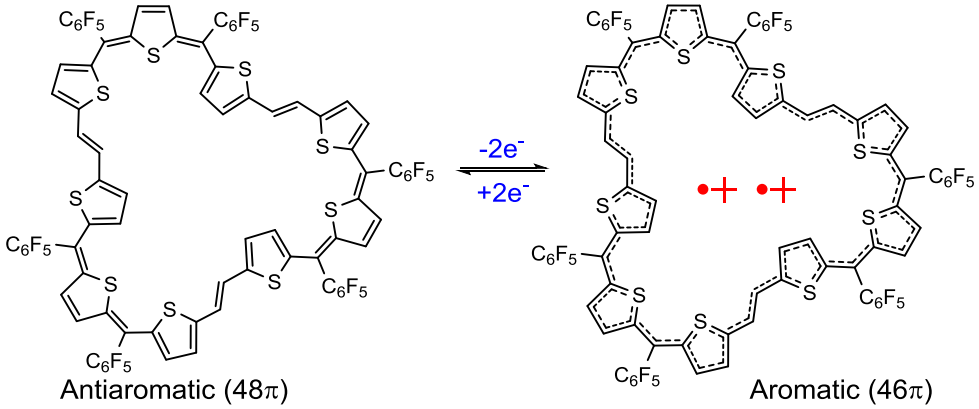

Scheme-IV.2: Reversible oxidation of 48π Expanded Isophlorin.

IV.3.4 Magnetic susceptibility measurements:

The radical nature of the oxidized species was analyzed by a SQUID magnetometer. The temperature dependence of susceptibility (χ_m) for **[IV.3]$^{2(.+)}$(SbCl$_6^-$)$_2$** and **[IV.3]$^{2(.+)}$(CF$_3$COO$^-$)$_2$** (**Figure-IV.13**) as measured by SQUID revealed a flat χ_m vs T plot above 25K indicating the singlet nature of diradical. Few examples of macrocyclic oligothiophenes have revealed a singlet character of polar pair upon two-electron oxidation[59, 71]. However, further decrease in temperature induced a sharp increase in its susceptibility suggestive of singlet to triplet transition. Such a transition is very rare for organic diradicals generated from macrocyclic oligothiophenes[59a].

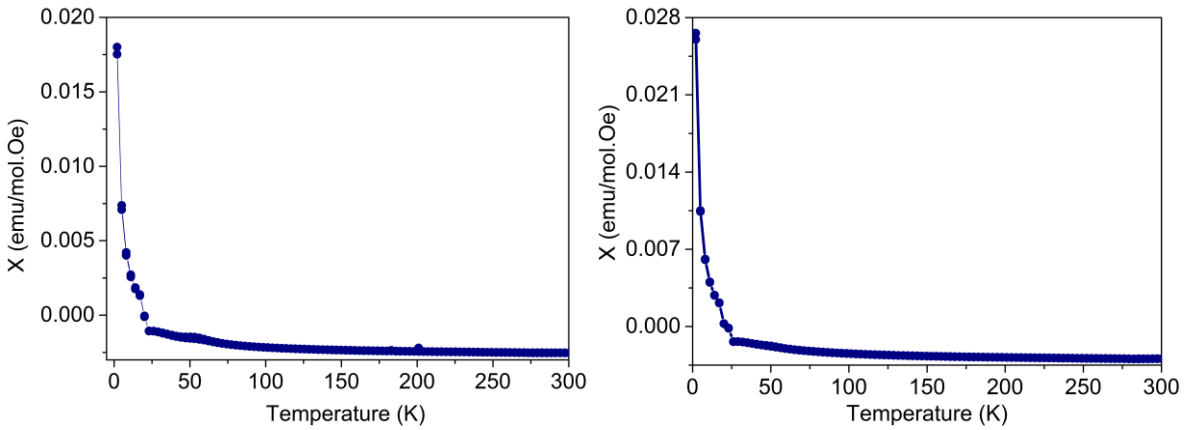

Figure-IV.13: χ vs T plot of **[IV.3]$^{2(.+)}$(SbCl$_6^-$)$_2$** (left) and **[IV.3]$^{2(.+)}$ (CF$_3$COO$^-$)$_2$** (right)**.**

IV.3.5. Cyclic voltammetric Studies:

In tune with the earlier analyses, cyclic voltammetric studies also suggested reversible oxidation of the 48π macrocycles (**Figure-IV.14**). Ideally two distinct waves can be expected for two one-electron oxidations. The observation of only one signal signified very little energy gap between the first and second oxidation. This was also further supported by titration studies employing electronic absorption spectroscopy, wherein the absorption peak of the second oxidation almost overlapped the first oxidation (**Figure-IV.14**). Such close energy gap between two successive oxidations can be attributed to the extended conjugated pathway of the macrocycle as similar to very lengthy oligomers[72].

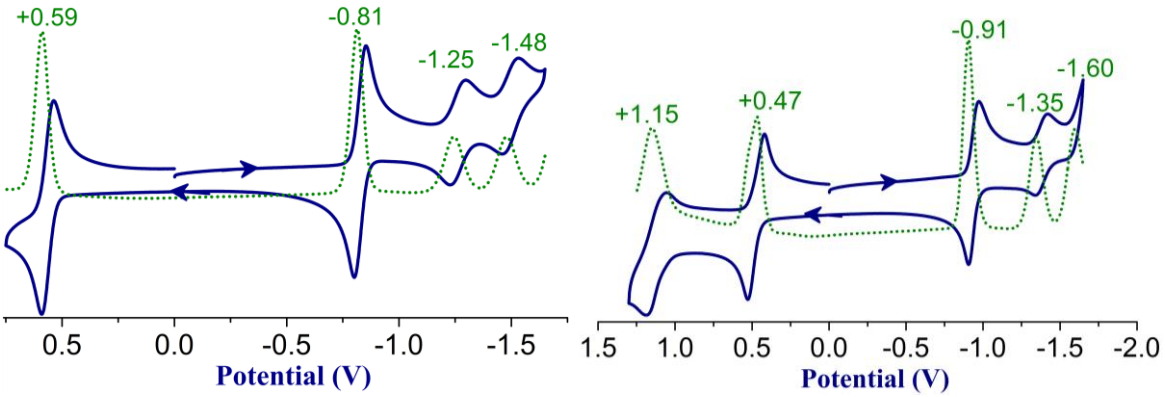

Figure-IV.14: Cyclic voltammograms (CV) and Differential pulse voltammogram (DPV) of **IV.1** (left) and **IV.5** (right) recorded in CH_2Cl_2 containing 0.1 M tetrabutylammonium perchlorate as the Supporting electrolyte recorded at a 50 mV s−1 scan rate.

.

IV.3.6. Single Crystal X-ray Diffraction Studies:

The molecular structure of all these macrocycles, **IV.2-IV.6,** and their trifluoroacetate salts was unambiguously determined from single crystal X-ray diffraction studies. Single crystals suitable for X-ray diffraction were grown from appropriate solvent combinations. All efforts to crystallize **IV.1** in a variety of solvents did not yield single crystals good enough for X-ray diffraction. However, single crystals of **IV.2**, **IV.3**, **IV.5** and **IV.6** suitable for X-ray diffraction was obtained through vapour diffusion technique from suitable solvent systems. Both **IV.2 (Figure-IV.15)** and **IV.3** (**Figure-IV.16**) were found to adopt a planar geometry with a threefold axis of symmetry. Both exhibited similar arrangement of the thiophene subunits in spite of the different substituents on the macrocycle. A thiophene from the (*E*)-1,2-dithienylethylene was found to be inverted such that the β-carbon atoms of these thiophene rings are exposed to central cavity of the macrocycle. Even the methyl substitution

on the β-carbon atoms could not prevent this ring inversion, to indicate the large cavity size of this giant macrocycle. The paratropic ring current effect in these macrocycles is substantiated by two different chemical shift values for the methyl protons in **IV.3** and the downfield chemical shifts for the protons of the inverted thiophene rings in **IV.1** and **IV.2**. In spite of their large structures, π-stacking was observed in their crystal packing. A very short distance of 3.16Å for **IV.3** and 3.44 Å for **IV.2** indicated unusual strong π-π interactions in such large macrocycles (**Figures-IV.15 and IV.16**).

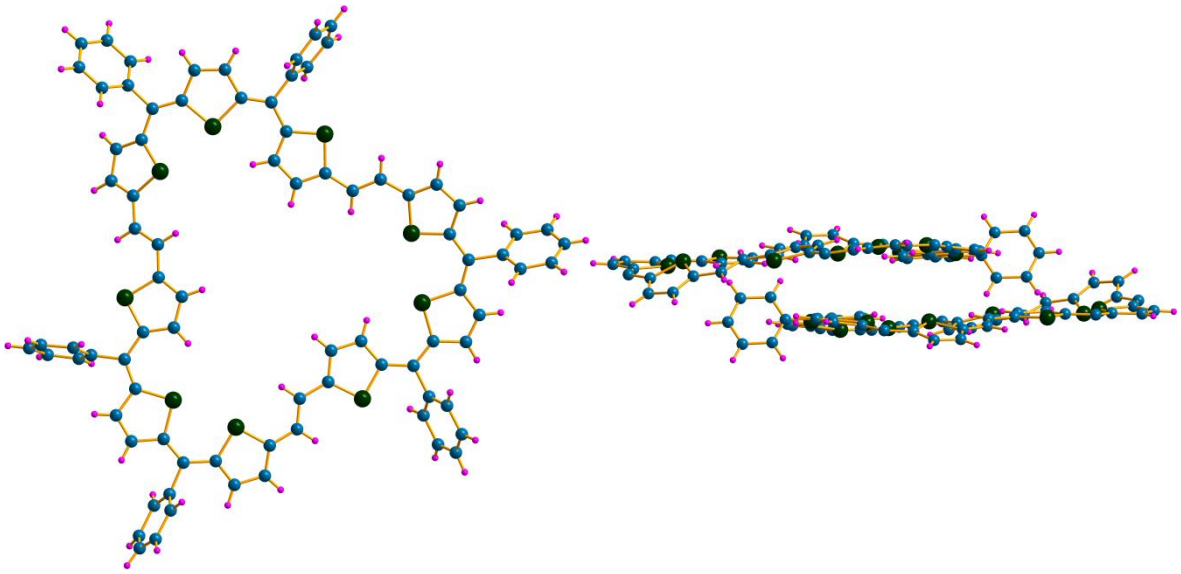

Figure-IV.15: Molecular structure of **IV.2** (left)**.** Solvent molecules are omitted for clarity. π-π Interactions observed in the crystal packing of **IV.2** (right).

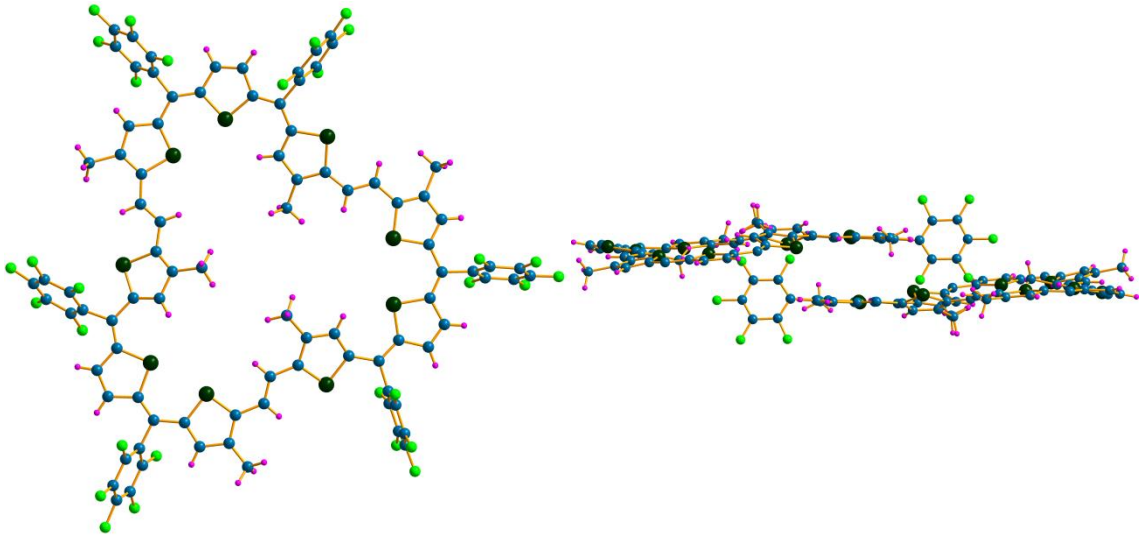

Figure-IV.16: Molecular structure of **IV.3** (left)**.** Solvent molecules are omitted for clarity. π-π Interactions observed in the crystal packing of **IV.3** (right)**.**

The molecular structure of **IV.5** (**Figure-IV.17**) was also found to be very similar to that of **IV.2** and **IV.3**. A furan unit connected through the ethylene unit was found to have an inverted configuration such that the β-carbons of the inverted heterocyclic rings were facing the ring current effects of the macrocycle. This macrocycle was also found to display remarkable π-π interactions as observed by the overlapping of two macrocycles within a short distance of 3.37 Å (**Figure-IV.17**).

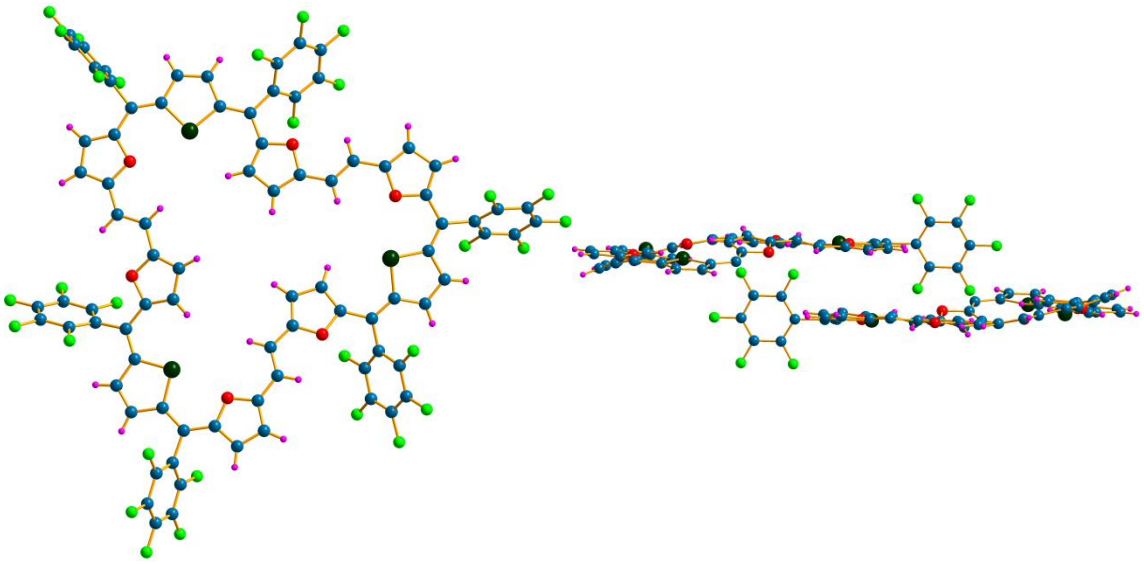

Figure-IV.17: Molecular structure of **IV.5 (**left**).** Solvent molecules are omitted for clarity. π-π Interactions observed in the crystal packing of **IV.5** (right)**.**

In a notable deviation from planarity for the 48π macrocycles, **IV.6** displayed a relatively non-planar confirmation (**Figure-IV.18**). Apart from the inversion of three furan rings, a *meso* pentafluorophenyl ring was also pulled right into the macrocyclic cavity. This positioning of the phenyl ring induced the loss of symmetry observed in **IV.6**, as supported by its ^{1}H NMR spectrum.

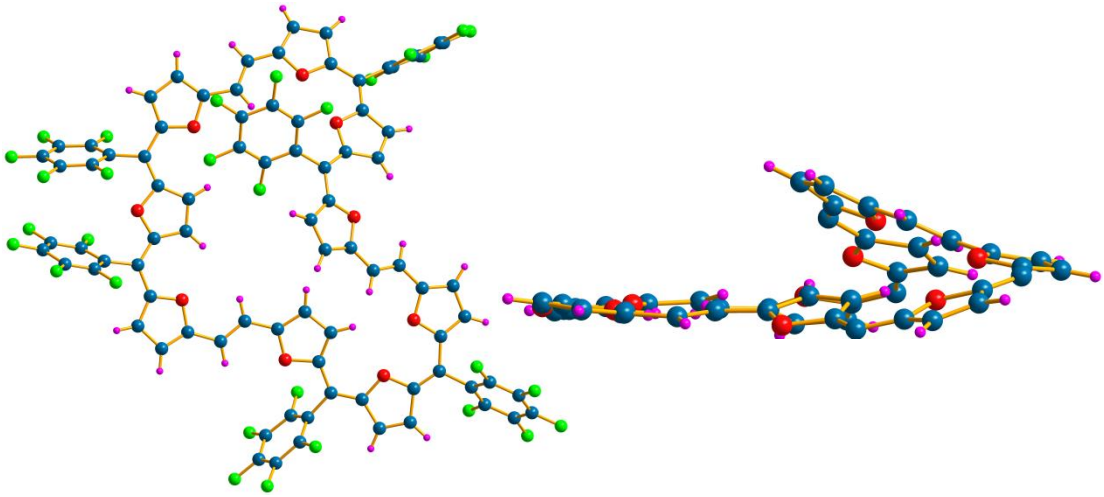

Figure-IV.18: Molecular structure of **IV.6.** Solvent molecules are omitted for clarity.

The dication diradicals of **IV.3**, **IV.5** and **IV.6** were crystallized as their TFA salts by slow evaporation of their solutions in trifluoroacetic acid. Both **[IV.3]**$^{2(.+)}$ and **[IV.6]**$^{2(.+)}$ were found to retain planar structure similar to that of their neutral molecules. In contrast, the dication diradical **[IV.5]**$^{2(.+)}$ displayed a marked change in its structure. The macrocycle adopted a figure-of-eight conformation with a twist at the center of the molecule (**Figure-IV.18**). This observation clearly distinguished the impact of the structure induced transformation in its electronic absorption spectrum of **[IV.5]**$^{2(.+)}$.

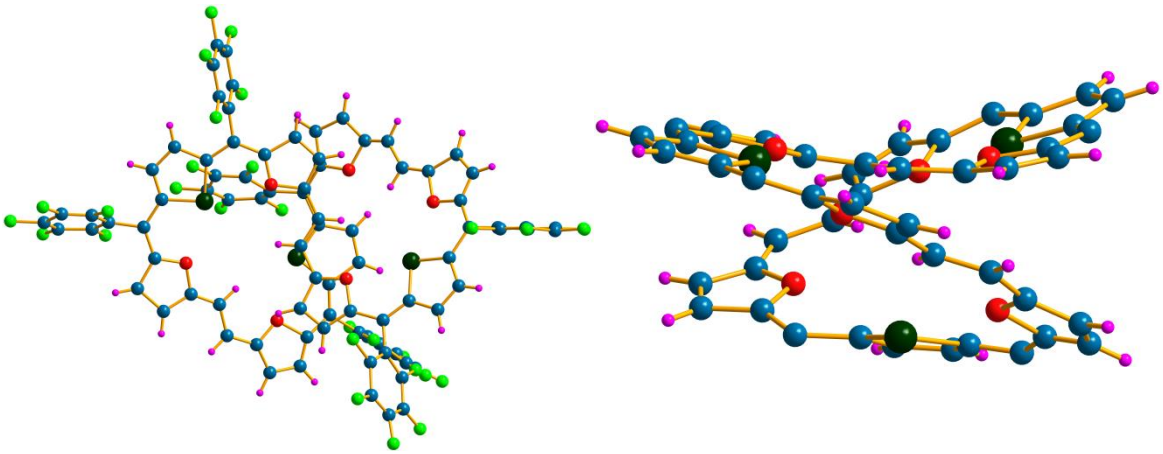

Figure-IV.19: Molecular structure of **[IV.5]**$^{2(.+)}$. TFA counter ions are omitted for clarity.

IV.4. Quantum mechanical calculations:

The antiaromatic character of 48π expanded isophlorins was further confirmed by Nucleus Independent Chemical Shift (NICS) calculations at global ring centers[49]. The computed NICS value of 2.95, 2.8, 3.65, 2.2, 4.14 and 3.61 for **IV.1**,**IV.2, IV.3, IV.4,IV.5,** and **IV.6** respectively, was suggestive of weak antiaromatic character. The estimated NICS values were found to have moderately negative values of -13.6, -13.27, -13.74, -12.94 and -12.2 for [**IV.1**]$^{2(.+)}$, [**IV.2**]$^{2(.+)}$, [**IV.3**]$^{2(.+)}$,[**IV.4**]$^{2(.+)}$ and [**IV.6**]$^{2(.+)}$ suggesting their aromatic character. In contrast, [**IV.5**]$^{2(.+)}$ was found to have a near zero NICS value as expected from the twist induced loss of aromaticity. The experimental value is in agreement with the estimated value of the HOMO-LUMO energy difference in the dications from DFT calculations (**Table-IV.2**).

Molecule	HOMO-LUMO (UV-Vis)eV	HOMO-LUMO (computed)eV
[**IV.1**]$^{2(.+)}$	0.79	1.05
[**IV.2**]$^{2(.+)}$	0.76	1.02
[**IV.3**]$^{2(.+)}$	0.79	1.12
[**IV.4**]$^{2(.+)}$	0.78	0.79
[**IV.5**]$^{2(.+)}$	0.99	1.21
[**IV.6**]$^{2(.+)}$	0.87	1.18

Table-IV.2: Energy gap between frontier molecular orbitals for the dication of 48π expanded isophlorins.

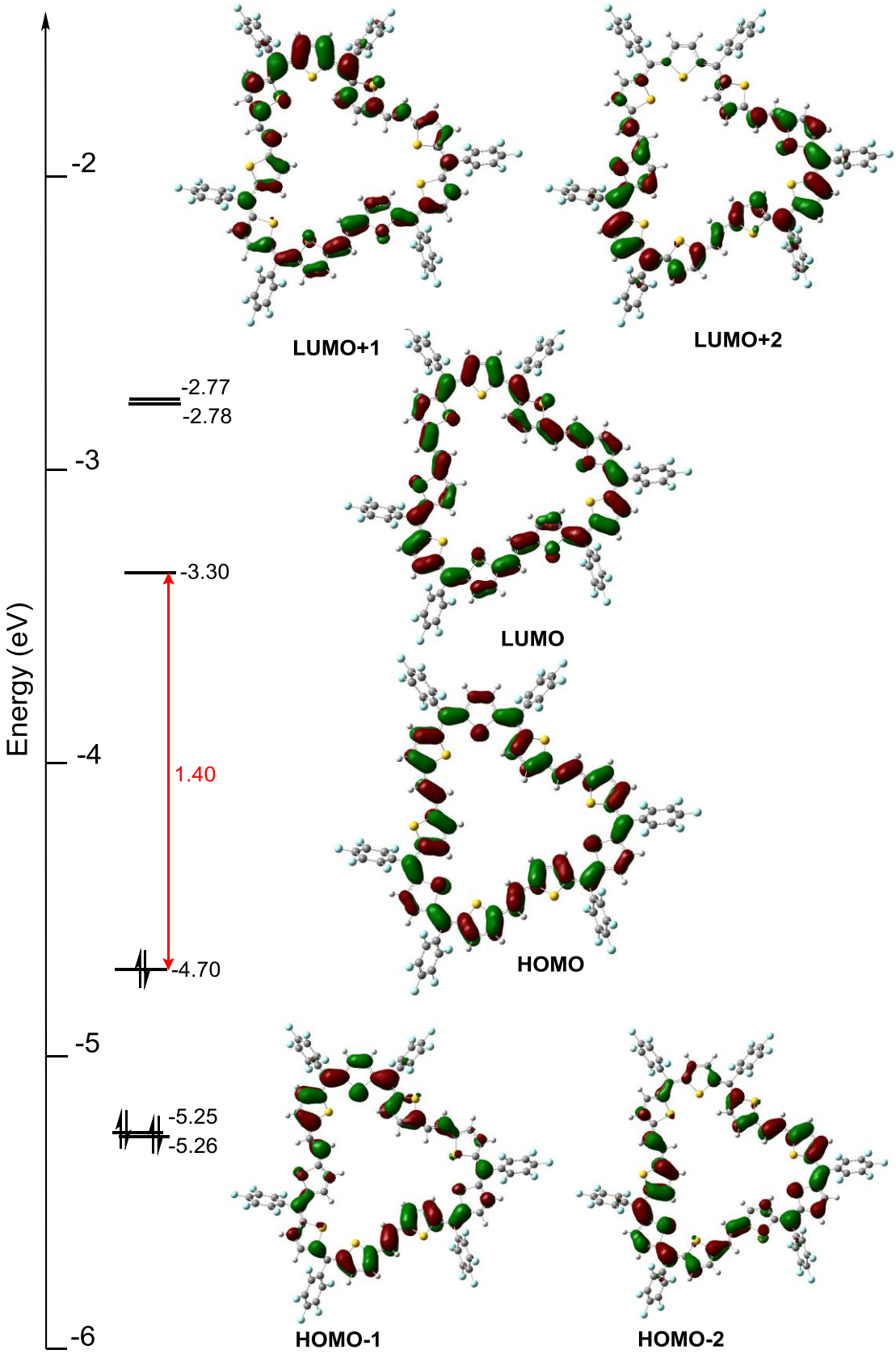

Figure-IV.20: Selected frontier MOs of **IV.1** calculated at the B3LYP/6-31G (d,p) level.

IV.5. Conclusions:

By varying the synthetic procedure employed for the 32π expanded isophlorins, larger planar 48π antiaromatic macrocycles could be synthesized in this simple and straightforward strategy. Single crystal X-ray diffraction studies revealed a planar geometry for most of the 48π antiaromatic expanded isophlorins described in this chapter. The planarity in large π-conjugated 48π like macrocycles are extremely rare and they even exhibited significant π-π interactions in the crystal packing. Till date, these molecules are the largest planar antiaromatic macrocycles to be characterized in the solid state. Even though the all-furan macrocycle did not adopt a twisted conformation, its unique non-planar structure was sufficient enough to reduce the antiaromatic properties. All the 48π expanded isophlorins exhibited significant deviation in their redox properties in contrast the smaller congeners of isophlorinoids. The 20π isophlorins derivatives of furan/thiophene/selenophene are known to form stable aromatic dications, while the expanded isophlorins with 32π electrons undergo relatively easier and reversible oxidation between neutral and aromatic dicationic states. Similar to 32π congeners, 48π macrocycles also undergo reversible two-electron oxidation as evidenced by mass spectrometry. Formally, these macrocycles belong to the (4n+2)π class of conjugated molecules and hence are expected to be aromatic nature. However, they were identified as paramagnetic species as observed from their ESR spectrum. This observation has not been familiar to any class of porphyrinoids including those reported by Vogel and Märkl. However, a similar observation has been observed for macrocyclic oligothiophenes, which are oxidized to the so called "polaron pair". This situation can be responsible for the Columbic repulsions between the charges by separating them in a lengthy conjugated pathway[71]. This is envisaged as weak spin-spin interaction between the two electrons in the HOMO of the dication. The weak delocalization was inferred from the ^{1}H NMR experiments and estimated low NICS values suggested reduced effect of ring current.

Upon oxidation, the macrocycles were also electronically modified as examined by absorption spectroscopy. Depending on the nature of the heteroatoms present in the core of the macrocycles, they are prone to structural modification in the dicationic state. While most of the thiophene based macrocycles retained their planarity, macrocycle with six furan sub units, **IV.5**, displayed a twisted conformation as confirmed by single crystal X-ray diffraction studies. Accordingly it also revealed the structure dependent electronic properties in such macrocyclic systems. The planar dications displayed a single intense absorption band. Twisted dication had two intense absorptions (hypsochromic and bathochromic) with respect

to its neutral macrocycle. Electronic absorption spectroscopy studies confirmed this structural modification to be reversible and dependent on the oxidation state of the macrocycle. Overall, the extension of the π conjugation in expanded isophlorins undergoes a phenomenal change in the electronic and redox properties. These observations clearly suggest the perimeter of the macrocycle as a good yard to tune the properties of these macrocycles.

IV.6. Experimental Section:

General synthetic procedure IV.1 - IV.6 and their cations: An equimolar concentration of ethylene bridged bis-thiophene/furan and the corresponding diol were dissolved in 75 ml dry dichloromethane and degassed with Argon for ten minutes. Then, a catalytic amount of boron trifluoride diethyl etherate ($BF_3.OEt_2$) was added under dark using a syringe. After stirring for an hour, two equivalents of DDQ were added and stirring continued for an additional 2 h. Then few drops of triethyl amine were added and the resultant solution was passed through a short basic Alumina column.This mixture was concentrated and further purified by silica gel column chromatography using CH_2Cl_2/hexane as eluent. The dications were generated by the addition of TFA to a solution of the macrocycle in dichloromethane. Evaporation of the solvent gave the dication as a metallic green solid. Dicationic salt of hexachloroantimonate was prepared as per earlier report.

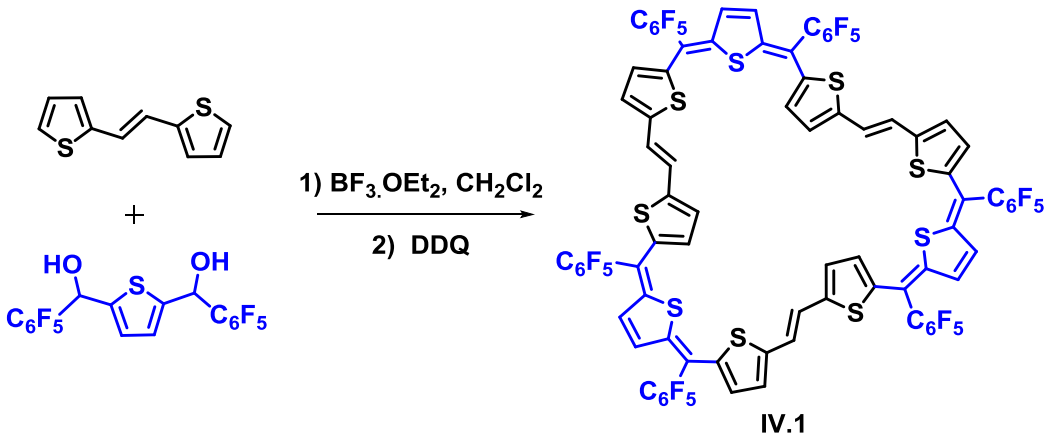

IV.1

IV.1: (E)-1,2-di(thiophen-2-yl)ethane (192 mg, 1 mmol) and thiophene-2,5-diylbis-((perfluorophenyl)methanol) (476 mg, 1 mmol) were reacted in presence of $BF_3.OEt_2$, (0.065 ml, 0.5 mmol), as described above to give **IV.1** in 10% yield. **^{1}H NMR** (500 MHz, acetone-d6, 206K) δ 8.72 (d, *J* = 3.9 Hz, 3H), 8.39 (d, *J* = 15.8 Hz, 3H), 8.08 (d, *J* = 4.1 Hz, 3H), 7.02 (d, *J* = 4.1 Hz, 3H), 6.75 (d, *J* = 15.8 Hz, 3H), 6.72 (d, *J* = 5.8 Hz, 3H), 6.65 (d, 6H). **^{19}F NMR** (471 MHz, acetone-d6, 196K) δ -141.60 (d, *J* = 20.8 Hz), -142.58 (d, *J* = 20.3 Hz), -

154.56 (t, *J* = 21.7 Hz), -156.28 (t, *J* = 20.8 Hz), -162.13 (t, *J* = 19.1 Hz), -162.90 (t, *J* = 19.7 Hz). **UV-Vis** (CH_2Cl_2): λ_{max} nm(ε) L mol^{-1} cm^{-1} = 565 (335,000). **HR-MS** (ESI-TOF): *m/z* =1890.8456; (found, $[M]^+$): 1890.8964 (calcd. For $C_{84}H_{24}F_{30}S_9$).

[**IV.1**]$^{2(.+)}$: **UV-Vis** (CH_2Cl_2): λ_{max} nm(ε) L mol^{-1} cm^{-1} = 906 (419,000), 1328 (31,000), 1560 (81,000). **HR-MS** (ESI-TOF): *m/z* =944.9454; (found, $[M]^{2+}$): 1890.8964 (calcd. (M) $C_{84}H_{24}F_{30}S_9$).

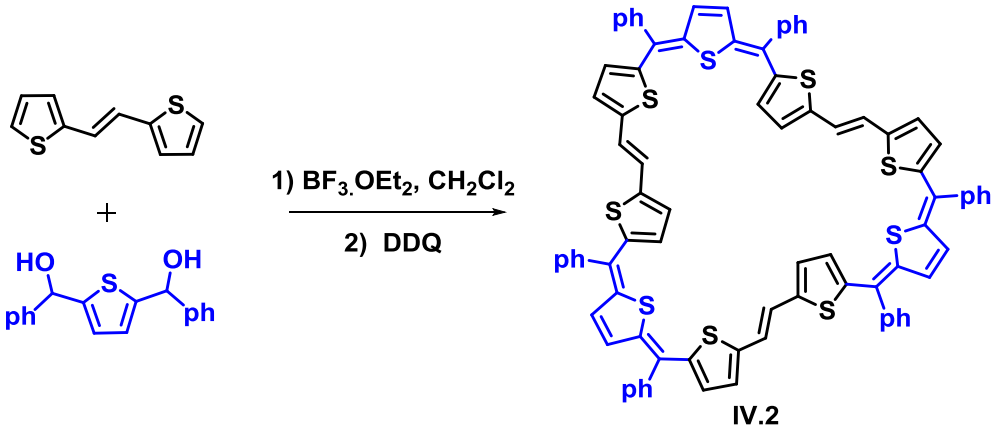

IV.2

IV.2: (E)-1,2-di(thiophen-2-yl)ethane (192 mg, 1 mmol) and thiophene-2,5-diylbis-(phenylmethanol) (296 mg, 1 mmol) were reacted in presence of $BF_3.OEt_2$, (0.065 ml, 0.5 mmol), as described above to give **IV.2** in 8% yield. **^{1}H NMR** (500 MHz, THF-d8, 196K) δ 8.62 (s, 3H), 8.22 (d, *J* = 11.8 Hz, 6H), 7.45 (d, *J* = 6.8 Hz, 33H), 7.27 (24H), 6.72 (d, *J* = 16.5 Hz, 7H), 6.07 (d, *J* = 13.9 Hz, 9H). **UV-Vis** (CH_2Cl_2): λ_{max} nm(ε) L mol^{-1} cm^{-1} = 569 (336,000).

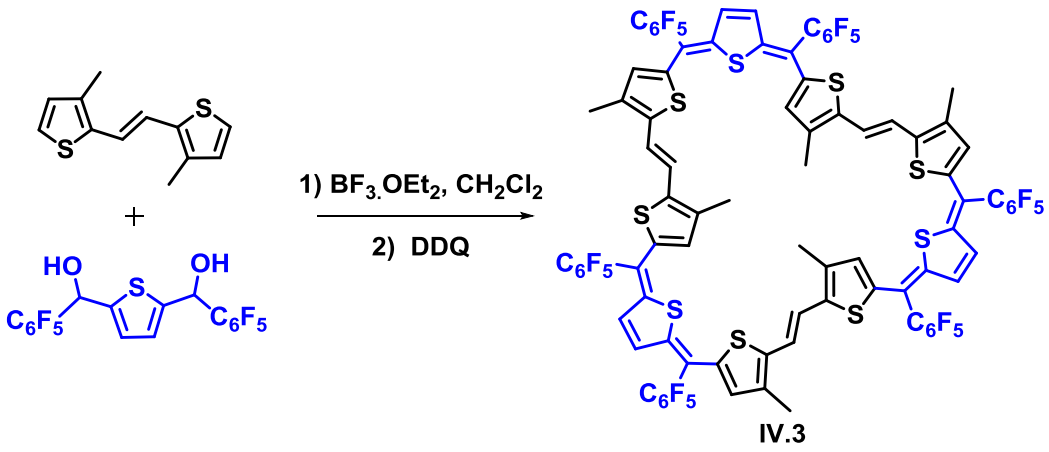

IV.3

IV.3: (E)-1,2-bis(3-methylthiophen-2-yl)ethene(220 mg, 1 mmol) and thiophene-2,5-diylbis-((perfluorophenyl)methanol)(476 mg, 1 mmol) were reacted in presence of $BF_3.OEt_2$, (0.065

ml, 0.5 mmol), as described above to give **IV.3** in 11% yield. **^{1}H NMR** (400 MHz, acetone-d6,183K) δ 9.03 (s, 3H), 8.75 (d, *J* = 15.4 Hz, 3H), 6.58 (d, *J* = 5.4 Hz, 3H), 6.52 (d, *J* = 5.2 Hz, 3H), 6.46 (s, 3H), 6.34 (d, *J* = 15.4 Hz, 3H), 3.57 (s, 9H), 1.80 (s, 9H). **^{19}F NMR** (376 MHz, acetone-d6, 213K) δ -141.63 (d, *J* = 21.5 Hz), -142.37 (d, *J* = 22.4 Hz), -154.49 (t, *J* = 17.9 Hz), -156.34 (t, *J* = 19.6 Hz), -162.28 (d, *J* = 21.7 Hz), -162.95 (t, *J* = 18.5 Hz). **UV-Vis** (CH_2Cl_2): λ_{max} nm (ε) L mol^{-1} cm^{-1} = 586 (419,000). **HR-MS** (ESI-TOF): *m/z* =1974.9844; (found, $[M]^+$): 1974.9855 (calcd. For $C_{90}H_{36}F_{30}S_9$).

[IV.3]$^{2(.+)}$: **UV-Vis** (CH_2Cl_2): λ_{max} nm(ε) L mol^{-1} cm^{-1} = 911 (548,000), 1330 (40,000), 1559 (31,000).

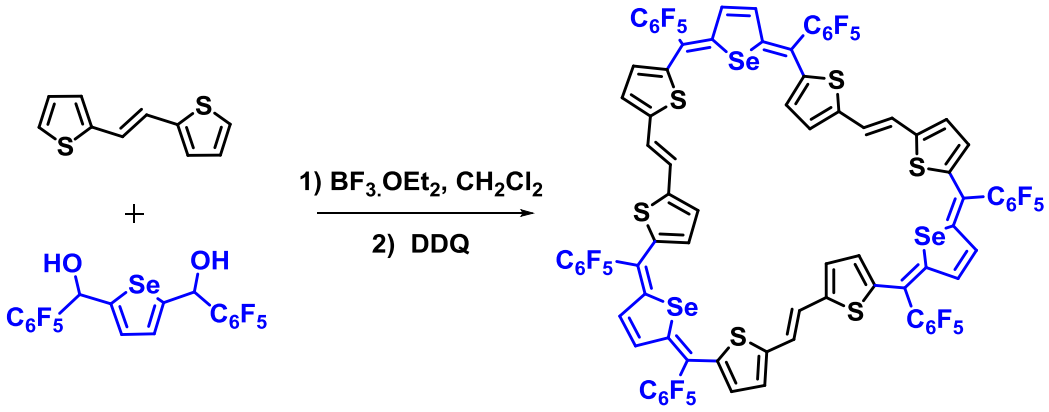

IV.4

IV.4: (E)-1,2-di(thiophen-2-yl)ethane (192 mg, 1 mmol) and selenophene-2,5-diylbis((perfluorophenyl)methanol) (523 mg, 1 mmol) were reacted in presence of $BF_3.OEt_2$, (0.065 ml, 0.5 mmol), as described above to give **IV.4** in 10% yield. **^{1}H NMR** (500 MHz, THF-d8, 190K) δ 8.45 (d, *J* = 3.1 Hz, 3H), 8.24 (6H), 6.83 (6H), 6.67 – 6.48 (m, 9H). **^{19}F NMR** (471 MHz, THF-d8, 192K) δ -142.84 (bs), -143.87 (bs), -156.93 (s), -158.45 (bs), -164.19 (bs), -164.76 (bs). **UV-Vis** (CH_2Cl_2): λ_{max} nm (ε) L mol^{-1} cm^{-1} = 556 (345,000). **HR-MS** (ESI-TOF): *m/z* =2031.6748; (found, $[M]^+$): 2031.7253 (calcd. For $C_{84}H_{24}F_{24}S_6Se_3$).

[IV.4]$^{2(.+)}$: **UV-Vis** (CH_2Cl_2): λ_{max}nm(ε) L mol^{-1} cm^{-1} = 886 (420,000), 1339 (33,000), 1585 (144,000).

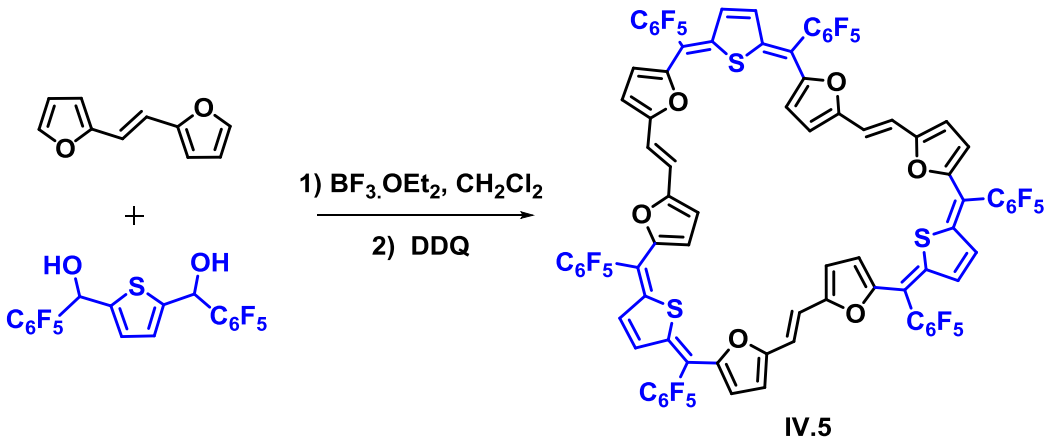

IV.5: (E)-1,2-di(furan-2-yl)ethane (160 mg, 1 mmol) and thiophene-2,5-diylbis((perfluorophenyl)methanol) (476 mg, 1 mmol) were reacted in presence of $BF_3.OEt_2$, (0.065 ml, 0.5 mmol), as described above to give **IV.5** in 12% yield.**^{1}H NMR** (500 MHz, THF-d8, 227K) δ 8.12 (d, *J* = 3.7 Hz, 3H), 7.94 (d, *J* = 15.6 Hz, 3H), 7.88 (d, *J* = 3.6 Hz, 3H), 6.55 (q, *J* = 5.9 Hz, 6H), 6.44 (d, *J* = 3.8 Hz, 3H), 6.30 (d, *J* = 15.6 Hz, 3H), 6.22 (d, *J* = 3.6 Hz, 3H). **UV-Vis** (CH_2Cl_2): λ_{max} nm(ε) L mol^{-1} cm^{-1} = 567 (261,000). **HR-MS** (ESI-TOF): *m/z* =1794.0131; (found, $[M]^+$): 1794.0256 (calcd. For $C_{84}H_{24}F_{24}O_6S_3$).

[IV.5]$^{2(.+)}$: **UV-Vis** (CH_2Cl_2): λ_{max}nm (ε) L mol^{-1} cm^{-1} = 458 (274,000), 885 (287,000), 1252 (39,000).

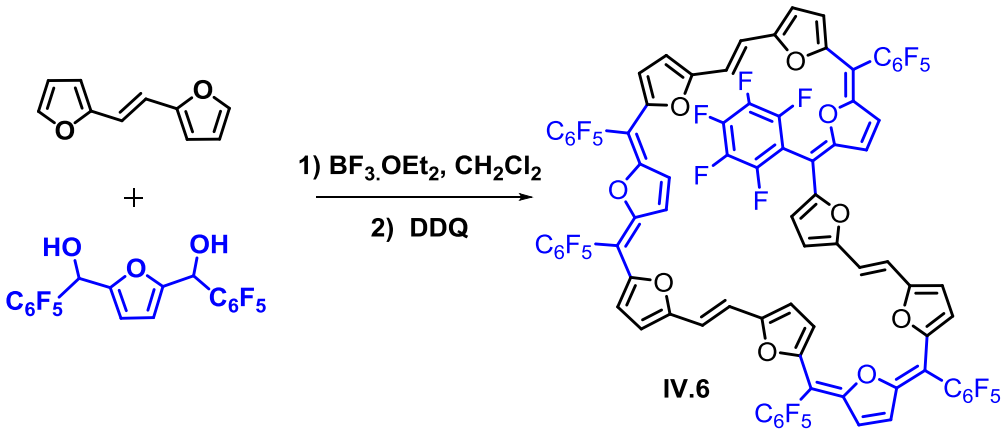

IV.6: (E)-1,2-di(furan-2-yl)ethane (160 mg, 1 mmol) and furan-2,5-diylbis((perfluorophenyl)methanol) (460 mg, 1 mmol) were reacted in presence of $BF_3.OEt_2$, (0.065 ml, 0.5 mmol), as described above to give **1c** in 8% yield. **^{1}H NMR** (400 MHz, ACETONE-D6) δ 9.14 (d, *J* = 3.8 Hz, 5H), 8.63 (d, *J* = 5.0 Hz, 6H), 8.49 (d, *J* = 4.8 Hz, 5H), 8.13 (d, *J* = 16.1 Hz, 5H), 7.91 (d, *J* = 3.6 Hz, 6H), 7.36 (d, *J* = 16.0 Hz, 4H), 6.95 (ddd, *J* = 29.4, 20.5, 10.5 Hz, 22H), 6.79 (s, 1H), 6.79 – 6.60 (m, 23H), 6.39 (t, *J* = 12.9 Hz, 7H), 6.34 – 6.25 (m, 7H), 6.17 (d, *J* = 6.2 Hz, 10H), 6.03 (s, 7H).

UV-Vis (CH_2Cl_2): λ_{max} nm(ε) L mol^{-1} cm^{-1} = 558 (234,000). **HR-MS** (ESI-TOF): *m*/*z* =1746.0852; (found, $[M]^+$): 1746.0941 (calcd. For $C_{84}H_{24}F_{24}O_6S_3$).

[IV.6]$^{2(\cdot+)}$: **UV-Vis** (CH_2Cl_2): λ_{max} nm(ε) L mol^{-1} cm^{-1} = 854 (400,000), 1262 (45,000), 1443 (54,000).

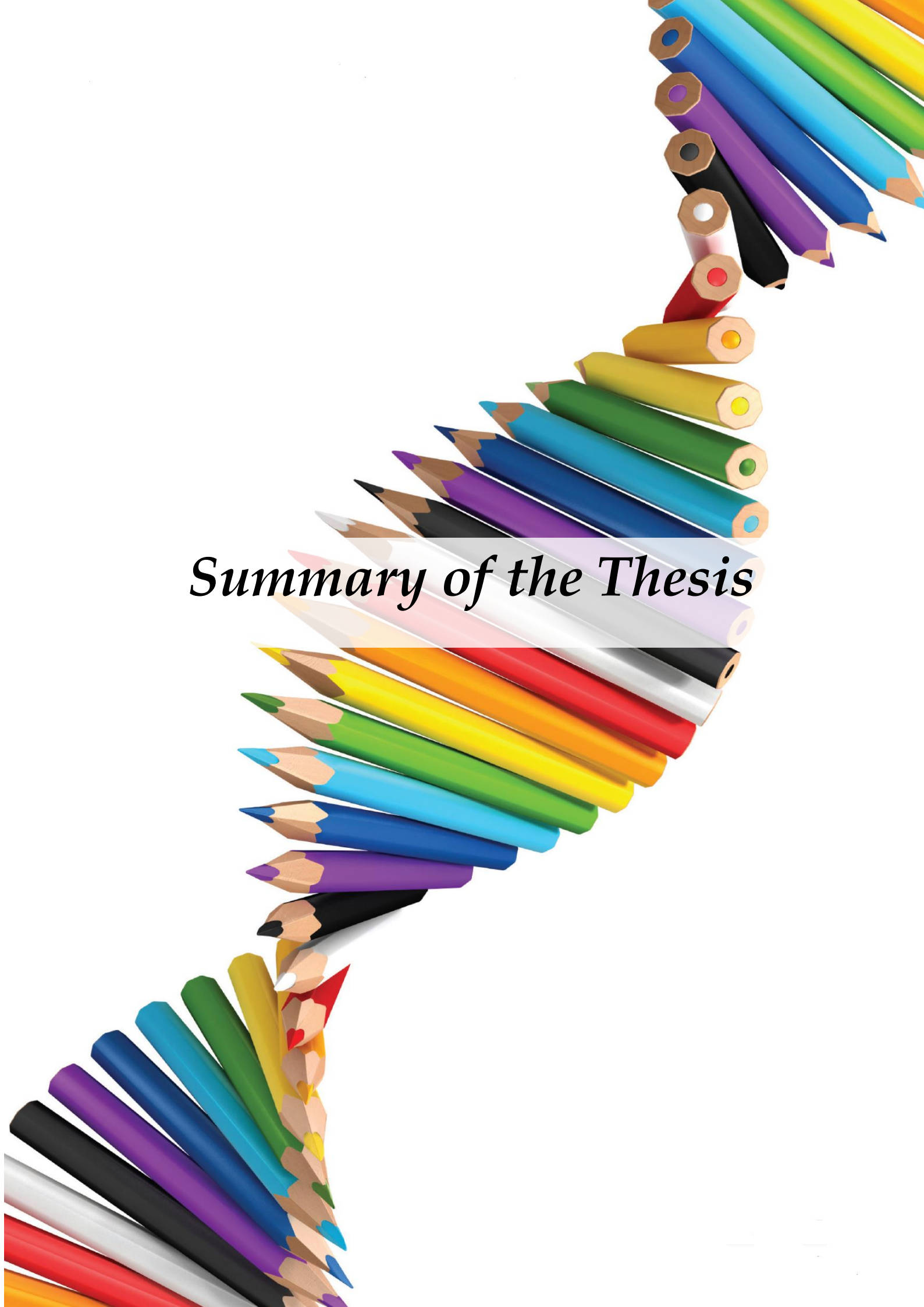

Summary of the Thesis

The thesis describes the synthesis, characterization and redox properties of the expanded isophlorins derived from heterocycles such as thiophene, furan and selenophene. From the synthetic view point, the one-pot synthesis of expanded isophlorins from thiophene and pentafluoro benzaldehyde yielded all possible types of π-conjugated cyclic systems. Detailed analyses and spectroscopic characterization distinguished the properties of the isolated macrocycles in terms of their structural features, electronic properties and redox potential. The most significant aspect of this thesis is in the discovery of neutral and dicationic paramagnetic species of expanded isophlorins. Even though thiophene based macrocycles were synthesized and studied in detail, the formation of a 25π radical had escaped the observation of synthetic porphyrin chemists. The versatility of thiophene's electronic and structural features is more suitable as a building block, than pyrrole, in the synthesis of π-conjugated macrocyclic radicals. The intermediate class of (4n+1)π electron radicals can act as a bridge to the already known aromatic and antiaromatic molecules. Given the fact that such radicals can undergo subtle one electron reduction, they appear to possess potential characteristics expected of ambipolar semiconductor.

The properties of expanded isophlorins exhibited a significant change with increase in the length of their π-conjugation. Extended π-circuits not only altered the structural features, but also induced concomitant alterations in the electronic properties with respect to the 20π antiaromatic isophlorins. Structurally, they either have a planar geometry or a twisted confirmation. For planar 32π expanded isophlorins, it was observed that a few heterocyclic rings were inverted depending on the composition of the heterocyclic rings in the macrocycle. However, ring inversion was a common feature in all the 48π expanded isophlorins. All the planar 32π, 40π and 48π expanded isophlorins were found to be antiaromatic in nature. Both experimental and computational studies indicated the reduced delocalization of π-electrons in comparison to the 20π isophlorins. Particularly for the ethylene bridged expanded isophlorins the experimental Δδ values calculated from their respective ^{1}H NMR spectrum decreased from 8 ppm for 32π systems to 2 ppm in 48π macrocycles. In support of this observation, the estimated NICS values also decreased with increase in the length of the conjugated pathway. 20π isophlorins were estimated to have a NICS values in the range of +40 to +30 ppm. As the conjugation expanded to 32π electrons, the estimated NICS values were observed in the region between +10 to +20 ppm. The largest of the planar systems bearing 48π electrons were estimated to have much lower NICS values in the range between 0 to +5 ppm. Curiously, the estimated NICS value of +17 for 25π radical strongly suggested antiaromatic feature of this

macrocycle. The value further increased to +35 for the corresponding oxidized 24π cation endorsing its antiaromatic character.

An important change was observed in the nature of the oxidized product of these antiaromatic macrocycles. Irrespective of the structural features, all of them underwent two-electron oxidation leading to the formation of (4n+2)π electron systems. The 30π dication derived by the oxidation of 32π macrocycles was found to be aromatic from their ^{1}H NMR spectrum and also form the estimated NICS values. The effect of ring current effects was more dramatic in the 30π aromatic dications as the calculated Δδ values were in the range of 25 to 20 ppm. Even though the estimated NICS values did confirm the aromatic behavior of dications, the value did not reflect the intensity of the π delocalization as observed from ^{1}H NMR spectroscopy. More intriguingly, the 46π dications derived by the oxidation of 48π expanded isophlorins were found to be paramagnetic as confirmed from magnetic measurements and ESR spectroscopy. Such a significant deviation can attributed to the increased perimeter of the macrocycles, which can favor the charge repulsion in extended π conjugation. This observation is peculiar to antiaromatic isophlorins and has not been noted in structurally similar porphyrinoids. The role of heterocyclic rings appears to be crucial since non-antiaromatic macrocyclic oligothiophenes are also reported to exhibit similar properties for their respective oxidized species. 40π octathiophene also exhibited paramagnetic behavior upon two-electron oxidation. More importantly it exhibited a not so common macrocycle splitting reaction leading to the formation of two 20π isophlorins upon reaction with a fullerene C_{60}. Even though the reaction is very surprising, further studies are required to study and explore the mechanism of this reaction.

In conclusion, this thesis reveals the unexplored facets of isophlorin and its expanded derivatives in particular, which can be extrapolated to antiaromatic systems in general. It can be easily observed that antiaromatic molecules possess redox characteristics dissimilar to the aromatic counterparts. The potential of antiaromatic molecules in organic electronics is yet to be discovered. Since they appear to possess better redox properties compared to aromatic molecules, it is expected that the findings described in this thesis would encourage the role of isophlorin and its expanded derivatives as organic semiconductors.

References

[1] P. J. Garratt, *Aromaticity*, Wiley:, New York, **1986**.
[2] a) R. Breslow, *Chem. Eng. News* **1965**, *43*, 90; b) Sondheim.F, *Acc. Chem. Res.* **1972**, *5*, 81; c) R. Breslow, *Acc. Chem. Res.* **1973**, *6*, 393.
[3] A. D. Allen, T. T. Tidwell, *Chem. Rev.* **2001**, *101*, 1333.
[4] R. B. Woodward, *Angew. Chem.* **1960**, *72*, 651.
[5] a) E. Vogel, W. Haas, B. Knipp, J. Lex, H. Schmickler, *Angew. Chem. Int. Ed.* **1988**, *27*, 406; b) H. Wilhelm, K. Bernd, S. Martin, L. Johann, V. Emanuel, *Angew. Chem., Int. Ed.* **1988**, *27*; c) E. Vogel, P. Rohrig, M. Sicken, B. Knipp, A. Herrmann, M. Pohl, H. Schmickler, J. Lex, *Angew. Chem., Int. Ed.* **1989**, *28*, 1651; d) M. Pohl, H. Schmickler, J. Lex, E. Vogel, *Angew. Chem., Int. Ed.* **1991**, *30*, 1693; e) R. Bachmann, F. Gerson, G. Gescheidt, E. Vogel, *J. Am. Chem. Soc.* **1992**, *114*, 10855; f) E. Vogel, M. Pohl, A. Herrmann, T. Wiss, C. König, J. Lex, M. Gross, J. P. Gisselbrecht, *Angew. Chem. Int. Ed.* **1996**, *35*, 1520.
[6] J. A. Cissell, T. P. Vaid, A. L. Rheingold, *J. Am. Chem. Soc.* **2005**, *127*, 12212.
[7] C. Liu, D.-M. Shen, Q.-Y. Chen, *J. Am. Chem. Soc.* **2007**, *129*, 5814.
[8] A. Weiss, M. C. Hodgson, P. D. W. Boyd, W. Siebert, P. J. Brothers, *Chem. Eur. J.* **2007**, *13*, 5982.
[9] J. S. Reddy, V. G. Anand, *J. Am. Chem. Soc.* **2008**, *130*, 3718.
[10] M. Kon-no, J. Mack, N. Kobayashi, M. Suenaga, K. Yoza, T. Shinmyozu, *Chem. Eur. J.* **2012**, *18*, 13361.
[11] Y. Matano, T. Nakabuchi, S. Fujishige, H. Nakano, H. Imahori, *J. Am. Chem. Soc.* **2008**, *130*, 16446.
[12] J. S. Reddy, V. G. Anand, *J. Am. Chem. Soc.* **2009**, *131*, 15433.
[13] a) M. Iyoda, J. Yamakawa, M. J. Rahman, *Angew. Chem., Int. Ed.* **2011**, *50*, 10522; b) F. Zhang, G. Gotz, H. D. F. Winkler, C. A. Schalley, P. Bauerle, *Angew. Chem. Int. Ed.* **2009**, *48*, 6632.
[14] D. F. (ed.), in *Handbook of Oligo- and Polythiophenes*, Wiley-VCH Verlag GmbH, Weinheim, **1999**.
[15] I. Perepichka, D. Perepichka, *Handbook of Thiophene-Based Materials: Applications in Organic Electronics and Photonics*, John Wiley & Sons, **2009**.
[16] J. Kromer, I. Rios-Carreras, G. Furhmann, C. Musch, M. Wunderlin, T. Debaerdemacker, E. Mena-Osteritz, P. Bauerle, *Angew. Chem., Int. Ed.* **2000**, *39*, 3481.
[17] E. Mena-Osteritz, P. Bauerle, *Adv. Mater. (Weinheim, Ger.)* **2001**, *13*, 243.
[18] G. Fuhrmann, T. Debaerdemaeker, P. Bauerle, *Chem. Commun* **2003**, 948.
[19] A. Strand, B. Thulin, O. Wennerström, O. Wennerström, A. Christensen, G. Schroll, *Acta Chem. Scand.* **1977**, *31b*, 521.
[20] a) Z. Y. Hu, J. L. Atwood, M. P. Cava, *J. Org. Chem.* **1994**, *59*, 8071; b) Z. Hu, J. L. Atwood, M. P. Cava, *The Journal of Organic Chemistry* **1994**, *59*, 8071.
[21] Z. Hu, C. Scordilis-Kelley, M. P. Cava, *Tetrahedron Lett.* **1993**, *34*, 1879.
[22] G. Markl, R. Ehrl, H. Sauer, P. Kreitmeier, T. Burgemeister, *Helv. Chim. Acta* **1999**, *82*, 59.
[23] G. Märkl, J. Stiegler, P. Kreitmeier, *Helv. Chim. Acta* **2001**, *84*, 2022.
[24] G. Märkl, R. Ehrl, P. Kreitmeier, T. Burgemeister, *Helv. Chim. Acta* **2000**, *83*, 495.
[25] G. Märkl, T. Knott, P. Kreitmeier, T. Burgemeister, F. Kastner, *Helv. Chim. Acta* **1998**, *81*, 1480.
[26] G. Märkl, H. Sauer, P. Kreitmeier, T. Burgemeister, F. Kastner, G. Adolin, H. Nöth, K. Polborn, *Angew. Chem. Int. Ed.* **1994**, *33*, 1151.
[27] G. Märkl, J. Stiegler, P. Kreitmeier, T. Burgemeister, *Helv. Chim. Acta* **2001**, *84*, 2037.

[28] a) J. E. McMurry, *Chem. Rev.* **1989**, *89*, 1513; b) M. Williams-Harry, A. Bhaskar, G. Ramakrishna, T. Goodson, III, M. Imamura, A. Mawatari, K. Nakao, H. Enozawa, T. Nishinaga, M. Iyoda, *J. Am. Chem. Soc.* **2008**, *130*, 3252.
[29] K. Nakao, M. Nishimura, T. Tamachi, Y. Kuwatani, H. Miyasaka, T. Nishinaga, M. Iyoda, *J. Am. Chem. Soc.* **2006**, *128*, 16740.
[30] a) J. L. Sessler, D. Seidel, *Angew. Chem., Int. Ed.* **2003**, *42*, 5134; b) T. K. Chandrashekar, S. Venkatraman, *Acc. Chem. Res.* **2003**, *36*, 676; c) M. Stepien, N. Sprutta, L. Latos-Grazynski, *Angew. Chem., Int. Ed.* **2011**, *50*, 4288; d) S. Saito, A. Osuka, *Angew. Chem., Int. Ed.* **2011**, *50*, 4342.
[31] a) J. Krömer, I. Rios-Carreras, G. Fuhrmann, C. Musch, M. Wunderlin, T. Debaerdemaeker, E. Mena-Osteritz, P. Bäuerle, *Angew. Chem. Int. Ed.* **2000**, *39*, 3481; b) M. Williams-Harry, A. Bhaskar, G. Ramakrishna, T. Goodson, M. Imamura, A. Mawatari, K. Nakao, H. Enozawa, T. Nishinaga, M. Iyoda, *J. Am. Chem. Soc.* **2008**, *130*, 3252.
[32] E. Vogel, P. Röhrig, M. Sicken, B. Knipp, A. Herrmann, M. Pohl, H. Schmickler, J. Lex, *Angew. Chem. Int. Ed.* **1989**, *28*, 1651.
[33] J. S. Reddy, S. Mandal, V. G. Anand, *Org. Lett.* **2006**, *8*, 5541.
[34] M. Ishida, S.-J. Kim, C. Preihs, K. Ohkubo, J. M. Lim, B. S. Lee, J. S. Park, V. M. Lynch, V. V. Roznyatovskiy, T. Sarma, P. K. Panda, C.-H. Lee, S. Fukuzumi, D. Kim, J. L. Sessler, *Nat Chem* **2013**, *5*, 15.
[35] T. Tanaka, N. Aratani, A. Osuka, *Chem-Asian J* **2012**, *7*, 889.
[36] M. Stępień, B. Szyszko, L. Latos-Grażyński, *J. Am. Chem. Soc.* **2010**, *132*, 3140.
[37] J. Sankar, S. Mori, S. Saito, H. Rath, M. Suzuki, Y. Inokuma, H. Shinokubo, K. Suk Kim, Z. S. Yoon, J.-Y. Shin, J. M. Lim, Y. Matsuzaki, O. Matsushita, A. Muranaka, N. Kobayashi, D. Kim, A. Osuka, *J. Am. Chem. Soc.* **2008**, *130*, 13568.
[38] K. M. Kadish, K. M. Smith, R. Guilard, *The Porphyrin Handbook, Vol. 6*, Academic Press, San Diego, **2000**.
[39] J. S. Lindsey, I. C. Schreiman, H. C. Hsu, P. C. Kearney, A. M. Marguerettaz, *J. Org. Chem.* **1987**, *52*, 827.
[40] a) P. Rothemund, *J. Am. Chem. Soc.* **1935**, *57*, 2010; b) P. Rothemund, *J. Am. Chem. Soc.* **1936**, *58*, 625.
[41] M. G. P. M. S. Neves, R. M. Martins, A. C. Tome, A. J. D. Silvestre, A. M. S. Silva, V. Felix, J. A. S. Cavaleiro, M. G. B. Drew, *Chem. Commun.* **1999**, 385.
[42] J.-Y. Shin, H. Furuta, K. Yoza, S. Igarashi, A. Osuka, *J. Am. Chem. Soc.* **2001**, *123*, 7190.
[43] J.-Y. Shin, H. Furuta, A. Osuka, *Angew. Chem. Int. Ed.* **2001**, *40*, 619.
[44] K. Nakasuji, K. Yoshida, I. Murata, *J. Am. Chem. Soc.* **1983**, *105*, 5136.
[45] Y. Morita, S. Nishida, in *Stable Radicals*, John Wiley & Sons, **2010**, pp. 81.
[46] R. Rathore, A. S. Kumar, S. V. Lindeman, J. K. Kochi, *J. Org. Chem.* **1998**, *63*, 5847.
[47] Gaussian 09, Revision D.01, M. J. Frisch, G. W. Trucks, H. B. Schlegel, G. E. Scuseria, M. A. Robb, J. R. Cheeseman, G. Scalmani, V. Barone, B. Mennucci, G. A. Petersson, H. Nakatsuji, M. Caricato, X. Li, H. P. Hratchian, A. F. Izmaylov, J. Bloino, G. Zheng, J. L. Sonnenberg, M. Hada, M. Ehara, K. Toyota, R. Fukuda, J. Hasegawa, M. Ishida, T. Nakajima, Y. Honda, O. Kitao, H. Nakai, T. Vreven, J. A. Montgomery, Jr., J. E. Peralta, F. Ogliaro, M. Bearpark, J. J. Heyd, E. Brothers, K. N. Kudin, V. N. Staroverov, R. Kobayashi, J. Normand, K. Raghavachari, A. Rendell, J. C. Burant, S. S. Iyengar, J. Tomasi, M. Cossi, N. Rega, J. M. Millam, M. Klene, J. E. Knox, J. B. Cross, V. Bakken, C. Adamo, J. Jaramillo, R. Gomperts, R. E. Stratmann, O. Yazyev, A. J. Austin, R. Cammi, C. Pomelli, J. W. Ochterski, R. L. Martin, K. Morokuma, V. G. Zakrzewski, G. A. Voth, P. Salvador, J. J. Dannenberg, S.

Dapprich, A. D. Daniels, Ö. Farkas, J. B. Foresman, J. V. Ortiz, J. Cioslowski, and D. J. Fox, Gaussian, Inc., Wallingford CT, 2009.
[48] Z. Chen, C. S. Wannere, C. Corminboeuf, R. Puchta, P. v. R. Schleyer, *Chem. Rev.* **2005**, *105*, 3842.
[49] P. V. Schleyer, C. Maerker, A. Dransfeld, H. J. Jiao, N. J. R. V. Hommes, *J. Am. Chem. Soc.* **1996**, *118*, 6317.
[50] D. Geuenich, K. Hess, F. Kohler, R. Herges, *Chem. Rev.* **2005**, *105*, 3758.
[51] S. Cho, Z. S. Yoon, K. S. Kim, M. C. Yoon, D. G. Cho, J. L. Sessler, D. Kim, *J Phys Chem Lett* **2010**, *1*, 895.
[52] a) P. D. W. Boyd, M. C. Hodgson, C. E. F. Rickard, A. G. Oliver, L. Chaker, P. J. Brothers, R. D. Bolskar, F. S. Tham, C. A. Reed, *J. Am. Chem. Soc.* **1999**, *121*, 10487; b) D. Sun, F. S. Tham, C. A. Reed, L. Chaker, M. Burgess, P. D. W. Boyd, *J. Am. Chem. Soc.* **2000**, *122*, 10704; c) D. V. Konarev, I. S. Neretin, Y. L. Slovokhotov, E. I. Yudanova, N. y. V. Drichko, Y. M. Shul'ga, B. P. Tarasov, L. L. Gumanov, A. S. Batsanov, J. A. K. Howard, R. N. Lyubovskaya, *Chem. - Eur. J.* , **2001**, *7*, 2605; d) D. Sun, F. S. Tham, C. A. Reed, L. Chaker, P. D. W. Boyd, *J. Am. Chem. Soc.* **2002**, *124*, 6604; e) P. D. Boyd, C. A. Reed, *Acc. Chem. Res.* **2005**, *38*, 235; f) J. Zhang, J. Tan, Z. Ma, W. Xu, G. Zhao, H. Geng, C. a. Di, W. Hu, Z. Shuai, K. Singh, D. Zhu, *J. Am. Chem. Soc.* **2013**, *135*, 558.
[53] Y. Tanaka, W. Hoshino, S. Shimizu, K. Youfu, N. Aratani, N. Maruyama, S. Fujita, A. Osuka, *J. Am. Chem. Soc.* **2004**, *126*, 3046.
[54] G. Märkl, R. Ehrl, H. Sauer, P. Kreitmeier, T. Burgemeister, *Helv. Chim. Acta* **1999**, *82*, 59.
[55] IUPAC. Compendium of Chemical Terminology, 2nd ed. (the "Gold Book"). Compiled by A. D. McNaught and A. Wilkinson. Blackwell Scientific Publications, Oxford (1997).
[56] J. Nakayama, S. Murabayashi, M. Hoshino, *Heterocycles* **1986**, *24*, 2639.
[57] a) M. Karplus, *J. Am. Chem. Soc.* **1963**, *85*, 2870; b) M. Karplus, *J. Chem. Phys.* **1959**, *30*, 11.
[58] a) J. J. Dannenberg, *Angew Chem Int Edit* **1975**, *14*, 641; b) J. A. E. H. van Haare, L. Groenendaal, E. E. Havinga, R. A. J. Janssen, E. W. Meijer, *Angew. Chem. Int. Ed.* **1996**, *35*, 638.
[59] a) F. Zhang, G. Gotz, E. Mena-Osteritz, M. Weil, B. Sarkar, W. Kaim, P. Bauerle, *Chem. Sci* **2011**, *2*, 781; b) M. Iyoda, K. Tanaka, H. Shimizu, M. Hasegawa, T. Nishinaga, T. Nishiuchi, Y. Kunugi, T. Ishida, H. Otani, H. Sato, K. Inukai, K. Tahara, Y. Tobe, *J. Am. Chem. Soc.* **2014**, *136*, 2389.
[60] Y. Xia, S. Viel, Y. Wang, F. Ziarelli, E. Laurini, P. Posocco, M. Fermeglia, F. Qu, S. Pricl, L. Peng, *Chem. Commun.* **2012**, *48*, 4284.
[61] T. V. Rybalova, I. Y. Bagryanskaya, *J. Struct. Chem.* **2009**, *50*, 741.
[62] J.-i. Setsune, Y. Katakami, N. Iizuna, *J. Am. Chem. Soc.* **1999**, *121*, 8957.
[63] J. L. Sessler, S. J. Weghorn, V. Lynch, M. R. Johnson, *Angew. Chem. Int. Ed. Engl.* **1994**, *33*, 1509.
[64] M. Bröring, J. Jendrny, L. Zander, H. Schmickler, J. Lex, Y.-D. Wu, M. Nendel, J. Chen, D. A. Plattner, K. N. Houk, E. Vogel, *Angew. Chem., Int. Ed.* **1995**, *34*, 2515.
[65] M. Broering, J. Jendrny, L. Zander, H. Schmickler, J. Lex, Y.-D. Wu, M. Nendel, J. Chen, D. A. Plattner, a. et, *Angew. Chem. Int. Ed. Engl.* **1995**, *34*, 2515.
[66] J.-i. Setsune, S. Maeda, *J. Am. Chem. Soc.* **2000**, *122*, 12405.
[67] J.-Y. Shin, H. Furuta, K. Yoza, S. Igarashi, A. Osuka, *J. Am. Chem. Soc.* **2001**, *123*, 7190.
[68] D. Seidel, V. Lynch, J. L. Sessler, *Angew. Chem. Int. Ed.* **2002**, *41*, 1422.

[69] V. G. Anand, S. Saito, S. Shimizu, A. Osuka, *Angew. Chem. Int. Ed. Engl.* **2005**, *44*, 7244.
[70] G. Karthik, J. M. Lim, A. Srinivasan, C. H. Suresh, D. Kim, T. K. Chandrashekar, *Chem. - Eur. J.* **2013**, *19*, 17011.
[71] T. Nishinaga, M. Tateno, M. Fujii, W. Fujita, M. Takase, M. Iyoda, *Org. Lett.* **2010**, *12*, 5374.
[72] J. Heinze, J. Mortensen, K. Mullen, R. Schenk, *J. Chem. Soc., Chem. Commun.* **1987**, 701.